Liquid-Phase Photo-induced Covalent Modification (PICM) of Single-Layer Graphene

単層グラフェンの液相光誘起共有結合修飾（PICM）

Guilin Feng

Graduate School of Information Science and Technology,

Hokkaido University

Supervisor: Hiroshi Uji-i

Table of Contents

Acknowledgements

Looking back to the four-year PhD study, it is a long journey with happiness and sadness. I can't image I am so close to the graduation since the scientific work is full of difficulty. There is a long list to thank everybody who gave me the help during these years.

First of all, I want to thank my supervisor Hiroshi Uji-i for giving me the opportunity to study in Japan. Hiroshi is very smart and he always had deep thinking on my project and gave me constructive suggestions during the PhD study. Hiroshi is rigorous on scientific work and always push me think deeply on my project, which have benefited me a lot. His thought and attitude on science will have greatly positive effect on my whole life. I sincerely thank Hiroshi for patiently guidance and selfless help, I want to say "thank you very much" to my professor Hiroshi Uji-i.

I want to thank Kenji Hirai, who gave huge help on my PhD study. Kenji is a highly efficient scientific worker. He can quickly response my request and gave me suggestions on summarizing my projects. During the period of PhD study, Kenji improved my communications, encouraged me a lot and gave me support on my scientific works. Many thanks to Kenji.

I want to thank Tomoko Inose who gave me help when I came to Japan. Tomoko showed me how to use the Raman microscopy and how to start the experiment in the laboratory. Without help from Tomoko, I was likely struggling in a tricky project. "Thank you, Tomoko".

I want to thank Farsai Taemaitree for helping on my communication and organizing the discussion with Hiroshi.

I also want to say "thank you" to my colleagues. Communication with English or Japanese was a big problem at the beginning of PhD study in Japan. In the study, I couldn't catch the points during the discussions with my professor. In the life, I didn't know how to address the house rent, how to adapt life in Japan. On these matters, Wen Han, Zhang Qiang and Li Jiangtao

helped me a lot. Especially, Han helped me a lot at the early period of my PhD study, “thank you, Han”. Zhang gave me suggestions related with studying and living in Japan. When I was anxious and helpless, Zhang encouraged me a lot, “thank you, Zhang”. Li has same hobby with me. Both we like skiing and we spent much time on skiing. It was enjoyable and relax time. “Li, thank you for your accompanying”.

I want to thank Fujita Yasuhiko and Shuichi Toyouchi for promoting my project and improving my scientific thoughts. Yasu and Shuichi are very smart and possess scientific thinking. They gave lots of constructive comments on my works, which made me know what is real collaboration and how to correctly carry out scientific works. Especially, Yasu gave me huge help on my first project. I would like to express my greatest attitude to him for his help on my experiments.

I want to thank Nozomu Suzuki for helping on DFT calculations. Suzuki sensei helped a lot on my first and second projects regarding on calculations. Thanks a lot.

I want to thank K. M. Muhammed Shameem for reading and improving my writing on the second project.

I want to express my appreciation to Cao En for spending time with me and encouraging me to go through the hard time.

I can’t forget to thank my girlfriend, Liu Xiaohong, who is really important in my PhD study and in my life. We start the relationship when I was in master student in Sichuan University. Liu is a very excellent girl and good at learning. She taught me a lot when I was master student. Without her, I am not sure if I would go abord or not. She encouraged me and gave me lots of strength for studying in Japan. I can’t express my all appreciation to Liu by words, “thank you, Xiaohong”

Many thanks to my family who always support me and encourage me during the four years. Especially in the fourth year, I lose my scholarship due to the extension. My family gave me

the financial support. Thank you very much for your help! Thank you very much for your moral support.

Again, thank you everybody, thank you for your help!

Finally, I want to thank China scholarship council (CSC) for financial support.

Abstract

Tailoring the electronic structure (bandgap engineering) of graphene is crucial for multi-purpose applications, especially in semiconductor devices. To this end, various efforts have been made to contribute to this modulation. Among them, chemical modification of graphene is a potential method, which can introduce sp^3 defects to graphene, accompanied by forming the covalent bond. By using chemical modification, the electronic nature, chemical and optical property of graphene can be well tailored. Recent years, the electrochemical and photo-induced chemical modification (PICM) at solid-phase has been most studied because of designable, high efficiency and reversible. Nonetheless, to spatially tailor the surface property of graphene, mask is required to prevent the reaction of graphene at the undesired area for the electrochemical method. In the case of solid-phase PICM, the reaction molecule is pre-deposited on graphene surface (forming solid film) followed by laser-irradiation generating the covalent grafting. However, the modified graphene is difficult for further application because of hard to keep clean and slightly low efficiency. In addition, both these two methods are involving complex organic molecules, which is difficult to understand and investigate the reaction mechanism of this covalent modification.

To response, liquid-phase PICM is attracted to develop mask-free, clean, and simplified chemical modification of graphene. Our research group previously investigated the PICM of graphene in pure water, demonstrating the liquid-phase PICM is available and reliable. Without any chemicals, the specifical pattern can be achieved by irradiating tightly focused laser at the liquid phase. Furthermore, the sp^2 hybridized carbon of graphene can be restored by high density of laser power or direct heating at high temperature, indicating the liquid-phase PICM induced defects is reversible. However, although the successful modification of graphene is obtained, low efficiency and low degree of functionalization extremely limits the further

investigation and applications. Thus, this thesis aims to develop high efficiency, a facile preparation process and controllable design of liquid-phase PICM of graphene. Also, by using this liquid-phase PICM, the reaction mechanism is deeply explored. After that, we aim to extend the application of PICM modified graphene investigating the electronic property.

In the first section (**chapter 2**), a high-efficiency liquid-phase PICM of graphene is established. In this study, we proposed a simple method to induce highly efficient modification of graphene in short-chain fatty acids (SCFAs) aqueous solutions. In-situ Raman is employed to monitor the efficiency of the liquid-phase PICM. By carefully analyzing, we found that SCFAs with alkyl chain present much higher PICM efficiency than those in pure water and formic acid, indicating the high-efficiency liquid-phase PICM reaction depends on alkyl chains. Furthermore, solid evidences (infrared and theoretical calculation) were conducted to analyze the attached groups on graphene. These results suggest radicals from the aqueous solution, such as alkyl, ester, and ether, can be stabilized to the graphene surface under laser irradiation and form the sp^3 hybridized bond. A greater downshift of the G-band in Raman spectra is observed upon the PICM with longer alkyl chains, suggesting alkyl chain is covalently attached and the charge doping effect can be controlled by the alkyl chain length of the SCFAs. Finally, we proposed a two stage radicals' reaction mechanism contributes to the high-efficiency liquid-phase PICM in the presence of SCFAs with alkyl chain.

In the second section (**chapter 3**), we further investigate the electronic property of photo-induced covalently modified graphene (PICM-G) by graphene-enhanced Raman scattering (GERS), thanks to that the liquid-phase PICM modified graphene is easily to be washed and spatially controllable. The PICM-G is fabricated following our study in chapter 2. The covalent patterning area can be easily obtained by this liquid-phase PICM method. We found that the GERS effect from the covalently patterned graphene substrate yields a significantly higher Raman enhancement of the absorbed fluorescent molecules compared to the pristine graphene.

The signal enhancement from the PICM region can be attributed to the modulation of electronic structure of graphene. Furthermore, the Langmuir-Blodgett (LB) technique is employed to deposit the mono and multilayer film of the probed 3,3'-Dioctadecyloxacarbocyanine Perchlorate (DiO) dye molecule on the PICM-G substrate. The Raman signal enhancement with respect to the layer thickness of probed molecule, excitation wavelength at the PICM region is discussed. To further estimate the GERS effect of the PICM graphene substrate, a most commonly used molecule (Rh6G) is employed. The GERS effect is estimated by calculating the ratio of peak intensity of from PCIM area to that of PG area, which shows highest than any reports (~25), indicating the Fermi level of PICM graphene with acetic is more appropriate than pristine graphene for GERS. Finally, we investigate the role of covalent grafting types on GERS enhancement factor (EF) by comparing the graphene substrates prepared in pure water and acetic acid solution. Our findings provide evidence that the functional groups within the chemically patterned region plays a critical role in determining the EF of GERS.

Abbreviations

PICM	Photo-induced covalent modification
FETs	Field-effect transistor
SCFAs	Short-chain fatty acids
DFT	Density functional theory
IR	Infrared
I_D	D-band Raman intensity
I_G	G -band Raman intensity
CCD	Coupled charge device
GERS	Graphene-enhanced Raman scattering
EF	Enhancement factor
PG	Pristine graphene
PICM-G	Photo-induced covalently modified graphene
LB	Langmuir-Blodgett
LUMO	Lowest unoccupied molecular orbital
HOMO	Highest occupied molecular orbital
DiO	3,3'-Dioctadecyloxacarbocyanine Perchlorate
Rh6G	Rhodamine 6G
I_{1094}	Intensity of DiO peak at 1094 cm^{-1}
I_m	Intensity of dye peaks at the modified area
I_p	Intensity of dye peaks at the pristine area

Chapter 1

General Introduction

1.1 Introduction to graphene

1.1.1 History of graphene and graphene's properties

Graphene is a one-atom-thick planar sheet of sp^2-bonded carbon atoms arranged in a hexagonal honeycomb lattice, which was firstly extracted from graphite by *Novoselov* and *Geim* in 2004.[1-3] This approach can produce high-quality monolayer graphene by repeatedly peeling highly oriented pyrolytic graphite (HOPG), leading to enormous scientific activities.[4-7] The basic structure of graphene is shown in Figure 1.1.[8] Carbon atoms are connected by molecular bonds, and the distance between two carbon atoms is ~0.142 nm. The thickness of monolayer graphene is ~0.34 nm. Generally, except for a particular definition, graphene means monolayer graphene. Due to carbon atoms in graphene being sp^2-bonded and the special structure, it makes graphene have unique properties.[9-12]

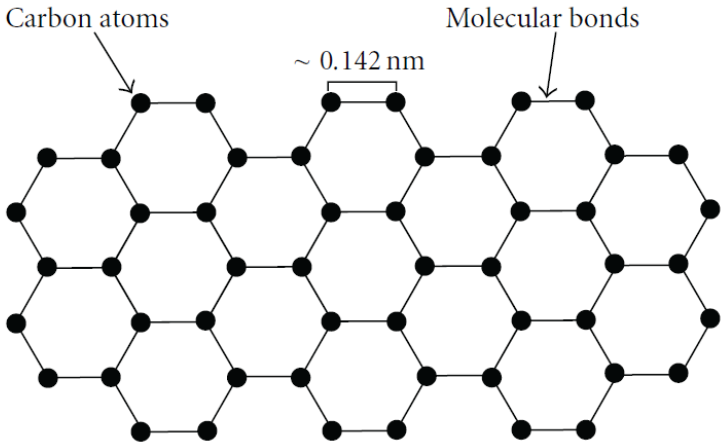

Figure 1.1 Schematic structure of graphene [adapted from[8]]

(1) Electronic property

The hybridized plane of sp^2 carbon of graphene forms a delocalized π band. The π electrons can freely move in the whole plane; thus, graphene has a good conductivity.[13, 14] At room temperature, its carrier mobility can reach 15,000 $cm^2/V{\cdot}s$.[15-17] As shown in Figure 1.2, the conduction band and valence band of graphene are crossed at the *K* point.[15] Each unit lattice of graphene has two carbon atoms causing the two tapered intersections (*K*, *K'*) points in each

Brillouin zone. The bandgap of graphene is zero due to its effective mass of electrons and holes being zero.[18, 19] The unique carrier of graphene makes it be a potential material in electrical fields.[20, 21]

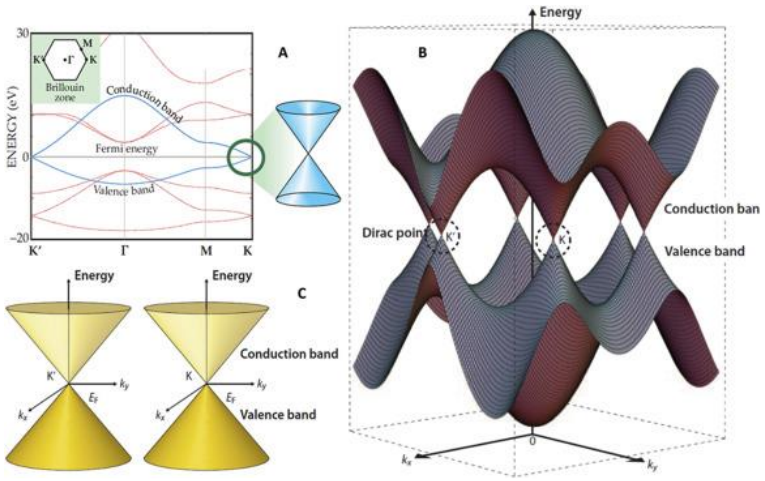

Figure 1.2 Band structure of graphene[adapted from[15]]

(2) Optical property

In addition to excellent carrier mobility, the single-layer graphene possesses ultra-high transparency.[22] As presented in Figure 1.3a, suspended graphene partially covered on an aperture. Thus, the opacities of different areas in one aperture can be fairly compared.[23] As a result, the light transmittance of single-layer graphene can be up to 97.7% comparing with the air (light transmittance in air is deemed as 100%). And the reflectance of light on graphene is less than 1%, which is negligible. A linear decrease of the light transmittance is observed with the increase of graphene layer numbers from 1-5 (5 layers, around 88%). And the opacity is independent with wavelength (Figure 1.3b). The light transmittance is almost same when the wavelength of light sources varying from 500 to 700 nm. In this report, the measured values of light transmittances align with theoretical calculation results estimated by a non-interacting massless Dirac fermions model. In this model, the high-frequency (dynamic) conductivity G for Dirac fermions depends on a universal constant, i.e., $G \approx \pi e^2/2h$. Where e is the electron charge and h is Planck's constant. The transparency of graphene is only related to a fine-

structure constant $\alpha = 2\pi e^2/2hc$ (c is the speed of light). Thus, the absorption of n-layer graphene can be predicted as $n\pi\alpha$. Although single-layer graphene has ultra-high transparency, it can be directly observed by optical microscopy when graphene supported on substrates (silicon, glass etc.). In addition, the transparency of graphene varied when its electronic structure of graphene is modified.[24, 25] *Robinson et al.* reported fluorinated graphene films on SiO_2 substrate.[26] The optical property of graphene changes after fluorination, which is attributed to the change of electronic property.

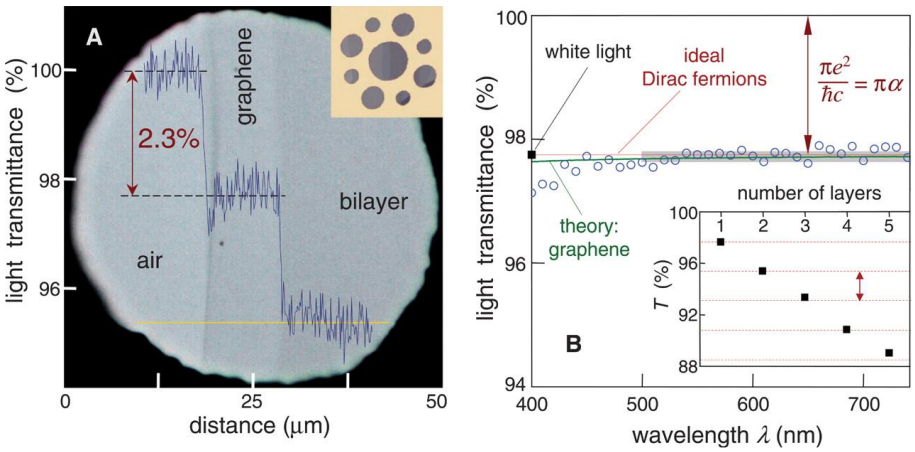

Figure 1.3 Optical absorbance of different layers' graphene suspended on porous membrane. [adapted from[23]]

(3) Thermal and mechanical property

The thermal conductivity of freely suspended graphene at room temperature can reach 3000-5000 W m^{-1} K^{-1}, which is dependent with the size of the graphene sheet (Figure 1.4a).[27-29] The supported substrates have significant influence on the thermal conductivity of graphene. For example, the measured thermal conductivity of SiO_2-supported graphene is ~600 W m^{-1} K^{-1} at room temperature.[30] And that of SiO_2-encased graphene shows only ~160 W m^{-1} K^{-1}.[31] The effect of the SiO_2 substrate on thermal conductivity is explained by the loss of phonons across the graphene-silicon and the effect of scattering of graphene-substrate interfacial phonons.[32, 33] Although the thermal conductivity of graphene decreases a lot for supported graphene, the

value is still much higher than most conductive substrates (for example, copper, silicon). Graphene also possesses excellent mechanical performance, which is evidenced by atomic force microscopy (AFM) for free-standing graphene membranes (inset of Figure 1.4b).[34, 35] The breaking strength of graphene can reach around 40 N m^{-1}, which is quite strong for ultrathin materials. With the increasing of graphene layers, the deformation force rises. The linear relationship between the applied force and deformation can be obtained when graphene layers reach 12 (Figure 1.4b), demonstrating the strong mechanical property of graphene. In addition, the mechanical loads of graphene affect the electronic structure.[36] The effect of strained graphene on electronic properties was studied by the field emission performance. The moderate tensile strain on graphene will open the bandgap of the graphene.[37-39]

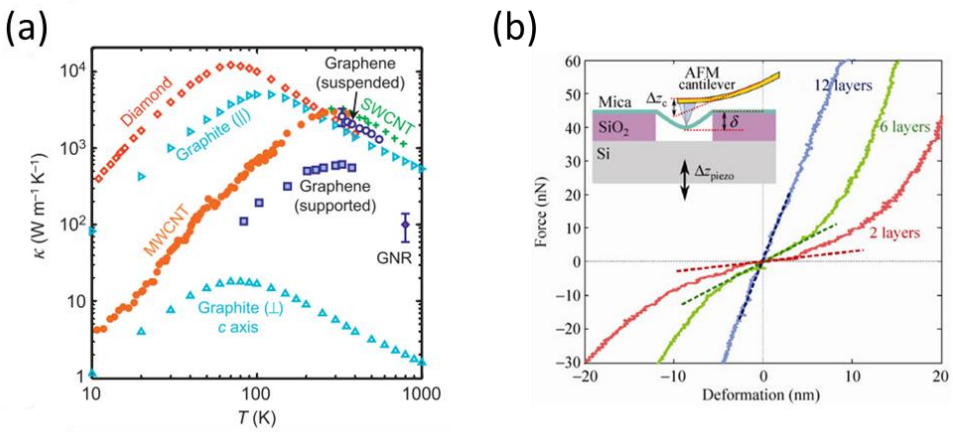

Figure 1.4 (a) the estimated thermal conductivity of graphene; [adapted from[27]] (b) mechanical test: different layers of suspended graphene on mica and bending test. [adapted from[34]]

1.1.2 Synthesis of graphene

As mentioned before, graphene was firstly obtained using mechanical exfoliation of graphite by a tape.[40] This method can give high-quality graphene, but it is not suitable for mass production and synthesizing the desired scale of graphene. In the past decade, various strategies have been established for the synthesis of graphene.[41-44] As presented in Figure 1.5, graphene synthesis can be categorized into two methods: top-down and bottom-up respectively.[45-47] In the top-down method, although mechanical exfoliation achieves few-layer graphene and is the cheapest method, the thickness of graphene varies to ~10 nm, which is relatively thicker than single-layer graphene (~0.345 nm).[7] Chemical exfoliation is an appropriate method for synthesizing graphene, which utilizes the colloidal suspension to reduce the interlayer van der Walls forces and increase the interlayer spacing. Then the graphene intercalated compounds (GICs) were exploited to single/few layers by rapid heating or sonication.[48] Chemical synthesis is mainly involving the chemical reduction of graphite oxide (GO). GO is usually synthesized through the oxidation of graphite using the Brodie method, Staudenmaier method, and Hummer's method.[49-51] H_2 or other reducing agents (phenyl hydrazine, ascorbic acid etc.) were used to remove the oxygen from GO.[52-55] Also, an electrochemical reduction can prepare the graphene from the GO.[56, 57] GO was suspended in water by sonication and deposited on surfaces by spin coating, forming single or double-layer graphene oxide. Then graphene film was prepared by thermally or chemically reducing the GO.[58] In the bottom-up method, pyrolysis is a chemical synthesis using the thermal process. For example, sodium and ethanol were put in a closed vessel with a molar ratio of ~1:1 to form graphene precursor at 220 ºC. Graphene can be achieved by pyritization of the graphene precursor after sonication and washing with water.[59] Pyrolysis of biomass sources can also achieve the graphene materials.[60] Feedstocks, such as cookies, chocolate, and grass, were thermal treated on the Cu foil to obtain biomass-derived high-quality graphene.[61] Although high-purity of graphene can be made by the pyrolysis, many defects are comprised. This method is not suitable for the safety and scale-up

production of defect-free graphene.

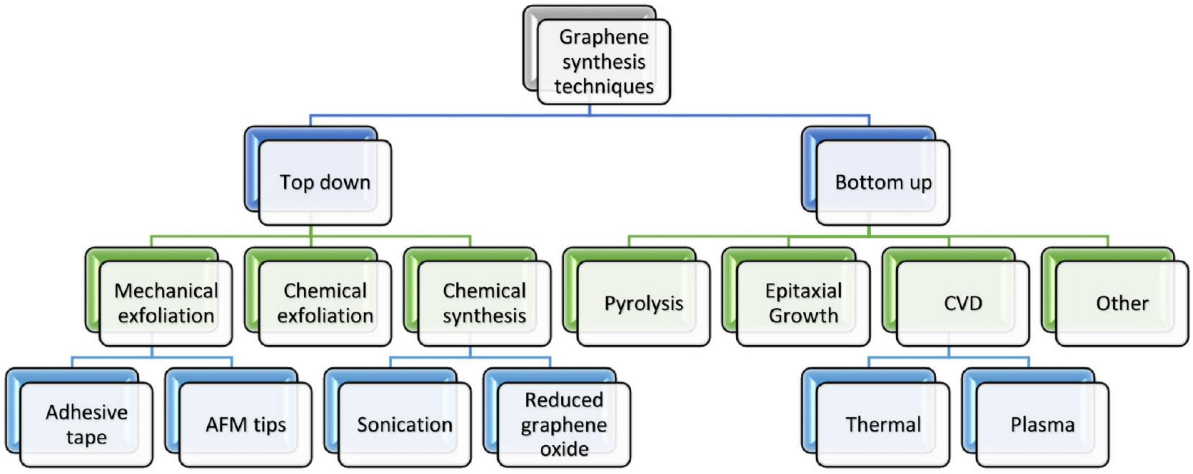

Figure 1.5 Strategies for graphene synthesis. [adapted from[45]]

Chemical vapor deposition (CVD) is a method that produces graphene by chemical reduction reaction.[62, 63] Molecules heated to a gaseous state or gaseous molecules at room temperature are used. And a substrate is pre-placed at high temperature to collect the gaseous precursors. The deposition of graphene is usually done on transition-metal substrates like Ni[64], Ru[65] and Cu[66] at high temperatures. The process of thermal CVD is shown in Figure 1.6a for the case of CH_4 and H_2. Figure 1.6b shows the growth kinetics. The metal performs two roles of substrate and catalyst.[67, 68] As the catalyst, the metal (Ni, Cu) can catalyze the reduction of CH_4 to C. The reduced C was subsequently deposited on the metal surface.

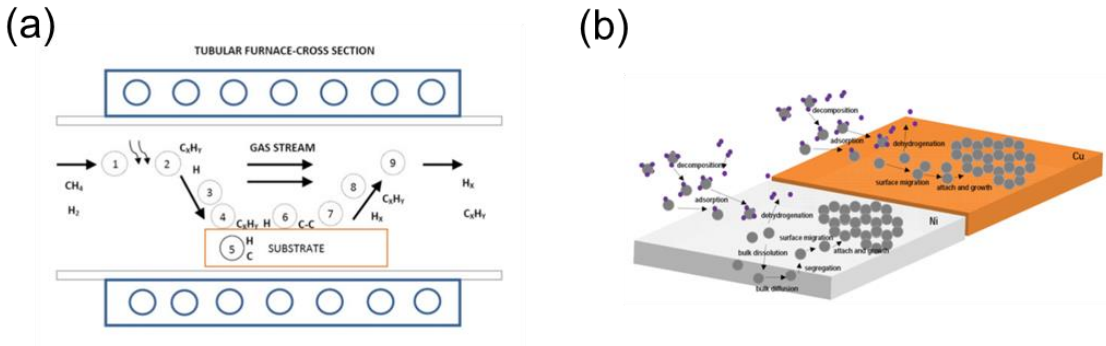

Figure 1.6 (a) schematic diagram of thermal CVD, (b) growth kinetics in CVD-produced graphene from CH_4 on Ni and Cu catalysts. [adapted from[62]]

With the development of the synthesis of graphene, the CVD method has been widely used and has become commercial owing to its high purity, low cost, and stability.[69, 70] CVD-produced graphene is often deposited on a transition metal substrate (Ni, Cu). However, to apply in various applications, graphene has to be transferred on a desired substrate (silicon, glass, etc.). As depicted in Figure 1.7, the polymer, PMMA, was applied to coat the surface of copper-supported graphene (copper/graphene/polymer), then the copper was etched by ammonium persulphate.[71] The achieved graphene/polymer is washed with deionized water and transferred to the desired substrate. In the final step, the polymer was removed by polymer annealing or solvent etch. In this thesis, single-layer graphene is synthesized using the CVD method and transferred to the targeted substrate.

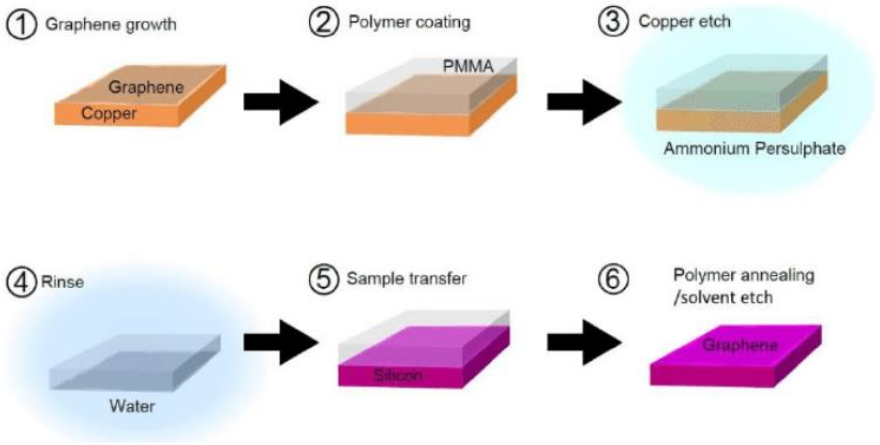

Figure 1.7 Transfer CVD-produced graphene to silicon substrate. [adapted from[71]]

1.1.3 Applications of graphene in electronic devices

As the latest member of carbon-based nano materials, graphene has become the subject of tremendous research and encourages lots of applications.[72-84] When it comes to electronical devices, graphene is a potential material due to the following advantages: (1) high mechanical strength; (2) fast carrier mobility; (3) high transparent; (4) ultrathin body; (5) special energy band structure; (6) flexibility; (7) thermal stability.[85-88] As a result, graphene has been utilized to graphene field-effect transistors (FETs),[89, 90] photodetectors,[91] graphene-based transparent electrodes,[92] and biosensors.[78] In this thesis, we study on the chemical modification (bandgap engineering) of graphene and investigate the electronic property of chemically modified graphene. Thus, we focus on introduction of application of graphene in FETs.

Ambipolar behaviors of graphene: graphene is considered as semiconductor with zero-bandgap energy structure. Dirac fermions can be continuously tuned between holes and electrons under electrostatic effect of gate voltage. The Fermi level lies at the intersection of a cone-like energy band structure, namely Dirac point, which has the same carrier density of both holes and electrons for pristine graphene without any voltage.[93] The carrier density presents as a function of voltage: $n_{e,\,h}=\alpha V_g$. Wherein, n_e, n_h are electrons density and holes density, respectively; α is charge injection rate; V_g is gate voltage. Thus, a linear relation between carrier density and gate voltage can be interred.[94] The resistivity can be understood as $1/\rho=en\mu$ and the Holzer coefficient is understood as $R_H=1/en$. The carrier density can be modulated between electrons and holes by the applied voltages.[95] For example, the holes and electrons can be induced in graphene under negative voltage and positive voltage, respectively (Figure 1.8a). Besides, around the Dirac point, the Holzer coefficient is being changed because the charge carrier is transmitted from electrons to holes or from holes to electrons. When the concentration of charge carrier reaches the minimum value, indicating minimum conductivity (Figure 1.8b).

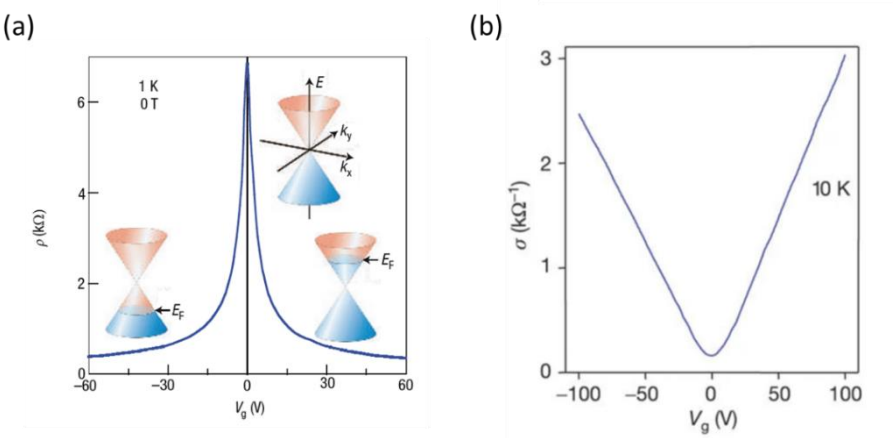

Figure 1.8 The field effect of graphene (a) correlation between resistivity and voltage; [adapted from[94]] (b) correlation between conductivity and voltage. [adapted from[95]]

The unique energy structure makes graphene have good opportunity in bottom-gated, top-gated, double-gated, and suspended FETs.[96-98] Figure 1.9 shows a single-layer graphene-based transistor by Al_2O_3 bottom-gating.[99] A typical "V-shape" can be observed in both Al_2O_3/Si and SiO_2/Si substrate. In this study, authors demonstrated Al_2O_3/Si substrate show enhanced performance and graphene has a great potential for field-effect transistors study.

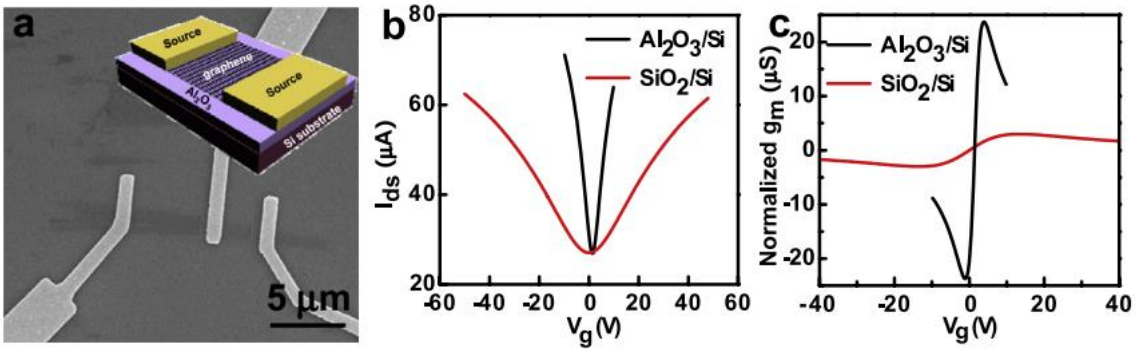

Figure 1.9 One typical application of graphene in field-effect transistor. [adapted from[99]]

Various FETs using graphene as the channel materials have been developed to realize the further miniaturization of integrated circuits. However, the zero-bandgap structure of graphene make it be difficult to achieve the channel cut off. Therefore, in order to improve the switch ratio of the device, a certain width of energy gap is required. Graphene nanoribbon (GNR)

possessing a wide bandgap has been reported to fabricate the device, which can achieve a high I_{on}/I_{off} ratio at room temperature.[100] As shown in Figure 1.10, GNR fabricated FETs exhibits high I_{on}/I_{off} ratio of 10^5 demonstrating that the GNR have substantial bandgap, which could afford the graphene transistors with orders of magnitude on/off switching at room temperature.

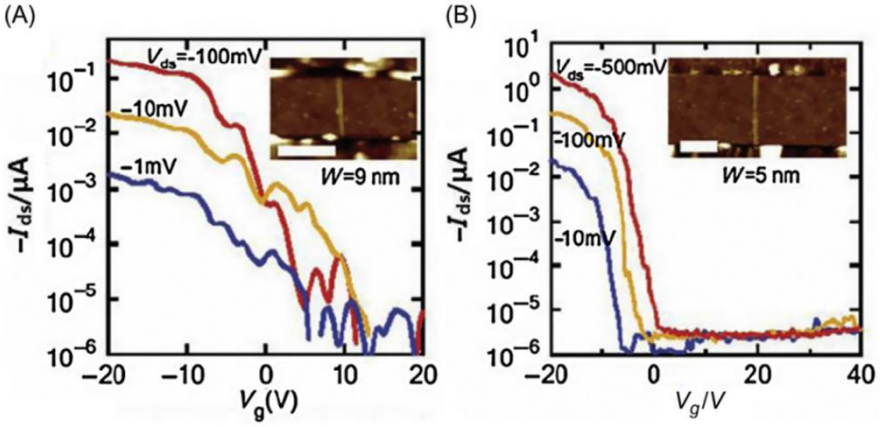

Figure 1.10 Graphene nanoribbon was applied in FETs and the switching ratio test. [adapted from[100]]

Besides, chemical approach is applied to tune the energy structure of graphene for switchable device. As shown in Figure 1.11, hydrogenated monolayer graphene prepared by hydrogen plasma was used in FETs, showing a current of over 10^3 on/off ratio on the sweep of a back-gate voltage at room temperature.[101] This study demonstrates the potential application of functionalized graphene in switchable FETs. By far, various studies have been reported to modify graphene and then applied in FETs or further application. A new field of graphene, how to open the graphene bandgap or how to tailor the electronic structure of graphene, has been attracted scientists' interests.

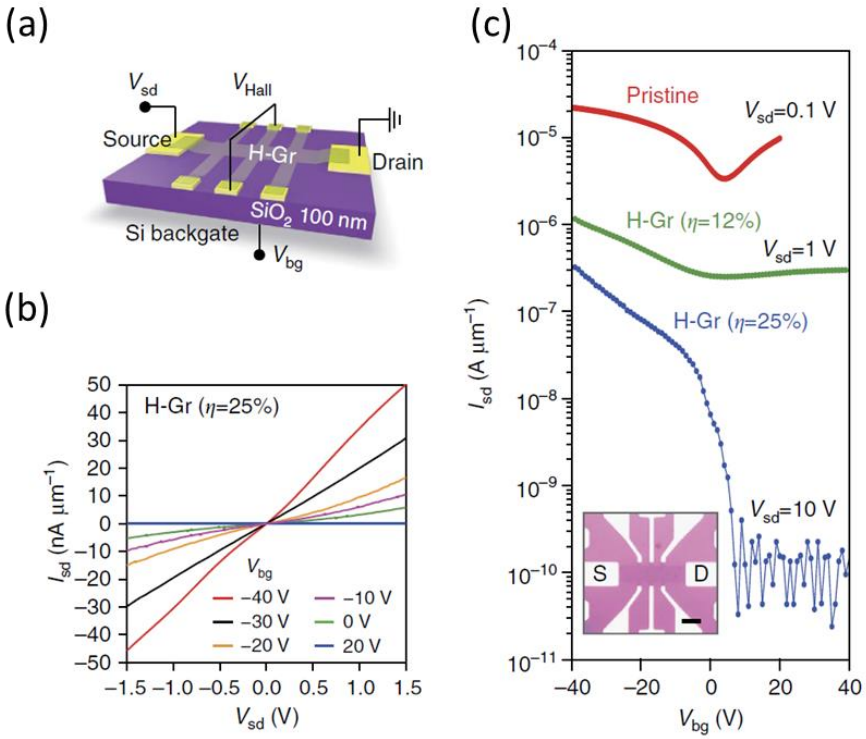

Figure 1.11 Hydrogenated monolayer graphene (H-Gr) for high on/off ratio graphene FETs. [adapted from[101]]

1.1.4 Bandgap engineering of graphene

To date, various techniques and methods have been proposed to open the bandgap of graphene and develop the application of graphene in FETs and semicoductors.[102-104,105] As shown in Figure 1.12a, the bandgap of graphene can be induced by supported substrate.[106] Epitaxial graphene on SiC is electron doped and Fermi level lies above the gap. Also, n or p-type doping can be achieved by substitution doping with nitrogen, boron, or both to modulate the band structure of graphene.[107-109] Figure 1.12b shows the doping sites and band structure of graphene.[110] The nitrogen-doped graphene is synthesized during the CVD method producing the graphene with the addition of nitrogen gas. After substitution, the nitrogen-doped graphene exhibits an n-type behavior. Similarly, p-type doping of graphene can be obtained by substitution of boron atoms further affecting the electron density distribution of graphene.[111] It has been reported large area of graphene h-BN hybrids has been successfully synthesized on the coper substrate (Figure 1.12c).[108] The small bandgap opening was observed. Theoretical computations suggesting bandgap opening in hybrid films with boron nitride (BN) is affected by hexagonal BN (h-BN) domain size. Figure 1.12d shows the bandgap opening through quantum confinement of electrons in graphene forming the graphene nanoribbon. Since no impurities are being introduced to graphene lattice, the carrier mobility will not be affected. Thus, the graphene nanoribbon with width <10 nm possesses a bandgap and have an enough carrier mobility facilitating high switching ratios.

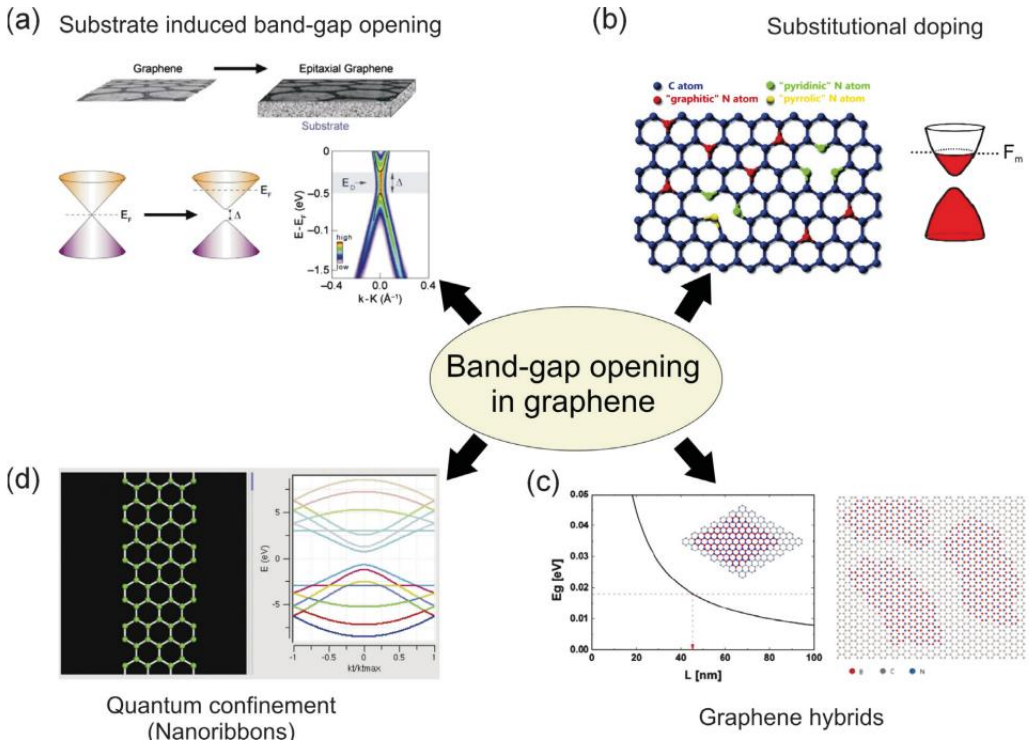

Figure 1.12 Various methods for bandgap opening of graphene. (a) substrate induced bandgap opening in graphene; (b) Substitutional doping of nitrogen in graphene lattice for bandgap opening; (c) Band gap opening in graphene h-BN hybrids; (d) Bandgap opening due to quantum confinement in graphene nanoribbons. [adapted from[104]]

In addition to the above methods, other several strategies have been developed to modulate the charge distribution of graphene. For intense, *Cao et al.* reported that bandgap of graphene can be opened by forming heterojunctions with 2D carbonitrides nitrogenated holey graphene, which has a large bandgap (186.6 meV).[112] *Nourbakhsh et al.* studied that single-layer graphene was exposed to oxygen plasma resulting in semi metallic to semiconducting behavior.[113] Covalent chemical modification also offers an effective pathway to tune the band structure of graphene.[114] For instance, *Li et al.* reported that graphene exposed to Cl_2 gas under UV light could introduce the Cl radicals to graphene surface (Figure 1.13).[115] The photochlorination reaction could form ~8 atom % Cl coverage and appear a bandgap. The research on bandgap engineering of graphene has been developed as a crucial and independent part of graphene'

science. It encourages and extends graphene in multi-purpose applications, such as FETs, sensors and photocatalysis.

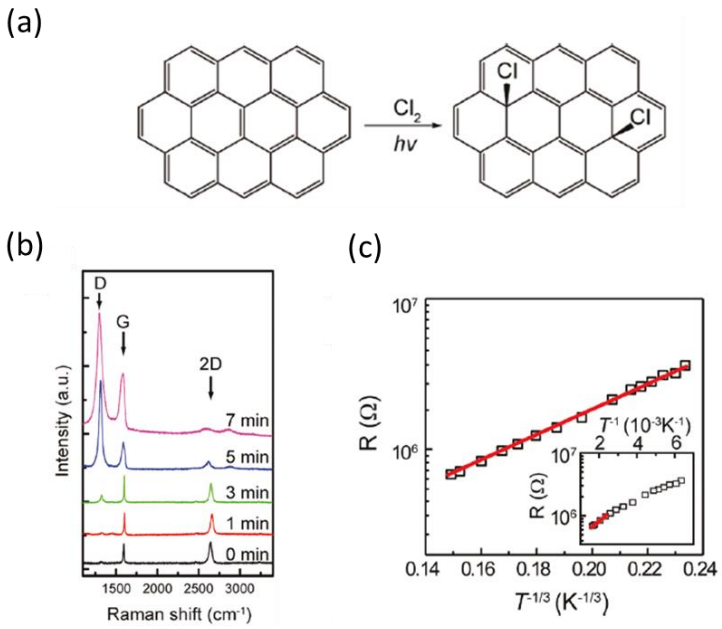

Figure 1.13 The photochemical chlorination of graphene for bandgap opening. [adapted from[115]]

1.2 Introduction to microscopic Raman spectroscopy and characterization on graphene

1.2.1 Raman spectroscopy

Raman spectroscopy is a technique where scattered light is used to measure the vibrational energy mode of a sample. It can extract information from a sample through the detection of Raman scattering. Raman scattering was theoretically predicted by *Adolf Smekal* in 1923 and first discovered by *C. V. Raman* together with his research patterner *K. S. Krishnan* in 1928.[116, 117] When a light (electromagnetic energy) interacts with a material, the light can either be reflected, absorbed, or scattered. In this scattering, the predominated mode is elastic, called Rayleigh scattering: the scattered light has the same energy (frequency and wavelength) as the incident light. If scattered light's energy (frequency and wavelength) changes, it is inelastic scattering (Raman scattering). Based on the energy difference between scattered light and incident light, the Raman scattering can be categorized into two types: Stokes Raman scattering and Anti-stokes Raman scattering (Figure 1.14).[118]

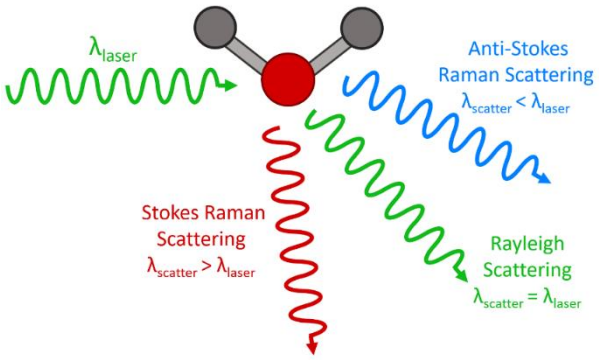

Figure. 1.14 Basic principle of Raman spectroscopy. [adapted from[118]]

(1) Stokes Raman scattering

When the wavelength (frequency) of scattered light is smaller than the incident light, the scattered light is called stokes Raman scattering. In the Stokes-Raman scattering, the photons emit less energy than incident light, and molecules get some energy. Therefore, these molecules

end up at higher vibrational states.

(2) Anti-stokes Raman scattering

When the wavelength (frequency) of scattered light is higher than the incident light, the scattered light is called anti-stokes Raman scattering. In the anti-stokes Raman scattering, the molecule's energy transfers to photons and ends at low vibrational states (ground state). Since most molecules are in the ground state at room temperature, there is a much lower possibility that a photon will be anti-stokes Raman scattering. As a result, most Raman measurements only consider the Stokes Raman scattering. The Jablonski diagram of stokes/anti-stokes Raman scattering is shown in Figure 1.10.[118, 119]

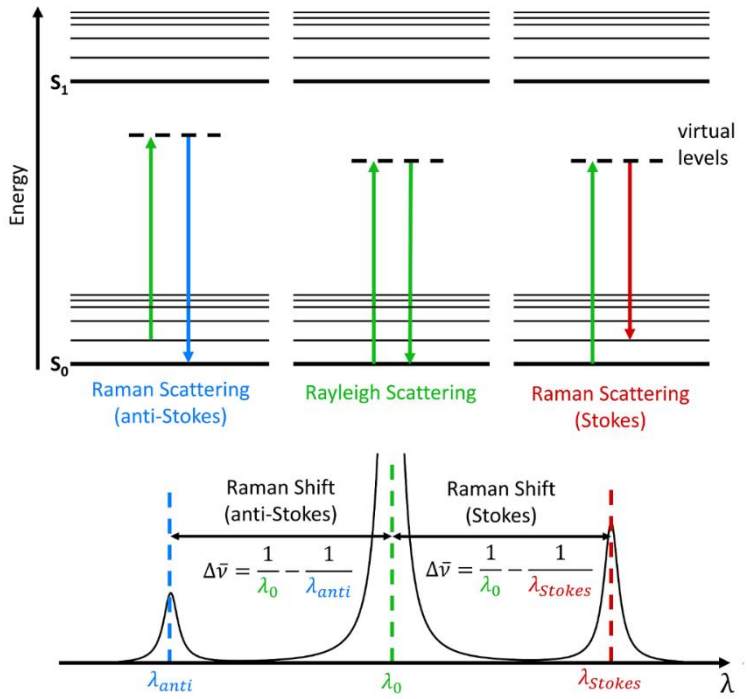

Figure 1.15 Jablonski Diagram showing the origin of Rayleigh, Stokes, and Anti-Stokes Raman Scatter. [adapted from[118]]

Raman shift

The Raman scattered light will depend on the wavelength of the excitation laser. It makes Raman scattered wavelength meaningless to compare spectra measured by different lasers. Therefore, the Raman scattered position is converted to Raman shift away from the excitation

laser. The Raman shift can be defined as an equation:[118]

$$\Delta\nu\ (cm^{-1}) = \left(\frac{1}{\lambda 0(nm)} - \frac{1}{\lambda 1(nm)}\right)$$

Wherein, the $\Delta\nu$ is the wavenumber of Raman shift; λ_0 is the wavelength of excitation laser (nm); λ_1 is the wavelength of Raman scattered light (nm). In Raman scattering, the molecular electronic ground states decide scattered light. Each molecule has a unique Raman spectrum. Namely, the Raman spectrum can be the fingerprint of the detected molecules. Therefore, Raman spectroscopy can be applied to detect and analyze the molecular structure. For instance, the Raman spectrum of the C-C stretching peak is around 919.7 cm^{-1}, and the C-H stretching peak is around 2900 cm^{-1}.[120] Taking advantage of the unique Raman spectrum, it is possible to distinguish complicated structures and even explore newly synthesized molecules. In addition, the Raman spectrum is a non-invasive measurement, easy for sample preparation, and can measure biological samples or fragile materials.[121]

1.2.2 Characterization on graphene by Raman spectroscopy

The use of Raman spectroscopy plays a critical role in the graphene field.[122-125] Figure 1.11 presents a typical Raman spectrum of graphene with defects.[126] Two characteristic peaks are intrinsic vibrations of graphene, namely, the G band (~1580 cm^{-1}) and 2D band (~2700 cm^{-1}) using laser excitation at 2.41eV. If the Raman spectrum is achieved from disordered graphene, several new peaks can be detected at ~1350 cm^{-1}(D band) and ~1625 cm^{-1} (D' band), indicating the defects of graphene.[127-130] The G band originates from a first-order Raman scattering process, corresponding to the double degenerate (iTO and iLO) phonons mode at the Brillouin center (E_{2g} symmetry).[131] Thus, the G band is only associated with graphene itself, which will not be affected by excitation energy. The D and G' (also named 2D) bands originate from the second-order process.[132, 133] Two iTO phonons near the *K* point for the 2D band, one iTO phonon and one defect for the D band. The frequency of the 2D band is approximately twice the D band, but the two phonons are not correction with any disorder or defects of graphene.[134, 135] Thus, we can generally observe G and 2D bands from pristine graphene (without defects). The D and 2D bands show the dispersive behavior because the frequency in Raman spectra changes as a function of the excitation energy. The D band frequency (ω_D) and 2D band (ω_{2D}) upshifts linearly with increasing laser energy (E_{laser}). As concluded in the literature, the slope between ω_D and E_{laser} ($\varphi_{\omega D}/\varphi_{Elaser}$) is about 50 cm^{-1}/eV and twice of that for the slope between ω_{2D} and E_{laser} ($\varphi_{\omega 2D}/\varphi_{Elaser}$).[136, 137] The D band is a significant sign to judge the successful modification of graphene, which has been widely used in graphene functionalization.[138-140] As presented Figure 1.16b, Raman spectroscopy was used to characterize the functionalization on exfoliated graphene.[141] After successfully introduce the nitrophenyl to graphene surface, strong D-band appeared in Raman spectra. It demonstrates that Raman scattering is sensitive to detect the defects on graphene, which is often employed for identifying the pristine graphene and functionalized graphene.[142-144]

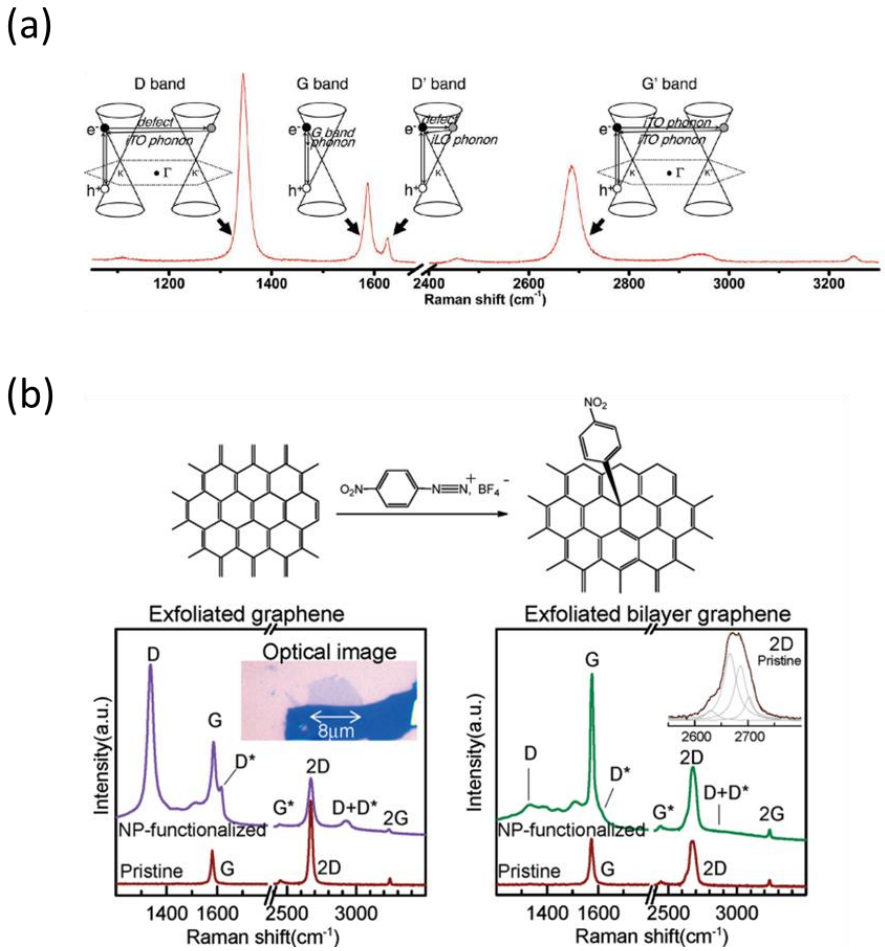

Figure 1.16 (a) Raman measurement on defect-contained graphene [adapted from[126]]; (b) Raman characterization on nitrophenyl (NP) functionalized exfoliated graphene. [adapted from[141]]

Graphene layer numbers Besides detecting the disorder or defects of graphene, the Raman spectrum can also analyze the layer numbers of graphene.[145-148] Two pieces of information on the Raman spectrum can be discussed, as shown in Figure 1.17.[149] The position of the 2D band change a lot as the graphene layers increase from 1 to 7. Secondly, the G band's intensity increases or the 2D *vs.* G band's intensity ratio decreases when the graphene layers up to 7. Furthermore, the 2D band becomes broader with the increasing layer numbers. Single-layer graphene shows a sharper 2D shape and lower peak position than multi-layer graphene. Thus, it is helpful to determine the number of graphene layers by the shape and position of the 2D

band. Which is the mainly used method to estimate single-layer graphene.[150, 151]

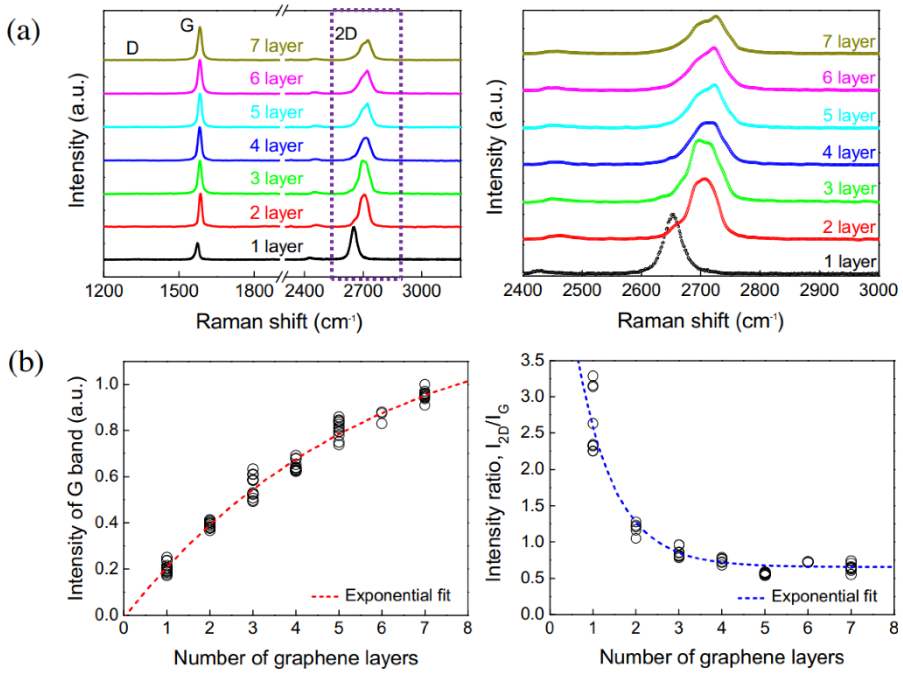

Figure 1.17 Raman spectra of graphene with different layers (a) spectra evolution, (b) intensities of G band and intensity ratio of 2D *vs.* G bands. [adapted from[149]]

Correlation between position of G, 2D and electronic property The position of G and 2D (pos (G), pos (2D)) can also reflect the degree of charge doping of graphene.[152, 153] As presented in Figure 1.18a, the electron or hole doping was manipulated by top-gated graphene transistor followed monitoring by Raman spectroscopy.[154] With the increasing of electron or hole concentrations, pos (G) shows the tendency of upshift.[149] In contrast, electron doping makes upshift of pos (2D) while downshift for hole doping. *Lee et al.* estimated the relation between charge doping and pos (G), pos (2D) since the positions are affected by degree of charge doping.[155] As shown in Figure 1.18b, the charge doping is separated from strain and estimated by the correlation between pos (G) and pos (2D). Thus, we can judge the charge doping degree of graphene by the pos (G) and pos (2D), which has been employed in functionalized graphene.[156, 157]

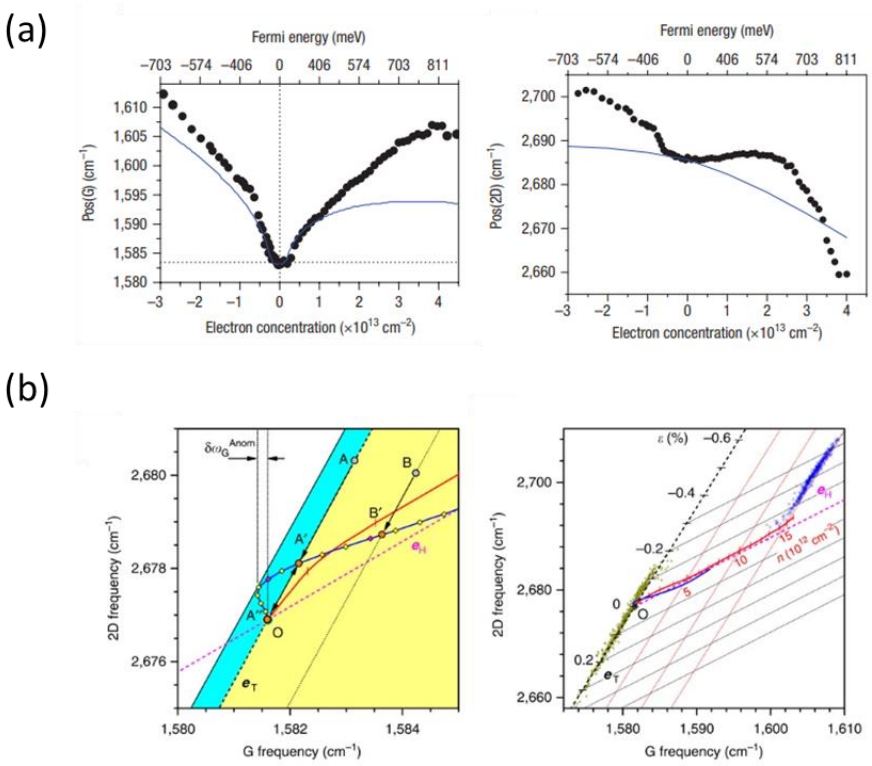

Figure 1.18 (a) The effect of electron or hole doping on position of G and 2D [adapted from[154]]; (b) estimating the charge doping from the correlation between position of G and 2D. [adapted from[155]]

1.2.3 Graphene enhanced Raman scattering (GERS)

Combination with graphene and Raman microscopy can detect a low quantity of organic molecules. Graphene as substrate absorbs the fluorescent dye molecules and enhances its Raman signal, called graphene-enhanced Raman Scattering (GERS).[158-161] The strong luminescence from dye molecules makes it be challenging to obtain the Raman signal due to much larger cross-sections of fluorescence signals than Raman signals.[162-164] Interestingly, in the GERS system, graphene can effectively quench the photo-generated luminescence of dye and eliminate the most fluorescence background, thanks to its large conductive surface area and superior molecule adsorption ability.[165, 166] Unlike conventional surface-enhanced Raman scattering (SERS), GERS demonstrates a clean and robust Raman signal response.[161] Currently, two types of graphene have been studied in the GERS application: pristine graphene and doped/functionalized graphene, respectively.

(1) Pristine graphene for GERS

As shown in Figure 1.19, pristine graphene as a substrate absorbs the Rh6G dye molecules.[167] When applying the incident laser on the Rh6G adsorbed graphene, the Raman peaks of the Rh6G can be observed, but no peak can be detected in the solution (Figure 1.13b). Since graphene's unique properties: smooth surface, high optical transmission in the visible range (97.7% for single layer graphene), and surface plasmon in the terahertz range, the mechanism of GERS is not due to electromagnetic mechanism.[168, 169] The Raman enhancement phenomenon in graphene can be attributed to charge transfer between graphene and detected molecules, which is the chemical mechanism.[170, 171]

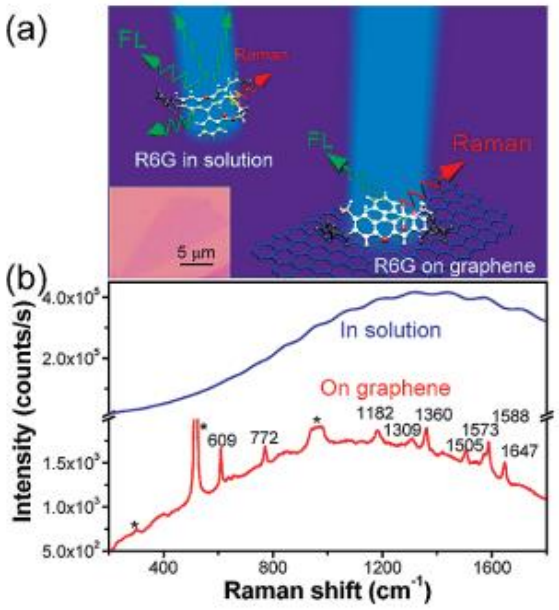

Figure 1.19 graphene enhanced Raman scattering (GERS) on pristine graphene. [adapted from[167]]

A deep investigation into the mechanism of GERS has been studied involving several parameters. For instance, molecular structure and energy level affecting the GERS effect (molecular selectivity) has been reported.[159] They found that GERS enhancement requires strong graphene-molecule coupling and thus induces effective charge transfer between the molecules and graphene. In addition, *Ling et al.* researched the "first layer effect" on GERS.[170] The distance between graphene and probed molecules strongly affects the GERS effect. Less distance shows higher Raman intensity on molecules, demonstrating that the GERS belongs to a chemical enhanced mechanism.

(2) Doped/functionalized graphene for GERS

Although the mechanism of GERS has been investigated in pristine graphene, the enhancement factor (EF) of GERS is only ~10^1-10^2, which is much lower than surface-enhanced Raman scattering (SERS). To achieve high GERS EF and give a clear understanding on GERS mechanism, modifying on graphene has been researched. For example, the charge-doped graphene modulated by the field effect transistor presents stronger Raman scattering intensities

of the probed molecule than pristine graphene. Here, the enhanced Raman signal at the charge modified graphene is attributed to the adjusted Fermi level of graphene can be appropriate to the highest occupied molecular orbital (HOMU) or lowest unoccupied molecular orbital (LUMO) of the molecule.[172] Furthermore, *Feng et al.* reported that the nitrogen-doped graphene was synthesized for investigating the GERS effect, which demonstrates quite better GERS EF than pristine one (Figure 1.20b).[173] In this study, DFT calculations explain the enhanced performance is due to the shifted Fermi level getting close to the LUMO of the probed molecule, promoting the charge transfer between graphene and dyes. Moreover, 4-nitrophenyl covalently grafted graphene is prepared for GERS study, which presents twice enhancement than pristine graphene.[174] These modified graphene confirm that the GERS effect is strongly dependent with Fermi level of graphene and vibrational energy of the probed molecules.

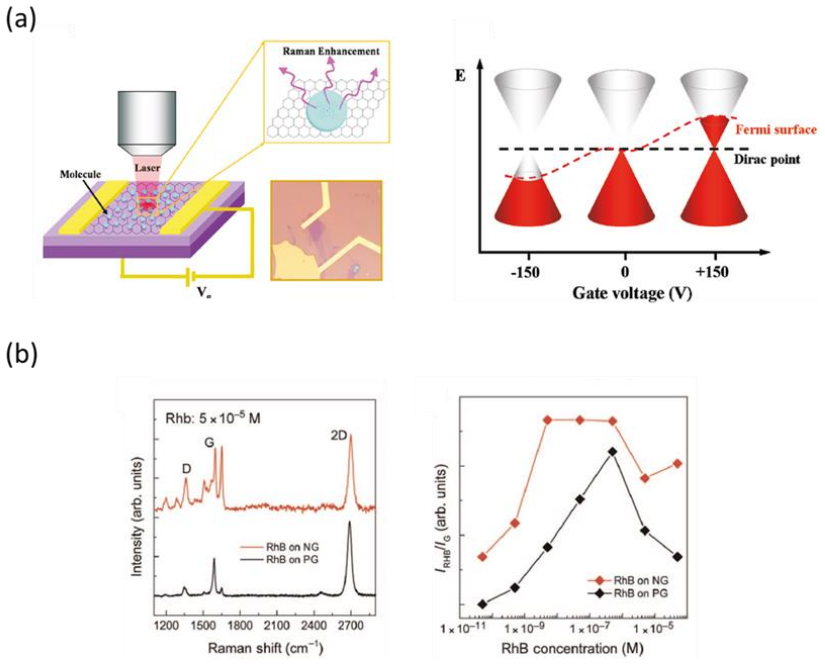

Figure 1.20 (a) Charge-doped graphene modulated by the field effect transistor for GERS and modulated Fermi level [adapted from[172]]; (b) Nitrogen-doped graphene for Raman enhancement on Rhodamine (RhB) and effect of concentration. Nitrogen-doped graphene (NG, red color); pristine graphene (PG, black color). [adapted from[173]]

1.3 Introduction to covalent chemical modification of graphene

Covalent chemical modification can introduce defects to graphene by forming the covalent bond. By this method, the charge distribution of graphene is modulated. Among the covalent modification methods, diazonium induced covalent modification is most studied because of high efficiency and controllable. Recent years, photo-induced chemical modification has been attracted the scientists' interest due to its designable, easy handling, and site-specifical control, which is beneficial for nano-modification of graphene.

1.3.1 Diazonium induced covalent modification of graphene

Diazonium compounds can contribute to covalent chemical modification of graphene. Generated radicals from the diazonium compound are efficiently stabilized on the surface of graphene.[175, 176] *Rodríguez González et al.* studied the covalent modification of graphite using several aryldiazonium salts.[177] X-ray photoelectron spectroscopy, Raman, and scanning tunnel microscope results demonstrated the successful modification was introduced to graphene. Radicals' reaction was concluded for the diazonium modification. Moreover, electrochemical method was used in the covalent functionalization of graphene combining with diazonium compounds (Figure 1.21).[178] Large-scale and highly efficient functionalization on graphene was achieved. The efficient functionalization is attributed to N-type graphene promoting the electron transfer from graphene to diazonium cations, resulting in reactive aryl radicals and reacting with the graphene surface.

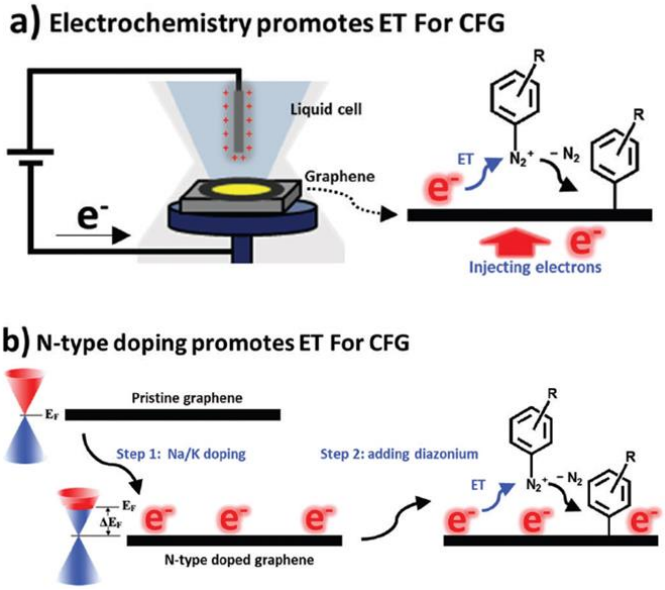

Figure 1.21 Electrochemical covalent modification on graphene [adapted from[178]]

1.3.2 Photo-induced covalent modification (PICM) of graphene

Photo-induced covalent modification (PICM) of graphene is a potential strategy to covalently modify graphene, which is easy handling and can site-specifically control the modification. The first report on the PICM of graphene can trace back to 2009. Liu *et al.* found that a Raman peak related to graphene defects (D-band) appeared only at the laser focused point in presence of benzoyl peroxide (Figure 1.16).[179] The electrical property of graphene was estimated by graphene FETs device, showing the reaction area of graphene increases the hole-doping level. This founding provides a novel way to site-specifically modify graphene, thus tailoring its chemical and electronic properties. Recent years, *Hirsch's* group presented a strategy to functionalize graphene covered with dibenzoyl peroxide (DBPO) solid film by laser-direct writing with 532 nm and reading with 633 nm, followed by de-functionalization by simple thermal annealing.[180] The sp^3 carbon defects can be locally introduced into graphene since this reaction is initiated by focused laser-irradiation.

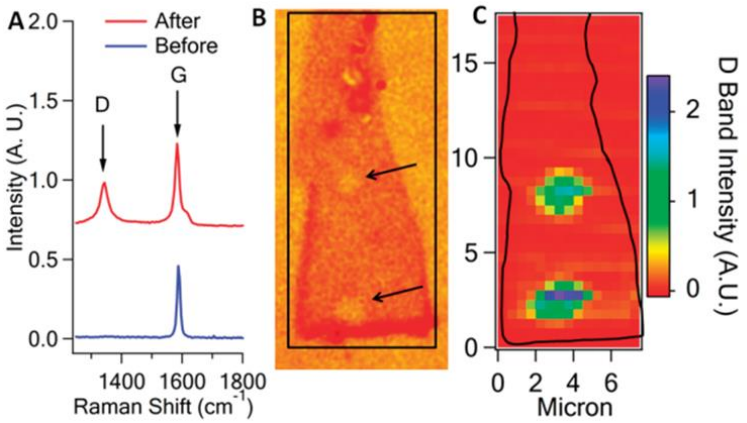

Figure 1.22 Photo-induced chemical reaction on single graphene absorbing with benzoyl peroxide [adapted from[179]]

Furthermore, our group reported the photo-oxidation of graphene in pure water, which can introduce the chemical defects in graphene at the liquid-phase (Figure 1.17).[181] Applying this PICM method can stabilize the oxygen species on the graphene surface. In addition, we demonstrated that the stabilized defects can be removed by the same laser with high density of

power or direct heating at high temperature. The reversible process of graphene indicates that such PICM method induced chemical defects, which can reversibly tailor the electronical property of graphene.

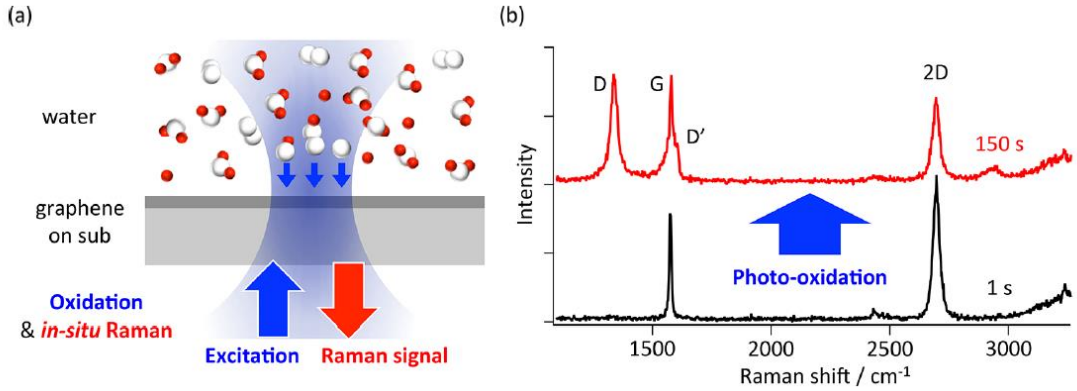

Figure 1.23 Photo-induced oxidation of pristine graphene [adapted from[181]]

1.4 Problem statement and research objectives

1.4.1 Problem statement

Although great efforts have been made to contribute to bandgap engineering of graphene, methods for precise patterning of nanostructures to achieve desirable electronic characteristics or reversible modulation of electronic property are still challenging. To response, covalent modification of graphene has been employed to overcome these issues. However, the current method has a relatively complex prepared process, is hard to control, low reaction efficiency or needs complicated organic molecules. In this context, photo-induced covalent modification (PICM) of graphene is an attractive method, which can easily introduce sp^3-hybridized carbon without any mask and modulate the charge distribution of graphene at a desired position. Currently, the PICM of graphene has been studied by using complex organic molecules at the solid-phase. The complex organic molecule, for example, 1-fluoro-3,3-dimethylbenziodoxole, is required for the PICM reaction. Although the high PICM efficiency can be found, the reaction mechanism is still mysterious because complex molecules' structures are used and graphene itself is not easy to be characterized after the modification. Moreover, the covalently modified graphene is hard to keep clean since the functionalization was generated at the solid phase. Thus, it is not convenient to use the modified graphene as a material in multi-purpose applications (FETs, sensors, catalysis etc.). Therefore, development towards the liquid-phase PICM method and investigations on reaction mechanisms is highly demanded. Furthermore, the studies on electronic property of chemically modified graphene are limited because of hard to prepare such materials. Thus, inspection of the electronic structure of liquid-phase PICM graphene is valuable to extend the further applications.

1.4.2 Research objectives

This thesis contains two objectives: (1) development of a facile and efficient liquid-phase PICM of graphene and reveal of reaction mechanism; (2) application of liquid-phase PICM functionalized graphene and investigation on the electronic property.

(1) Development of a facile and efficient liquid-phase PICM of graphene and reveal of reaction mechanism

Although PICM of graphene has been realized under the designed conditions, the efficiency of reaction and mechanism of PICM remain challenges for further study and application. Our group reported that the PICM in pure water is a promising strategy to induce sp^3-type defects on graphene at the liquid-phase. However, the PICM efficiency is not satisfied. It often takes several minutes to reach high-degree modification, which is hard to generate a scale-up chemical modification of graphene. In addition to this, the reaction mechanism is an opening question. In response, we aimed to develop a facile and efficient PICM of graphene at the liquid-phase. The systematic research on short-chain fatty acids uncovers the reaction mechanism.

(2) Application of liquid-phase PICM functionalized graphene and investigation on the electronic property

After establishing the efficient PICM method and understanding the reaction mechanism, we aim to extend application of the photo-induced covalently modified graphene (PICM-G) and investigate the electronic property. To realize it, the PICM-G was selected as a substrate to detect a low quantity of fluorescent molecules, thanks to that graphene as substrate can quench the photoluminescence and obtain the Raman signal of dyes, namely the graphene-enhanced Raman scattering (GERS). As mentioned in the chapter 1.2.3, the GERS mechanism has been demonstrated as charge transfer, which is strongly associated with the Fermi level of graphene, as well as the energy level of the probed molecule. In this study, we compared the pristine graphene (PG) and photo-induced covalently modified graphene (PICM-G) as substrates

regarding the GERS intensity of dye molecules. The distinct GERS effect at PG and PICM-G region

The different GERS effects could reflect the modulated electronic structure of PICM functionalized graphene. Finally, we concluded the relation between charge doping degree and GERS intensity.

1.5 References

1. Allen, M. J.; Tung, V. C.; Kaner, R. B., Honeycomb Carbon: A Review of Graphene. *Chem. Rev.* **2010**, 110, 132−145.

2. Wang, G.; Yang, J.; Park, J.; Gou, X.; Wang, B.; Liu, H.; Yao, J., Facile Synthesis and Characterization of Graphene Nanosheets. *J. Phys. Chem. C* **2008**, 112, 8192−8195.

3. Novoselov, K. S.; Geim, A. K.; Morozov, S. V.; Jiang, D.; Zhang, Y.; Dubonos, S. V.; Grigorieva, I. V.; Firsov, A. A., Electric Field Effect in Atomically Thin Carbon Films. *Science* **2004**, 306, 666−669.

4. Katsnelson, M. I., Graphene: Carbon in Two Dimensions. *Mater. Today* **2007**, 10, 20−27.

5. Li, X.; Zhang, G.; Bai, X.; Sun, X.; Wang, X.; Wang, E.; Dai, H., Highly conducting graphene sheets and Langmuir-Blodgett films. *Nat. Nanotechnol.* **2008**, 3 (9), 538-42.

6. Chen, L.; Hernandez, Y.; Feng, X.; Mullen, K., From nanographene and graphene nanoribbons to graphene sheets: chemical synthesis. *Angew. Chem. Int. Ed. Engl.* **2012**, 51 (31), 7640-54.

7. Yi, M.; Shen, Z. A Review on Mechanical Exfoliation for the Scalable Production of Graphene. *J. Mater. Chem. A* **2015**, 3, 11700−11715.

8. Roberts, M. W.; Clemons, C. B.; Wilber, J. P.; Young, G. W.; Buldum, A.; Quinn, D. D., Continuum Plate Theory and Atomistic Modeling to Find the Flexural Rigidity of a Graphene Sheet Interacting with a Substrate. *J. Nanotechnol.* **2010**, 868492.

9. Huang, X.; Qi, X.; Boey, F.; Zhang, H., Graphene-based composites. *Chem. Soc. Rev.* **2012**, 41 (2), 666-86.

10. Ghany, N. A. A.; Elsherif, S. A.; Handal, H. T., Revolution of Graphene for different applications: State-of-the-art. *Surf. Interfaces* **2017**, 9, 93-106.

11. Castro Neto, A. H.; Guinea, F.; Peres, N. M. R.; Novoselov, K. S.; Geim, A. K., The Electronic Properties of Graphene. *Rev. Mod. Phys.* **2009**, 81, 109−162.

12. Abergel, D. S. L.; Apalkov, V.; Berashevich, J.; Ziegler, K.; Chakraborty, T., Properties of Graphene: A Theoretical Perspective. *Adv. Phys.* **2010**, 59, 261−482.

13. Mehmood, A.; Mubarak, N. M.; Khalid, M.; Walvekar, R.; Abdullah, E. C.; Siddiqui, M. T. H.; Baloch, H. A.; Nizamuddin, S.; Mazari, S. Graphene Based Nanomaterials for Strain Sensor Application—a Review. *J. Environ. Chem. Eng.* **2020**, 8, 103743.

14. Zhang, J.; Zhao, C.; Liu, N.; Zhang, H.; Liu, J.; Fu, Y. Q.; Guo, B.; Wang, Z.; Lei, S.; Hu, P., Tunable electronic properties of graphene through controlling bonding configurations of doped nitrogen atoms. *Sci. Rep.* **2016**, 6, 28330.

15. Wang, J.; Ma, F.; Liang, W.; Sun, M., Electrical properties and applications of graphene, hexagonal boron nitride (h-BN), and graphene/h-BN heterostructures. *Mater. Today Phys.* **2017**, 2, 6-34.

16. Wu, X.; Chuang, Y.; Contino, A.; Soree, B.; Brems, S.; Tokei, Z.; Heyns, M.; Huyghebaert, C.; Asselberghs, I., Boosting Carrier Mobility of Synthetic Few Layer Graphene on SiO_2 by Interlayer Rotation and Decoupling. *Adv. Mater. Interfaces* **2018**, 5 (14), 1800454

17. Ci, H.; Chen, J.; Ma, H.; Sun, X.; Jiang, X.; Liu, K.; Shan, J.; Lian, X.; Jiang, B.; Liu, R.; Liu, B.; Yang, G.; Yin, W.; Zhao, W.; Huang, L.; Gao, T.; Sun, J.; Liu, Z., Transfer-Free Quasi-Suspended Graphene Grown on a Si Wafer. *Adv. Mater.* **2022**, 34 (51), e2206389.

18. Ando, T. The Electronic Properties of Graphene and Carbon Nanotubes. *NPG Asia Mater.* **2009**, 1, 17−21.

19. Jang, M. S.; Kim, H.; Son, Y. W.; Atwater, H. A.; Goddard, W. A., Graphene field effect transistor without an energy gap. *Proc. Natl. Acad. Sci. U. S. A.* **2013**, 110, 8786-8789.

20. Gosling, J. H.; Makarovsky, O.; Wang, F.; Cottam, N. D.; Greenaway, M. T.; Patanè, A.; Wildman, R. D.; Tuck, C. J.; Turyanska, L.; Fromhold, T. M. Universal mobility characteristics of graphene originating from charge scattering by ionised impurities. *Commun. Phys.* **2021**, 4 (1), 1−8.

21. Massicotte, M.; Soavi, G.; Principi, A.; Tielrooij, K. J., Hot carriers in graphene-fundamentals and applications. *Nanoscale* **2021**, 13, 8376−8411.

22. Ma, L. P.; Wu, Z.; Yin, L.; Zhang, D.; Dong, S.; Zhang, Q.; Chen, M. L.; Ma, W.; Zhang, Z.; Du, J.; Sun, D. M.; Liu, K.; Duan, X.; Ma, D.; Cheng, H. M.; Ren, W., Pushing the conductance and transparency limit of monolayer graphene electrodes for flexible organic light-emitting diodes. *Proc. Natl. Acad. Sci. U. S. A.* **2020**, 117 (42), 25991-25998.

23. Nair, R. R.; Blake, P.; Grigorenko, A. N.; Novoselov, K. S.; Booth, T. J.; Stauber, T.; Peres, N. M.; Geim, A. K., Fine structure constant defines visual transparency of graphene. *Science* **2008**, 320 (5881), 1308.

24. Nair, R. R.; Ren, W. C.; Jalil, R.; Riaz, I.; Kravets, V. G.; Britnell, L.; Blake, P.; Schedin, F.; Mayorov, A. S.; Yuan, S. J.; Katsnelson, M. I.; Cheng, H. M.; Strupinski, W.; Bulusheva, L. G.; Okotrub, A. V.; Grigorieva, I. V.; Grigorenko, A. N.; Novoselov, K. S.; Geim, Fluorographene: A Two-Dimensional Counterpart of Teflon. *Small* **2010**, 6, 2877–2884.

25. Feng, W.; Long, P.; Feng, Y.; Li, Y., Two-Dimensional Fluorinated Graphene: Synthesis,

Structures, Properties and Applications. *Adv. Sci.* **2016**, 3 (7), 1500413.

26. Robinson, J. T.; Burgess, J. S.; Junkermeier, C. E.; Badescu, S. C.; Reinecke, T. L.; Perkins, F. K.; Zalalutdniov, M. K.; Baldwin, J. W.; Culbertson, J. C.; Sheehan, P. E.; Snow, E. S., Properties of fluorinated graphene films. *Nano Lett.* **2010**, 10 (8), 3001-3005.

27. Pop, E.; Varshney, V.; Roy, A. K., Thermal properties of graphene: Fundamentals and applications. *MRS Bull.* **2012**, 37, 1273−1281.

28. Nika, D. L.; Askerov, A. S.; Balandin, A. A., Anomalous size dependence of the thermal conductivity of graphene ribbons. *Nano Lett.* **2012**, 12 (6), 3238-44.

29. Nika, D. L.; Ghosh, S.; Pokatilov, E. P.; Balandin, A. A., Lattice Thermal Conductivity of Graphene Flakes: Comparison with Bulk Graphite. *Appl. Phys. Lett.* **2009**, 94 (20), 203103.

30. Seol, J. H.; Jo, I.; Moore, A. L.; Lindsay, L.; Aitken, Z. H.; Pettes, M. T.; Li, X.; Yao, Z.; Huang, R.; Broido, D.; et al. Two-Dimensional Phonon Transport in Supported Graphene. *Science* **2010**, 328 (5975), 213−216.

31. Jang, W.; Chen, Z.; Bao, W.; Lau, C. N.; Dames, C., Thickness-dependent thermal conductivity of encased graphene and ultrathin graphite. *Nano Lett.* **2010**, 10 (10), 3909-13.

32. Fu, Y.; Hansson, J.; Liu, Y.; Chen, S.; Zehri, A.; Samani, M. K.;Wang, N.; Ni, Y.; Zhang, Y.; Zhang, Z.-B.; Wang, Q.; Li, M.; Lu, H.; Sledzinska, M.; Torres, C. M. S.; Volz, S.; Balandin, A. A.; Xu, X.; Liu, J. Graphene Related Materials for Thermal Management. *2D Mater.* **2020**, 7, 012001.

33. Kim, H. G.; Kihm, K. D.; Lee, W.; Lim, G.; Cheon, S.; Lee, W.; Pyun, K. R.; Ko, S. H.; Shin, S., Effect of graphene-substrate conformity on the in-plane thermal conductivity of

supported graphene. *Carbon* **2017**, 125, 39-48.

34. Castellanos-Gomez, A.; Poot, M.; Amor-Amorós, A.; Steele, G. A.; van der Zant, H. S. J.; Agraït, N.; Rubio-Bollinger, G., Mechanical properties of freely suspended atomically thin dielectric layers of mica. *Nano Res.* **2012**, 5 (8), 550-557.

35. Papageorgiou, D. G.; Kinloch, I. A.; Young, R. J., Mechanical properties of graphene and graphene-based nanocomposites. *Prog. Mater. Sci.* **2017**, 90, 75-127.

36. San-Jose, P.; Gutierrez-Rubio, A.; Sturla, M.; Guinea, F. Electronic structure of spontaneously strained graphene on hexagonal boron nitride. *Phys. Rev. B* **2014**, 90, 115152

37. Akinwande, D.; Brennan, C. J.; Bunch, J. S.; Egberts, P.; Felts, J. R.; Gao, H.; Huang, R.; Kim, J.-S.; Li, T.; Li, Y.; Liechti, K. M.; Lu, N.; Park, H. S.; Reed, E. J.; Wang, P.; Yakobson, B. I.; Zhang, T.; Zhang, Y.-W.; Zhou, Y.; Zhu, Y., A review on mechanics and mechanical properties of 2D materials—Graphene and beyond. *Extreme Mech. Lett.* **2017**, 13, 42-77.

38. Monteverde, U.; Pal, J.; Migliorato, M. A.; Missous, M.; Bangert, U.; Zan, R.; Kashtiban, R.; Powell, D., Under pressure: Control of strain, phonons and bandgap opening in rippled graphene. *Carbon* **2015**, 91, 266-274.

39. Zhan, D.; Yan, J.; Lai, L.; Ni, Z.; Liu, L.; Shen, Z., Engineering the electronic structure of graphene. *Adv. Mater.* **2012**, 24 (30), 4055-69.

40. Balandin, A. A.; Ghosh, S.; Bao, W.; Calizo, I.; Teweldebrhan, D.; Miao, F.; Lau, C. N. Superior Thermal Conductivity of Single Layer Graphene. *Nano Lett.* **2008**, 8, 902−907.

41. Viculis, L. M.; Mack, J. J.; Kaner, R. B., A chemical route to carbon nanoscrolls. *Science*

2003, 299 (5611), 1361.

42. Guo, H.-L.; Wang, X.-F.; Qian, Q.-Y.; Wang, F.-B.; Xia, X.-H., A Green Approach to the Synthesis of Graphene Nanosheets. *ACS Nano* **2009**, 3, 2653−2659.

43. Kumar, R.; Sahoo, S.; Joanni, E.; Singh, R. K.; Yadav, R. M.; Verma, R. K.; Singh, D. P.; Tan, W. K.; Pérez del Pino, A.; Moshkalev, S. A.; Matsuda, A., A review on synthesis of graphene, h-BN and MoS_2 for energy storage applications: Recent progress and perspectives. *Nano Res.* **2019**, 12 (11), 2655-2694.

44. Li, X.; Colombo, L.; Ruoff, R. S., Synthesis of Graphene Films on Copper Foils by Chemical Vapor Deposition. *Adv. Mater.* **2016**, 28 (29), 6247-6252.

45. Bhuyan, M. S. A.; Uddin, M. N.; Islam, M. M.; Bipasha, F. A.; Hossain, S. S., Synthesis of graphene. *Int. Nano Lett.* **2016**, 6 (2), 65-83.

46. Edwards, R. S.; Coleman, K. S., Graphene synthesis: relationship to applications. *Nanoscale* **2013**, 5 (1), 38-51.

47. Pang, Y. X.; Yew, M.; Yan, Y.; Khine, P.; Filbert, A.; Manickam, S.; Foo, D. C. Y.; Sharmin, N.; Lester, E.; Wu, T.; Pang, C. H., Application of supercritical fluid in the synthesis of graphene materials: a review. *J. Nanopart. Res.* **2021**, 23, 204.

48. Wu, Y. H.; Yu, T.; Shen, Z. X. Two-Dimensional Carbon Nanostructures: Fundamental Properties, Synthesis, Characterization, and Potential Applications. *J. Appl. Phys.* **2010**, 108(7), 071301.

49. Tkachev, S. V.; Buslaeva, E. Y.; Gubin, S. P., Graphene: A novel carbon nanomaterial. *Inorg. Mater.* **2010**, 47 (1), 1-10.

50. Park, S.; Ruoff, R. S., Chemical methods for the production of graphenes. *Nat. Nanotechnol.* **2009**, 4 (4), 217-24.

51. Hummers, W.; Offeman, R., Preparation of Graphitic Oxide. *J.Am. Chem. Soc.* **1958**, 80, 1339−1339.

52. Shin, H. J.; Kim, K. K.; Benayad, A.; Yoon, S. M.; Park, H. K.; Jung, I. S.; Jin, M. H.; Jeong, H. K.; Kim, J. M.; Choi, J. Y.; Lee, Y. H., Efficient Reduction of Graphite Oxide by Sodium Borohydride and Its Effect on Electrical Conductance. *Adv. Funct. Mater.* **2009**, 19 (12), 1987-1992.

53. Pham, V. H.; Cuong, T. V.; Nguyen-Phan, T. D.; Pham, H. D.; Kim, E. J.; Hur, S. H.; Shin, E. W.; Kim, S.; Chung, J. S., One-step synthesis of superior dispersion of chemically converted graphene in organic solvents. *Chem. Commun.* **2010**, 46 (24), 4375-7.

54. Zhu, C.; Guo, S.; Fang, Y.; Dong, S. Reducing Sugar: New Functional Molecules for the Green Synthesis of Graphene Nanosheets. *ACS Nano* **2010**, 4, 2429−2437.

55. Zhang, J.; Yang, H.; Shen, G.; Cheng, P.; Zhang, J.; Guo, S., Reduction of graphene oxide via L-ascorbic acid. *Chem. Commun.* **2010**, 46 (7), 1112-1114.

56. Sundaram, R. S.; Gómez-Navarro, C.; Balasubramanian, K.; Burghard, M.; Kern, K., Electrochemical Modification of Graphene. *Adv. Mater.* **2008**, 20 (16), 3050-3053.

57. Compton, O. C.; Jain, B.; Dikin, D. A.; Abouimrane, A.; Amine, K.; Nguyen, S. T., Chemically Active Reduced Graphene Oxide with Tunable C/O Ratios. *ACS Nano* **2011**, 5, 4380−4391.

58. Marcano, D. C.; Kosynkin, D. V.; Berlin, J. M.; Sinitskii, A.; Sun, Z.; Slesarev, A.;

Alemany, L. B.; Lu, W.; Tour, J. M. Improved synthesis of graphene oxide. *ACS Nano* **2010**, 4 (8), 4806−4814.

59. Choucair, M.; Thordarson, P.; Stride, J. A., Gram-scale production of graphene based on solvothermal synthesis and sonication. *Nat. Nanotechnol.* **2009**, 4 (1), 30-33.

60. Prekodravac, J. R.; Kepić, D. P.; Colmenares, J. C.; Giannakoudakis, D. A.; Jovanović, S. P., A comprehensive review on selected graphene synthesis methods: from electrochemical exfoliation through rapid thermal annealing towards biomass pyrolysis. *J. Mater. Chem. C* **2021**, 9 (21), 6722-6748.

61. Ruan, G.; Sun, Z.; Peng, Z.; Tour, J. M., Growth of Graphene from Food, Insects, and Waste. *ACS Nano* **2011**, 5 (9), 7601−7607

62. Muñoz, R.; Gómez-Aleixandre, C., Review of CVD Synthesis of Graphene. *Chem. Vap. Deposition* **2013**, 19 (10-11-12), 297-322.

63. Zhang, Y.; Zhang, L.; Zhou, C. Review of Chemical Vapor Deposition of Graphene and Related Applications. *Acc. Chem. Res.* **2013**, 46, 2329−2339.

64. Kim, K. S.; Zhao, Y.; Jang, H.; Lee, S. Y.; Kim, J. M.; Kim, K. S.; Ahn, J. H.; Kim, P.; Choi, J. Y.; Hong, B. H., Large-scale pattern growth of graphene films for stretchable transparent electrodes. *Nature* **2009**, 457 (7230), 706-710.

65. Sutter, P. W.; Flege, J. I.; Sutter, E. A., Epitaxial graphene on ruthenium. *Nat. Mater.* **2008**, 7 (5), 406-411.

66. Reina, A.; Jia, X.; Ho, J.; Nezich, D.; Son, H.; Bulovic, V.; Dresselhaus, M. S.; Kong, J. Large area, few-layer graphene films on arbitrary substrates by chemical vapor deposition.

Nano Lett. **2009**, 9 (1), 30−35.

67. Chen, B.; Huang, H.; Ma, X.; Huang, L.; Zhang, Z.; Peng, L. M., How good can CVD-grown monolayer graphene be? *Nanoscale* **2014**, 6 (24), 15255-15261.

68. Al-Hilfi, S. H.; Derby, B.; Martin, P. A.; Whitehead, J. C., Chemical vapour deposition of graphene on copper-nickel alloys: the simulation of a thermodynamic and kinetic approach. *Nanoscale* **2020**, 12 (28), 15283-15294.

69. Deokar, G.; Avila, J.; Razado-Colambo, I.; Codron, J. L.; Boyaval, C.; Galopin, E.; Asensio, M. C.; Vignaud, D., Towards high quality CVD graphene growth and transfer. *Carbon* **2015**, 89, 82-92.

70. Deokar, G.; Jin, J.; Schwingenschlögl, U.; Costa, P. M. F. J., Chemical vapor deposition-grown nitrogen-doped graphene's synthesis, characterization and applications. *NPJ 2D Mater. Appl.* **2022**, 6 (1), 17.

71. Goniszewski, S.; Gallop, J.; Adabi, M.; Gajewski, K.; Shaforost, O.; Klein, N.; Sierakowski, A.; Chen, J.; Chen, Y.; Gotszalk, T.; Hao, L., Self-supporting graphene films and their applications. *IET Circuits, Devices & Syst.* **2015**, 9 (6), 420-427.

72. Pumera, M., Graphene-based nanomaterials for energy storage. *Energy Environ. Sci.* **2011**, 4 (3), 668-674.

73. Raccichini, R.; Varzi, A.; Passerini, S.; Scrosati, B., The role of graphene for electrochemical energy storage. *Nat. Mater.* **2015**, 14 (3), 271-279.

74. El-Kady, M. F.; Shao, Y.; Kaner, R. B., Graphene for batteries, supercapacitors and beyond. *Nat. Rev. Mater.* **2016**, 1 (7), 16033.

75. Madurani, K. A.; Suprapto, S.; Machrita, N. I.; Bahar, S. L.; Illiya, W.; Kurniawan, F., Progress in Graphene Synthesis and its Application: History, Challenge and the Future Outlook for Research and Industry. *ECS J. Solid State Sci. Technol.* **2020**, 9 (9), 093013.

76. Bitounis, D.; Ali-Boucetta, H.; Hong, B. H.; Min, D. H.; Kostarelos, K., Prospects and challenges of graphene in biomedical applications. *Adv. Mater.* **2013**, 25 (16), 2258-68.

77. He, Q. Y.; Wu, S. X.; Yin, Z. Y.; Zhang, H. Graphene-Based Electronic Sensors. *Chem. Sci.* **2012**, 3(6), 1764−1772.

78. Morales-Narváez, E.; Baptista-Pires, L.; Zamora-Gálvez, A.; Merkoci, A. Graphene-Based Biosensors: Going Simple. *Adv. Mater.* **2017**, 29 (7), 1604905.

79. Biswas, C.; Lee, Y. H., Graphene Versus Carbon Nanotubes in Electronic Devices. *Adv. Funct. Mater.* **2011**, 21 (20), 3806-3826.

80. Avouris, P., Graphene: electronic and photonic properties and devices. *Nano Lett.* **2010**, 10 (11), 4285-94.

81. Yin, Z.; Zhu, J.; He, Q.; Cao, X.; Tan, C.; Chen, H.; Yan, Q.; Zhang, H., Graphene-Based Materials for Solar Cell Applications. *Adv. Energy Mater.* **2014**, 4 (1), 1300574.

82. Yoo, E.; Zhou, H. Li-Air Rechargeable Battery Based on Metal-Free Graphene Nanosheet Catalysts. *ACS Nano* **2011**, 5, 3020−3026.

83. Velasco, A.; Ryu, Y. K.; Boscá, A.; Ladrón-De-Guevara, A.; Hunt, E.; Zuo, J.; Pedrós, J.; Calle, F.; Martinez, J. Recent Trends in Graphene Supercapacitors: From Large Area to Microsupercapacitors. *Sustain. Energy Fuels* **2021**, 5 (5), 1235−1254.

84. Li, G.; Law, W.-C.; Chan, K. C., Floating, highly efficient, and scalable graphene membranes for seawater desalination using solar energy. *Green Chem.* **2018**, 20 (16), 3689-3695.

85. Weiss, N. O.; Zhou, H.; Liao, L.; Liu, Y.; Jiang, S.; Huang, Y.; Duan, X., Graphene: an emerging electronic material. *Adv. Mater.* **2012**, 24 (43), 5782-825.

86. Basu, J.; Basu, J. K.; Bhattacharyya, T. K. The evolution of graphene-based electronic devices. *Int. J. Smart Nano Mater.* **2010**, 1(3), 201−223.

87. Yang, J.; Hu, P.; Yu, G., Perspective of graphene-based electronic devices: Graphene synthesis and diverse applications. *APL Mater.* **2019**, 7 (2), 020901.

88. You, R.; Liu, Y. Q.; Hao, Y. L.; Han, D. D.; Zhang, Y. L.; You, Z., Laser Fabrication of Graphene-Based Flexible Electronics. *Adv. Mater.* **2020**, 32 (15), e1901981.

89. Reddy, D.; Register, L. F.; Carpenter, G. D.; Banerjee, S. K., Graphene field-effect transistors. *J. Phys. D: Appl. Phys.* **2011**, 45 (1), 019501.

90. Zhan, B.; Li, C.; Yang, J.; Jenkins, G.; Huang, W.; Dong, X., Graphene field-effect transistor and its application for electronic sensing. *Small* **2014**, 10 (20), 4042-4065.

91. Mueller, T.; Xia, F.; Avouris, P., Graphene photodetectors for high-speed optical communications. *Nat. Photonics* **2010**, 4 (5), 297-301.

92. Ma, Y.; Zhi, L., Graphene-Based Transparent Conductive Films: Material Systems, Preparation and Applications. *Small Methods* **2019**, 3 (1), 1800199.

93. Sun, Y.; Sun, M.; Xie, D., Graphene Electronic Devices. *Graphene*, **2018**; pp 103-155.

94. Geim, A. K.; Novoselov, K. S., The Rise of Graphene. *Nat. Mater.* **2007**, 6, 183−191.

95. Novoselov, K. S.; Geim, A. K.; Morozov, S. V.; Jiang, D.; Katsnelson, M. I.; Grigorieva, I. V.; Dubonos, S. V.; Firsov, A. A., Two-dimensional gas of massless Dirac fermions in graphene. *Nature* **2005**, 438 (7065), 197-200.

96. Xu, H. L.; Zhang, Z. Y.; Xu, H. T.; Wang, Z. X.; Wang, S.; Peng, L. M., Top-Gated Graphene Field-Effect Transistors with High Normalized Transconductance and Designable Dirac Point Voltage. *ACS Nano* **2011**, 5, 5031−5037.

97. Novoselov, K. S.; Geim, A. K.; Morozov, S. V.; Jiang, D.; Zhang, Y.; Dubonos, S. V.; Grigorieva, I. V.; Firsov, A. A. Electric Field Effect in Atomically Thin Carbon Films. *Science* **2004**, 306, 666−669.

98. Kim, S.; Nah, J.; Jo, I.; Shahrjerdi, D.; Colombo, L.; Yao, Z.; Tutuc, E.; Banerjee, S. K., Realization of a high mobility dual-gated graphene field-effect transistor with Al_2O_3 dielectric. *Appl. Phys. Lett.* **2009**, 94 (6), 062107.

99. Liao, L.; Bai, J.; Qu, Y.; Huang, Y.; Duan, X., Single-layer graphene on Al_2O_3/Si substrate: better contrast and higher performance of graphene transistors. *Nanotechnol.* **2010**, 21 (1), 015705.

100. Li, X.; Wang, X.; Zhang, L.; Lee, S.; Dai, H. Chemically Derived, Ultrasmooth Graphene Nanoribbon Semiconductors. *Science* **2008**, 319 (5867), 1229−1232.

101. Son, J.; Lee, S.; Kim, S. J.; Park, B. C.; Lee, H. K.; Kim, S.; Kim, J. H.; Hong, B. H.; Hong, J., Hydrogenated monolayer graphene with reversible and tunable wide band gap and its field-effect transistor. *Nat. Commun.* **2016**, 7, 13261.

102. Xia, F.; Farmer, D. B.; Lin, Y. M.; Avouris, P., Graphene field-effect transistors with high on/off current ratio and large transport band gap at room temperature. *Nano Lett.* **2010**, 10 (2), 715-8.

103. Kim, K. H.; Seo, S. E.; Park, C. S.; Kim, S.; Lee, S.; Ryu, C. M.; Yong, D.; Park, Y. M.; Kwon, O. S., Open-Bandgap Graphene-Based Field-Effect Transistor Using Oligo(phenylene-ethynylene) Interfacial Chemistry. *Angew. Chem. Int. Ed. Engl.* **2022**, 61 (41), e202209726.

104. Jariwala, D.; Srivastava, A.; Ajayan, P. M., Graphene synthesis and band gap opening. *J. Nanosci. Nanotechnol.* **2011**, 11 (8), 6621-6641.

105. Xu, X.; Liu, C.; Sun, Z.; Cao, T.; Zhang, Z.; Wang, E.; Liu, Z.; Liu, K., Interfacial engineering in graphene bandgap. *Chem. Soc. Rev.* **2018**, 47 (9), 3059-3099.

106. Zhou, S. Y.; Gweon, G. H.; Fedorov, A. V.; First, P. N.; de Heer, W. A.; Lee, D. H.; Guinea, F.; Castro Neto, A. H.; Lanzara, A., Substrate-induced bandgap opening in epitaxial graphene. *Nat. Mater.* **2007**, 6 (10), 770-775.

107. Li, Y.; Zhou, Z.; Shen, P.; Chen, Z. Spin Gapless Semiconductor−Metal−Half-Metal Properties in Nitrogen-Doped Zigzag Graphene Nanoribbons. *ACS Nano* **2009**, 3, 1952−1958.

108. Ci, L.; Song, L.; Jin, C.; Jariwala, D.; Wu, D.; Li, Y.; Srivastava, A.; Wang, Z. F.; Storr, K.; Balicas, L.; Liu, F.; Ajayan, P. M., Atomic layers of hybridized boron nitride and graphene domains. *Nat. Mater.* **2010**, 9 (5), 430-435.

109. Li, J.; Shenoy, V. B., Graphene quantum dots embedded in hexagonal boron nitride sheets. *Appl. Phys. Lett.* **2011**, 98 (1), 013105.

110. Wei, D.; Liu, Y.; Wang, Y.; Zhang, H.; Huang, L.; Yu, G. Synthesis of N-Doped Graphene by Chemical Vapor Deposition and Its Electrical Properties. *Nano Lett.* **2009**, 9, 1752−1758.

111. Panchakarla, L. S.; Subrahmanyam, K. S.; Saha, S. K.; Govindaraj, A.; Krishnamurthy, H. R.; Waghmare, U. V.; Rao, C. N. R., Synthesis, Structure, and Properties of Boron- and Nitrogen-Doped Graphene. *Adv. Mater.* **2009**, 21, 4726–4730.

112. Cao, X.; Shi, J.-j.; Zhang, M.; Jiang, X.-h.; Zhong, H.-x.; Huang, P.; Ding, Y.-m.; Wu, M., Band Gap Opening of Graphene by Forming Heterojunctions with the 2D Carbonitrides Nitrogenated Holey Graphene, g-C3N4, and g-CN: Electric Field Effect. *J. Phys. Chem. C* **2016**, 120 (20), 11299-11305.

113. Nourbakhsh, A.; Cantoro, M.; Vosch, T.; Pourtois, G.; Hofkens, J.; Heyns, M. M.; Sels, B. F.; De Gendt, S., Transition from Metallic to Semiconducting Behavior in Oxygen Plasma-treated Single-layer Graphene. *MRS Proceedings* **2011**, 1336.

114. Liao, L.; Peng, H.; Liu, Z., Chemistry makes graphene beyond graphene. *J. Am. Chem. Soc.* **2014**, 136 (35), 12194-12200.

115. Li, B.; Zhou, L.; Wu, D.; Peng, H.; Yan, K.; Zhou, Y.; Liu, Z. Photochemical Chlorination of Graphene. *ACS Nano* **2011**, 5, 5957−5961.

116. Smekal, A. Zur Quantentheorie der Streuung und Dispersion. *Zeitschrift fr. Physik* **1925**, 32 (1), 241−244.

117. Raman, C. V.; Krishnan, K. S. A New Type of Secondary Radiation. *Nature* **1928**, 121, 501−502.

118. Edinburgh Instruments, what is Raman Spectroscopy? *https://www.edinst.com/blog/what-is-raman-spectroscopy/*

119. Smith, E.; Dent, G., Modern Raman Spectroscopy- A Practical Approach; *John Wiley & Sons, Ltd.: England*, **2005**.

120. Hu, Z.; Wang, X.; Wang, W.; Zhang, Z.; Gao, H.; Mao, Y., Raman spectroscopy for detecting supported planar lipid bilayers composed of ganglioside-GM1/sphingomyelin/cholesterol in the presence of amyloid-beta. *Phys. Chem. Chem. Phys.* **2015**, 17 (35), 22711-22720.

121. Dodo, K.; Fujita, K.; Sodeoka, M., Raman Spectroscopy for Chemical Biology Research. *J. Am. Chem. Soc.* **2022**, 144 (43), 19651-19667.

122. Malard, L. M.; Pimenta, M. A.; Dresselhaus, G.; Dresselhaus, M. S., Raman spectroscopy in graphene. *Phys. Rep.* **2009**, 473 (5-6), 51-87.

123. Ferrari, A. C.; Meyer, J. C.; Scardaci, V.; Casiraghi, C.; Lazzeri, M.; Mauri, F.; Piscanec, S.; Jiang, D.; Novoselov, K. S.; Roth, S.; Geim, A. K., Raman spectrum of graphene and graphene layers. *Phys. Rev. Lett.* **2006**, 97 (18), 187401.

124. Ni, Z.; Wang, Y.; Yu, T.; Shen, Z., Raman spectroscopy and imaging of graphene. *Nano Res.* **2010**, 1 (4), 273-291.

125. Ferrari, A. C.; Basko, D. M., Raman spectroscopy as a versatile tool for studying the properties of graphene. *Nat. Nanotechnol.* **2013**, 8 (4), 235-246.

126. Xu, W.; Mao, N.; Zhang, J., Graphene: a platform for surface-enhanced Raman spectroscopy. *Small* **2013**, 9 (8), 1206-1224.

127. Das, A.; Chakraborty, B.; Sood, A., Raman Spectroscopy of Graphene on Different Substrates and Influence of Defects. *Bull. Mater. Sci.* **2008**, 31, 579−584.

128. Gupta, A.; Chen, G.; Joshi, P.; Tadigadapa, S.; Eklund., Raman Scattering from High-Frequency Phonons in Supported n-Graphene Layer Films. *Nano Lett.* **2006**, 6, 2667−2673.

129. Cancado, L. G.; Jorio, A.; Ferreira, E. H.; Stavale, F.; Achete, C. A.; Capaz, R. B.; Moutinho, M. V.; Lombardo, A.; Kulmala, T. S.; Ferrari, A. C., Quantifying defects in graphene via Raman spectroscopy at different excitation energies. *Nano Lett.* **2011**, 11 (8), 3190-3196.

130. Eckmann, A.; Felten, A.; Mishchenko, A.; Britnell, L.; Krupke, R.; Novoselov, K. S.; Casiraghi, C., Probing the nature of defects in graphene by Raman spectroscopy. *Nano Lett.* **2012**, 12 (8), 3925-3930.

131. Lazzeri, M.; Attaccalite, C.; Wirtz, L.; Mauri, F., Impact of the electron-electron correlation on phonon dispersion: Failure of LDA and GGA DFT functionals in graphene and graphite. *Phys. Rev. B* **2008**, 78 (8), 081406.

132. Zólyomi, V.; Koltai, J.; Kürti, J., Resonance Raman spectroscopy of graphite and graphene. *Phys. Status Solidi B* **2011**, 248 (11), 2435-2444.

133. Carozo, V.; Almeida, C. M.; Fragneaud, B.; Bedê, P. M.; Moutinho, M. V. O.; Ribeiro-Soares, J.; Andrade, N. F.; Souza Filho, A. G.; Matos, M. J. S.; Wang, B.; Terrones, M.; Capaz, R. B.; Jorio, A.; Achete, C. A.; Cançado, L. G., Resonance effects on the Raman spectra of graphene superlattices. *Phys. Rev. B* **2013**, 88 (8), 085401.

134. Frank, O.; Mohr, M.; Maultzsch, J.; Thomsen, C.; Riaz, I.; Jalil, R.; Novoselov, K. S.; Tsoukleri, G.; Parthenios, J.; Papagelis, K.; Kavan, L.; Galiotis, C. Raman 2D-Band Splitting in Graphene: Theory and Experiment. *ACS Nano* **2011**, 5, 2231−2239.

135. Rao, C. N. R.; Biswas, K.; Subrahmanyam, K. S.; Govindaraj, A., Graphene, the new nanocarbon. *J. Mater. Chem.* **2009**, 19 (17), 2457–2469.

136. Pocsik, I.; Hundhausen, M.; Koos, M.; Ley, L., Origin of the D peak in the Raman spectrum of microcrystalline graphite. *J. Non-Cryst. Solids* **1998**, 227, 1083−1086.

137. Matthews, M. J.; Pimenta, M. A.; Dresselhaus, G.; Dresselhaus, M. S.; Endo, M. Origin of Dispersive Effects of The Raman D Band in Carbon Materials. *Phys. Rev. B* **1999**, 59, R6585−R6588.

138. Gao, G.; Liu, D.; Tang, S.; Huang, C.; He, M.; Guo, Y.; Sun, X.; Gao, B., Heat-Initiated Chemical Functionalization of Graphene. *Sci. Rep.* **2016**, 6, 20034.

139. Englert, J. M.; Dotzer, C.; Yang, G.; Schmid, M.; Papp, C.; Gottfried, J. M.; Steinruck, H. P.; Spiecker, E.; Hauke, F.; Hirsch, A., Covalent bulk functionalization of graphene. *Nat. Chem.* **2011**, 3 (4), 279-286.

140. Mali, K. S.; Greenwood, J.; Adisoejoso, J.; Phillipson, R.; De Feyter, S., Nanostructuring graphene for controlled and reproducible functionalization. *Nanoscale* **2015**, 7 (5), 1566-1585.

141. Niyogi, S.; Bekyarova, E.; Itkis, M. E.; Zhang, H.; Shepperd, K.; Hicks, J.; Sprinkle, M.; Berger, C.; Lau, C. N.; deHeer, W. A.; Conrad, E. H.; Haddon, R. C., Spectroscopy of covalently functionalized graphene. *Nano Lett.* **2010**, 10 (10), 4061-4066.

142. Englert, J. M.; Vecera, P.; Knirsch, K. C.; Schäfer, R. A.; Hauke, F.; Hirsch, A. Scanning-Raman-Microscopy for the Statistical Analysis of Covalently Functionalized Graphene. *ACS Nano* **2013**, 7, 5472−5482.

143. Lucchese, M. M.; Stavale, F.; Ferreira, E. H. M.; Vilani, C.; Moutinho, M. V. O.; Capaz, R. B.; Achete, C. A.; Jorio, A., Quantifying ion-induced defects and Raman relaxation length in graphene. *Carbon* **2010**, 48 (5), 1592-1597.

144. Sampathkumar, K.; Diez-Cabanes, V.; Kovaricek, P.; del Corro, E.; Bouša, M.; Hošek, J.; Kalbac, M.; Frank, O., On the Suitability of Raman Spectroscopy to Monitor the Degree of Graphene Functionalization by Diazonium Salts. *J. Phys. Chem. C* **2019**, 123 (36), 22397-22402.

145. Hao, Y.; Wang, Y.; Wang, L.; Ni, Z.; Wang, Z.; Wang, R.; Koo, C. K.; Shen, Z.; Thong, J. T., Probing layer number and stacking order of few-layer graphene by Raman spectroscopy. *Small* **2010**, 6 (2), 195-200.

146. Das, A.; Chakraborty, B.; Sood, A. K. Raman Spectroscopy of Graphene on Different Substrates and Influence of Defects. *Bull. Mater. Sci.* **2008**, 31, 579−584.

147. Graf, D.; Molitor, F.; Ensslin, K.; Stampfer, C.; Jungen, A.; Hierold, C.; Wirtz, L., Spatially Resolved Raman Spectroscopy of Single- and Few-Layer Graphene. *Nano Lett.* **2007**, 7, 238−242.

148. Park, J. S.; Reina, A.; Saito, R.; Kong, J.; Dresselhaus, G.; Dresselhaus, M. S., G′ band Raman spectra of single, double and triple layer graphene. *Carbon* **2009**, 47 (5), 1303-1310.

149. Kumar, V.; Kumar, A.; Lee, D. J.; Park, S. S., Estimation of Number of Graphene Layers Using Different Methods: A Focused Review. *Materials* **2021**, 14 (16), 4590.

150. Papanai, G. S.; Sharma, I.; Gupta, B. K., Probing number of layers and quality assessment of mechanically exfoliated graphene via Raman fingerprint. *Mater. Today Commun.* **2020**, 22, 100795.

151. Wang, Y. Y.; Ni, Z. H.; Yu, T.; Shen, Z. X.; Wang, H. M.; Wu, Y. H.; Chen, W.; Wee, A. T. S., Raman Studies of Monolayer Graphene: The Substrate Effect. *J. Phys. Chem. C* **2008**, 112, 10637−10640.

152. Das, A.; Chakraborty, B.; Piscanec, S.; Pisana, S.; Sood, A. K.; Ferrari, A. C., Phonon renormalization in doped bilayer graphene. *Phys. Rev. B* **2009**, 79 (15), 155417.

153. Bong, J. H.; Sul, O.; Yoon, A.; Choi, S. Y.; Cho, B. J., Facile graphene n-doping by wet chemical treatment for electronic applications. *Nanoscale* **2014**, 6 (15), 8503-8508.

154. Das, A.; Pisana, S.; Chakraborty, B.; Piscanec, S.; Saha, S. K.; Waghmare, U. V.; Novoselov, K. S.; Krishnamurthy, H. R.; Geim, A. K.; Ferrari, A. C.; Sood, A. K., Monitoring dopants by Raman scattering in an electrochemically top-gated graphene transistor. *Nat. Nanotechnol.* **2008**, 3 (4), 210-215.

155. Lee, J. E.; Ahn, G.; Shim, J.; Lee, Y. S.; Ryu, S., Optical separation of mechanical strain from charge doping in graphene. *Nat. Commun.* **2012**, 3, 1024.

156. Wu, G.; Tang, X.; Meyyappan, M.; Lai, K. W. C., Doping effects of surface functionalization on graphene with aromatic molecule and organic solvents. *Appl. Surf. Sci.* **2017**, 425, 713-721.

157. Velpula, G.; Phillipson, R.; Lian, J. X.; Cornil, D.; Walke, P.; Verguts, K.; Brems, S.; Uji, I. H.; De Gendt, S.; Beljonne, D.; Lazzaroni, R.; Mali, K. S.; De Feyter, S., Graphene Meets Ionic Liquids: Fermi Level Engineering via Electrostatic Forces. *ACS Nano* **2019**, 13 (3), 3512-3521.

158. Ling, X.; Xie, L.; Fang, Y.; Xu, H.; Zhang, H.; Kong, J.; Dresselhaus, M. S.; Zhang, J.; Liu, Z., Can graphene be used as a substrate for Raman enhancement? *Nano Lett.* **2010**, 10 (2),

553-561.

159. Huang, S.; Ling, X.; Liang, L.; Song, Y.; Fang, W.; Zhang, J.; Kong, J.; Meunier, V.; Dresselhaus, M. S., Molecular selectivity of graphene-enhanced Raman scattering. *Nano Lett.* **2015**, 15 (5), 2892-2901.

160. Lai, H.; Xu, F.; Zhang, Y.; Wang, L., Recent progress on graphene-based substrates for surface-enhanced Raman scattering applications. *J. Mater. Chem. B* **2018**, 6 (24), 4008-4028.

161. Zhang, N.; Tong, L.; Zhang, J., Graphene-Based Enhanced Raman Scattering toward Analytical Applications. *Chem. Mater.* **2016**, 28 (18), 6426-6435.

162. Perez-Jimenez, A. I.; Lyu, D.; Lu, Z.; Liu, G.; Ren, B., Surface-enhanced Raman spectroscopy: benefits, trade-offs and future developments. *Chem. Sci.* **2020**, 11 (18), 4563-4577.

163. Zhao, Z.; Chen, C.; Wei, S.; Xiong, H.; Hu, F.; Miao, Y.; Jin, T.; Min, W., Ultra-bright Raman dots for multiplexed optical imaging. *Nat. Commun.* **2021**, 12 (1), 1305.

164. Silva, W. R.; Keller, E. L.; Frontiera, R. R., Determination of resonance Raman cross-sections for use in biological SERS sensing with femtosecond stimulated Raman spectroscopy. *Anal. Chem.* **2014**, 86 (15), 7782-7787.

165. Silver, A.; Kitadai, H.; Liu, H.; Granzier-Nakajima, T.; Terrones, M.; Ling, X.; Huang, S., Chemical and Bio Sensing Using Graphene-Enhanced Raman Spectroscopy. *Nanomater.* **2019**, 9 (4), 516.

166. Kim, J.; Cote, L. J.; Kim, F.; Huang, J. Visualizing Graphene Based Sheets by Fluorescence Quenching Microscopy. *J. Am. Chem. Soc.* **2010**, 132 (1), 260−267.

167. Xie, L.; Ling, X.; Fang, Y.; Zhang, J.; Liu, Z. Graphene as a Substrate to Suppress Fluorescence in Resonance Raman Spectroscopy. *J. Am. Chem. Soc.* **2009**, 131, 9890−9891.

168. Nie, S.; Emory, S. R. Probing Single Molecules and Single Nanoparticles by Surface-Enhanced Raman Scattering. *Science* **1997**, 275, 1102−1106.

169. Heeg, S.; Mueller, N. S.; Wasserroth, S.; Kusch, P.; Reich, S., Experimental tests of surface-enhanced Raman scattering: Moving beyond the electromagnetic enhancement theory. *J. Raman Spectrosc.* **2020**, 52 (2), 310-322.

170. Ling, X.; Zhang, J., First-layer effect in graphene-enhanced Raman scattering. *Small* **2010**, 6 (18), 2020-2025.

171. Ling, X.; Moura, L. G.; Pimenta, M. A.; Zhang, J., Charge-Transfer Mechanism in Graphene-Enhanced Raman Scattering. *J. Phys. Chem. C* **2012**, 116 (47), 25112-25118.

172. Xu, H.; Chen, Y.; Xu, W.; Zhang, H.; Kong, J.; Dresselhaus, M. S.; Zhang, J., Modulating the charge-transfer enhancement in GERS using an electrical field under vacuum and an n/p-doping atmosphere. *Small* **2011**, 7 (20), 2945-2952.

173. Feng, S.; Dos Santos, M. C.; Carvalho, B. R.; Lv, R.; Li, Q.; Fujisawa, K.; Elías, A. L.; Lei, Y.; Perea-López, N.; Endo, M.; et al., Ultrasensitive molecular sensor using N-doped graphene through enhanced Raman scattering. *Sci. Adv.* **2016**, 2 (7), e1600322.

174. Valeš, V.; Kovaříček, P.; Fridrichová, M.; Ji, X.; Ling, X.; Kong, J.; Dresselhaus, M. S.; Kalbáč, M., Enhanced Raman scattering on functionalized graphene substrates. *2D Mater.* **2017**, 4 (2), 025087.

175. Greenwood, J.; Phan, T. H.; Fujita, Y.; Li, Z.; Ivasenko, O.; Vanderlinden, W.; Van

Gorp, H.; Frederickx, W.; Lu, G.; Tahara, K.; et al., Covalent Modification of Graphene and Graphite Using Diazonium Chemistry: Tunable Grafting and Nanomanipulation. *ACS Nano* **2015**, 9, 5520−5535.

176. Wetzl, C.; Silvestri, A.; Garrido, M.; Hou, H. L.; Criado, A.; Prato, M., The Covalent Functionalization of Surface-Supported Graphene: An Update. *Angew. Chem. Int. Ed. Engl.* **2023**, 62 (6), e202212857.

177. Rodriguez Gonzalez, M. C.; Brown, A.; Eyley, S.; Thielemans, W.; Mali, K. S.; De Feyter, S., Self-limiting covalent modification of carbon surfaces: diazonium chemistry with a twist. *Nanoscale* **2020**, 12 (36), 18782-18789.

178. Xia, Y.; Sun, L.; Eyley, S.; Daelemans, B.; Thielemans, W.; Seibel, J.; De Feyter, S., Grafting Ink for Direct Writing: Solvation Activated Covalent Functionalization of Graphene. *Adv. Sci.* **2022**, e2105017.

179. Liu, H.; Ryu, S.; Chen, Z.; Steigerwald, M. L.; Nuckolls, C.; Brus, L. E., Photochemical Reactivity of Graphene. *J. Am. Chem. Soc.* **2009**, 131, 17099−17101.

180. Edelthalhammer, K. F.; Dasler, D.; Jurkiewicz, L.; Nagel, T.; Al-Fogra, S.; Hauke, F.; Hirsch, A., Covalent 2D-Engineering of Graphene by Spatially Resolved Laser Writing/Reading/Erasing. *Angew. Chem. Int. Ed. Engl.* **2020**, 59 (51), 23329-23334.

181. Toyouchi, S.; Wolf, M.; Feng, G.; Fujita, Y.; Fortuni, B.; Inose, T.; Hirai, K.; De Feyter, S.; Uji-i, H., All-Optical and One-Color Rewritable Chemical Patterning on Pristine Graphene under Water. *J. Phys. Chem. Lett.* **2022**, 3796-3803.

Chapter 2

Liquid-Phase Photo-induced Covalent Modification (PICM) of Single-Layer Graphene by Short-Chain Fatty Acids

The results reported in this chapter are based on the following publication:

Feng, G.; Inose, T.; Suzuki, N.; Wen, H.; Taemaitree, F.; Wolf, M.; Toyouchi, S.; Fujita, Y.; Hirai, K.; Uji-i, H., Liquid-phase photo-induced covalent modification (PICM) of single-layer graphene by short-chain fatty acids. *Nanoscale,* 2023, 15, 4932–4939.

2.1 Abstract

We report an efficient photo-induced covalent modification (PICM) of graphene by short-chain fatty acids (SCFAs) with an alkyl chain at the liquid-solid interface for spatially resolved chemical functionalization of graphene. Light irradiation on monolayer graphene under an aqueous solution of the SCFAs with an alkyl chain efficiently introduces sp^3-hybridized defects, where the reaction rates of PICM are significantly higher than those in pure water. Raman and IR spectroscopy revealed that a high density of methyl, methoxy, and acetate groups is covalently attached to the graphene surface while it was partially oxidized by other oxygen-containing functional groups, such as OH and COOH. A greater downshift of the G-band in Raman spectra was observed upon the PICM with longer alkyl chains, suggesting that the charge doping effect can be controlled by the alkyl chain length of the SCFAs. The systematic research and exploration of covalent modification in SCFAs provide new insight and a potentially facile method for bandgap engineering of graphene.

2.2 Introduction

Graphene, a two-dimensional material consisting of a single atomic layer of sp^2 hybridized carbon, has attracted great attention as a next-generation material for opto-electronic devices, energy storage, catalysis, (bio-)chemical sensors, and so on since its isolation in 2004.[1-7] This is mainly due to its ultra-thin/light body along with its excellent mechanical strength/flexibility, high carrier mobility, unique optical properties, and high thermal conductivity.[8, 9] However, the absence of a bandgap in graphene limits the advanced applications, especially in switching devices such as field-effect transistors.[10, 11] To overcome this obstacle, several effective techniques to modify its electronic properties have been reported (known as bandgap engineering in graphene), for instance, by introducing sp^3-type defects in graphene. Unlike physical defects like vacancy, boundary, and edge defects, the sp^3-type defects can be

reversibly introduced by electrochemical reactions, radical species, and electron or light irradiation.[12-14]

For practical applications, spatially resolved chemical modification remains challenging, although it is expected to be useful for site-specific control of wettability, catalytic or optical activity, molecular affinity, and electron conductivity.[15-18] Several methods for spatially resolved chemical modifications have been proposed, including masking, stamping, and light-induced ones.[1, 19, 20] Among these, photo-induced chemical modification (PICM) is a promising method. Liu *et al.* reported the photochemical reactivity of graphene in a toluene solution of benzoyl peroxide. They found that a Raman peak related to graphene defects (D-band) appeared only at the laser focus, where they suggested that photo-induced phenyl radicals attacked the basal plane of graphene forming covalent bonds.[21] Mitoma *et al.* found that excitation of graphene by visible light in the presence of water could result in graphene oxidation, which modifies the electronic transport properties, suggesting local bandgap engineering.[22] We have extended this approach to deposit metal electrodes on the graphene upon visible laser light focusing on the interface between an aqueous solution of metal ions and the graphene surface.[23] We reported that multiple metal elements could be deposited on graphene in a site-specific manner just by changing the ion solution and revealed the excellent electric contact between the deposited metal and graphene. Besides the spatially resolved nature, PICM offers reversible graphene chemical patterning. Hirsch's group presented a strategy to functionalize graphene covered with dibenzoyl peroxide (DBPO) solid film by laser-direct writing with 532 nm and reading with 633 nm, followed by de-functionalization (erasing chemical patterns) by simple thermal annealing.[24] We recently reported an all-optical method for spatially resolved and reversible PICM of graphene in pure water using a one-color laser.[14] These reversible PICM offers a facile and flexible tool for site-specific control and tunability over the physicochemical properties of graphene.

Herein, we report that short-chain fatty acids (SCFAs) with an alkyl chain can offer an extraordinarily efficient PICM on graphene at the liquid phase. The PICM was performed in a site-specific manner by tightly focusing visible laser light (488 nm) on a graphene surface covered by an aqueous solution of the SCFAs. To investigate the alkyl chain length dependence on the PICM, HCOOH (Formic acid) and $CH_3(CH_2)_nCOOH$ (n = 0: acetic acid, n = 1: propionic acid, n = 2: butyric acid) were systematically investigated by means of Raman/IR spectroscopy. *In-situ* Raman spectroscopy was carried out to record the change in the D-band intensity as a function of the irradiation time and the intensity ratio of the D- and G-bands (I_D/I_G) to evaluate defect formation in graphene. SCFAs with an alkyl chain (n = 0, 1, 2) showed a higher reaction yield and rate than without alkyl chain (HCOOH), demonstrating that the alkyl chains ($-CH_2)_nCH_3$) play a vital role in dense functionalization. The difference in the reaction rates and the shift of G-band peak position (G^-) between the SCFAs further confirm the roles of alkyl chains in introducing a high degree of charge doping effect on graphene. Raman and IR spectroscopy detected methyl, methoxy, and acetate groups at the modified area on graphene. This study proposes a plausible reaction mechanism for the liquid-phase PICM of graphene and paves a way to tune the charge doping effect for graphene bandgap engineering.

2.3 Results and discussion

Figure 2.1a illustrates a typical PICM configuration at a liquid-solid interface on graphene monolayers supported by a dielectric substrate. A laser line at 488 nm (laser power: 0.1 ~ 10 MW/cm^2) was tightly focused with an objective lens (NA ~ 0.95) on a graphene surface in the presence of water or an aqueous solution of the SCFAs. Raman spectra were simultaneously recorded using the same objective lens and a spectrograph equipped with a charge-coupled device (CCD), allowing in-situ Raman monitoring during the PICM processes. To confirm the spatial distribution of the PICM, Raman mapping around the modified area is taken under weak laser power (0.1 MW/cm^2) to ensure that the Raman excitation light would not induce further

PICM. Figure 2.1b presents typical Raman spectra of a graphene monolayer before and after PICM under an aqueous solution of acetic acid at a laser power of 6 MW/cm^2. Before the PICM (0 s), only the G-band at 1595 cm^{-1} and 2D-band at 2697 cm^{-1} were observed, indicating pristine graphene, where the G-band is assigned to the graphitic E_{2g} mode from sp^2-hybridized carbon atoms and 2D-band to the double resonance scattering process between nonequivalent K points in the Brillouin zone of graphene.[25] In contrast, after the PICM, an additional peak around 1350 cm^{-1} appears, which can be assigned to the D-band (defect mode[27]). Since the D-band disappears after thermal treatment of the graphene at 350 ˚C in the air, as shown in Figure 2A1, it is mainly due to a chemical defect instead of a physical one in accordance with literature[27]. The same decrease of I_D/I_G in acetic and propionic acid solution suggests similar defects are introduced on graphene. The small difference in I_D/I_G ratio after heating (0.21 for acetic acid and 0.26 for propionic acid) could be attributed to the functional groups on graphene surface. Figure 2.1c shows D-band intensity maps before and after PICM at a fixed point. Before high-power laser irradiation, the Raman intensity map does not show any features (Figure 2.1c top left). After high-power laser irradiation, however, the Raman map shows a point with high D-band intensity (Figure 2.1c top right). Since the laser focus was fixed precisely at this point during the PICM process, the map indicates that the PICM was induced only around the laser focal point. The full-width half-maxima (FWHM) of this point was estimated to be ca. 1.2 μm (Figure 2.1c bottom), which is larger than the diffraction limit (~260 nm). This suggests that radicals or hot electrons generated upon light irradiation diffuse over the diffraction limit and react with the nearby graphene surface or surrounding molecules.[14, 22]

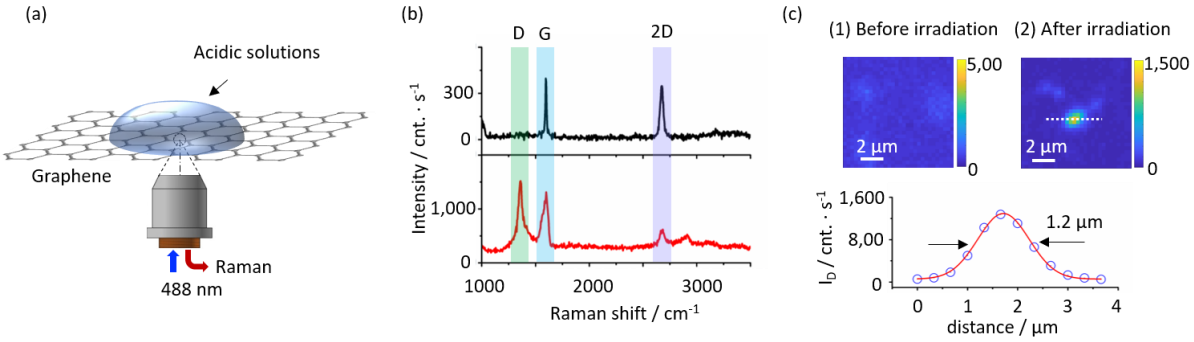

Figure 2.1 Principle of PICM on graphene at the liquid solid interface. (a) A schematic illustration of *in-situ* Raman spectroscopy during PICM. A 488 nm laser was used for both PCIM and Raman spectroscopy. (b) Typical Raman spectra of a graphene monolayer before (black) and after (red) PICM for 0 and 120 s, respectively, at an interface between graphene and an aqueous solution of acetic acid. (c) Typical maps of the Raman intensity at 1350 cm^{-1} before and after PICM at a laser focal point (above) and a line profile along (open circle) the white dashed line in the map after irradiation with a Gaussian fitting (solid red line) (FWHM ~ 1.2 μm).

In this study, we compare the PICM processes of graphene monolayers in pure water, formic acid (HCOOH), acetic acid, propionic acid, and butyric acid; $CH_3(CH_2)_nCOOH$ (n = 0, 1, 2, respectively). Figure 2.2 displays Raman spectra of graphene after the PICM for 120 s in an aqueous solution of each molecule. In all cases, D-band was confirmed after PICM. However, the intensity of the D-band in the case of the SCFAs with an alkyl chain is significantly higher than those of pure water and formic acid. The D to G ratio (I_D/I_G) reaches about 1 for the SCFAs with alkyl chain, while it remains below 0.5 for water and formic acid under the employed illumination condition. Another striking difference between them is the graphene Raman intensity after the PICM. The Raman peak intensities after PICM with the SCFAs with alkyl chain were significantly enhanced (typically reaches 10,000 counts / s) compared to those before the PICM (typically 2,000 counts / s), while it remains the same in the case of water and

formic acid. It is likely that graphene electronic structures are modified by the PICM with SCFAs with an alkyl chain.

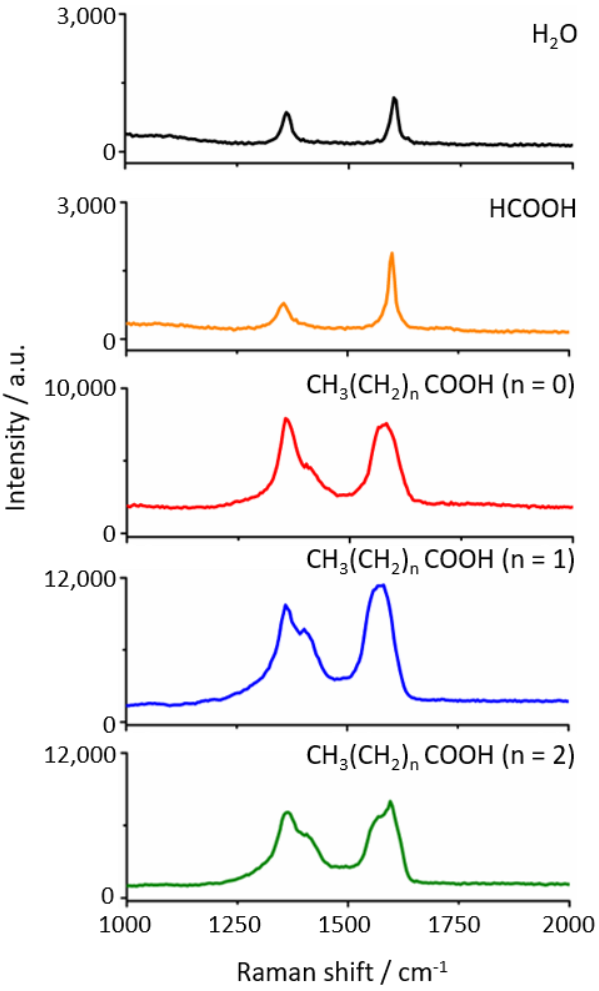

Figure 2.2 Raman spectra of graphene after 120 s PICM in H_2O, formic acid, acetic acid (n = 0), propionic acid (n = 1), and butyric acid (n = 2), respectively, from the top to the bottom panels.

To investigate the PICM dynamics, in-situ Raman monitoring was conducted during the PICM process in water and an aqueous solution of acetic acid (0.1 M). Figure 2.3a and 2.3b, respectively, present waterfall plots of the Raman scattering as a function of time during the PICM process in water and 0.1 M acetic acid aqueous solution (the plots in propionic and butyric acid are presented in Figure 2A2). The corresponding I_D/I_G ratios as a function of time

for the solutions are summarized in Figure 2.3c. $I_D/(I_D+I_G)$ ratios are also estimated and show almost the same trend as I_D/I_G (Figure 2A3), indicating a slight change of I_G at the initial state is negligible for kinetics analysis. Hereafter, the reaction is analysed based on the I_D/I_G. First, water and the formic acid solution show a similar trend, i.e., I_D/I_G values gradually increase as a function of time. In contrast, the SCFAs with alkyl chain reveal completely different behaviour; at the first stage (0 - 10 s in the case of acetic acid), G- and D-bands show a similar trend as water and formic acid, while the intensity of both G- and D-bands suddenly increase by a factor of 5 ~ 6 (Figure 2.3b and Figure 2A2). The maximum I_D/I_G values reach a plateau at ~1 within 20 s for acetic acid and at 0.8 within 40 s for propionic and butyric acid, while it takes a few minutes in the case of water and formic acid solution. These results imply that the PICM mechanism for SCFAs with an alkyl chain differs from that for water and formic acid solution. In addition, we observed I_D decreases after a period of PICM time and this suggests the more functional groups on graphene make larger changes of electronic structures of graphene, resulting in maximum of D peak intensity during PICM process at the certain excitation energy due to resonant Raman scattering.[28]

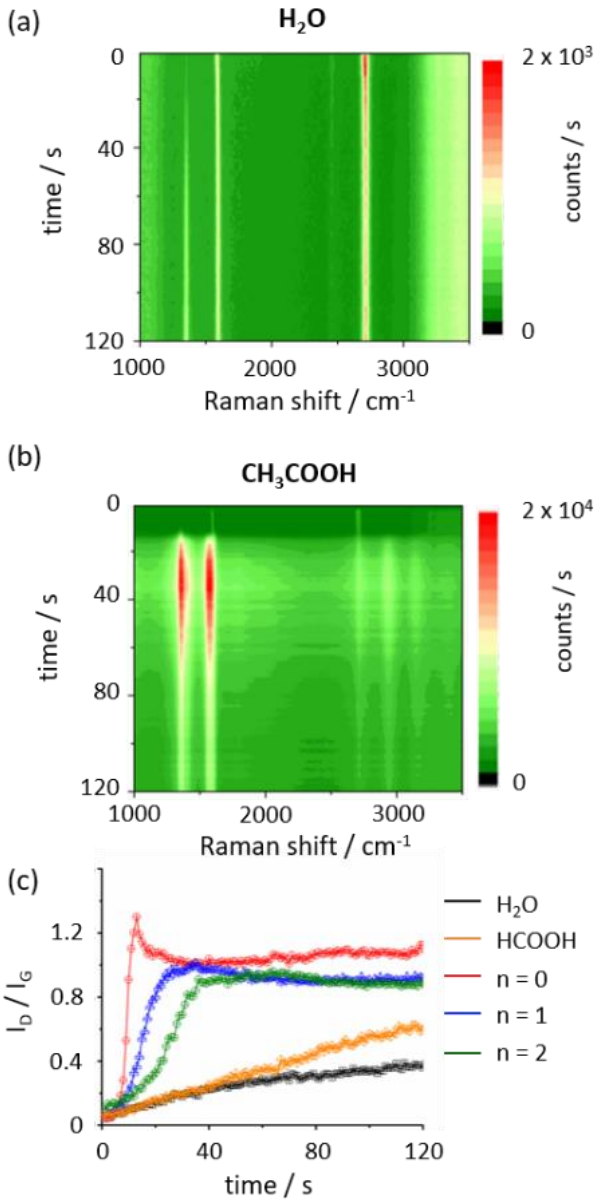

Figure 2.3 Time-course of Raman spectroscopy during the PICM. Waterfall plot of Raman spectra of graphene modified in H_2O (a) and acetic acid (b), respectively. (c) The intensity ratio between D and G bands (I_D/I_G) as a function of time for the PICM in H_2O (black), formic acid (orange), acetic acid ($n = 0$) (red), propionic acid ($n = 1$) (blue), and butyric acid ($n = 2$) (green), respectively.

Since the I_D/I_G ratio is related to the reactions of graphene and follows an exponential fashion at the abrupt increase in the initial part of the time course, the initial reaction rate constant can be estimated from the rise in I_D/I_G plot with the following equation,[22]

$$I_D/I_G(t) \propto \exp(kt) - 1 \quad (1)$$

where the time constant k is defined as the rate of loss of sp^2 carbon atoms of graphene during PICM process. As summarized in Table 2.1, k values for SCFAs with an alkyl chain are 100 times higher than those of water and formic acid. The fitting details were presented in Figure 2A4. A successive decrease was found in the reaction rate with increasing alkyl chain length, suggesting the length of the alkyl chain affects the generated radical's activity.

Table 2.1 The reaction rate in H_2O, and aqueous solution (0.1 M) of formic acid, acetic acid, propionic acid, and butyric acid, respectively.

Reagents	k (min^{-1})
water	1.53×10^{-3}
formic acid	1.32×10^{-3}
acetic acid (n = 0)	2.98×10^{-1}
propionic acid (n = 1)	9.42×10^{-2}
butyric acid (n = 2)	2.92×10^{-2}

In order to identify the chemical reactions of the PICM on graphene, detailed analyses with luminescence, IR, and Raman spectroscopy have been conducted. For the spectroscopic analyses, a wide area of monolayer graphene was periodically modified by laser light in 1 M acetic acid aqueous solution, as shown in Figure 2.4a, on which the modified area (corresponding to the luminescent area in Figure 2.4a) showed I_D/I_G values over 1.0 (Figure 2A5). The heterogenous luminescent intensities could be attributed to the spatial heterogeneity of the PICM efficiency caused by the tiny deviation in the laser focus during stage movements (Figure 2.4a). Additionally, weak/no luminescent spot corresponds probably to the spots of multiple-layered graphene (details see Figure 2A5). A luminescence spectrum at the modified region is shown in Figure 2.4b (excitation: 349 nm). The modified graphene in acetic acid

solution emits luminescence around 620 nm (Figure 2.4b), which is likely due to fragmentation of π-conjugation in graphene by the PICM. The functional groups-induced localized states in π-π* gap of sp^2 sites in graphene may cause a broad emission band.[29] In addition, functionalized groups, such as C-O, C=O and COOH, could have contribution to the fluorescence.[30] A detailed analysis of the luminescence property is shown in Figure 2A6.

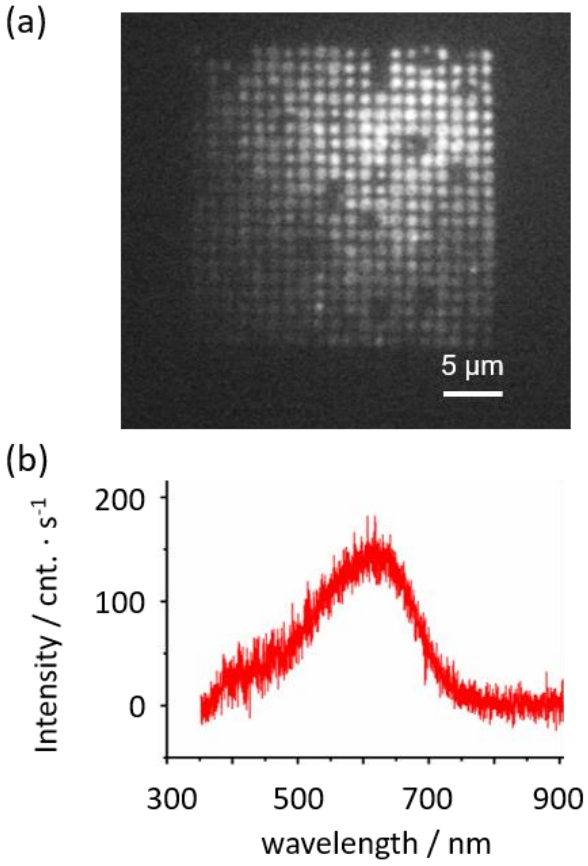

Figure 2.4 Luminescence microscopy/spectroscopy after the patterned PICM of a graphene monolayer in acetic acid aqueous solution. (a) Raman/luminescence wide-field image of the modified graphene upon excitation at 488 nm. (b) A luminescence spectrum at the modified area upon excitation at 349 nm.

An IR spectrum was taken on the modified area to investigate chemical functionalization on the graphene surface (Figure 2.5). Note that graphene's broad IR absorption across the measured frequency range was analytically removed by a 3rd order polynomial fitting to the

raw spectrum. From Figure 2.5, a number of IR peaks were detected. Those can be assigned to O–H stretching at 3650 cm^{-1} (broad), C–H stretching at 2918 and 2851 cm^{-1}, C=O stretching from ester groups at 1741 cm^{-1}, C=C stretching at 1637 cm^{-1}, C–H bending at 1465 cm^{-1}, C–O stretching at 1274 and 1200 cm^{-1}, and C–O–C stretching from ester groups at 1155, 1050 and 995 cm^{-1} (as listed in Table 2.2). Intense C–H stretching absorption suggests the presence of methyl functional groups on the graphene surface. Also, strong absorption from ether groups (C–O–C stretching) was measured, and, in correspondence with the strong C–H absorption, it is likely that a certain amount of methoxy groups exist on the surfaces. Also, from the fingerprint region, C=O and C–O stretching were identified with similar intensities, suggesting the presence of ester and/or carboxylic groups, while the amount of the carboxylic is presumably limited given the weak O–H stretching. Thus, along with the strong C–H absorption, a certain number of acetate group is likely formed on the graphene surface.

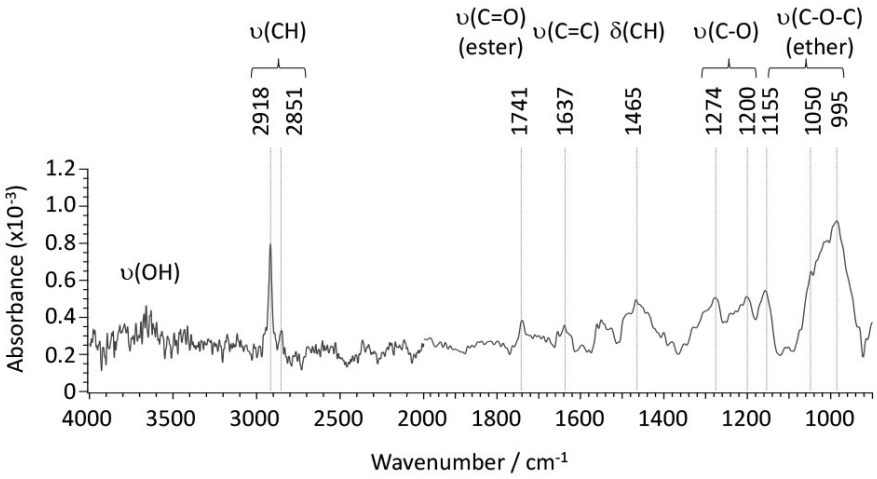

Figure 2.5 IR spectrum of a graphene monolayer after the PICM in acetic acid aqueous solution.

Table 2.2 Assignment of IR peaks and expected origins

Wavenumber (cm^{-1})	Assignment	Origin
3650 (broad)	O-H stretching	Hydroxy
2918, 2851	C-H stretching	Methyl, Methoxy, Acetate
1741	C=O stretching (ester)	Acetate
1637	C=C stretching	Graphene
1465	C-H bending	Methyl, Methoxy, Acetate
1274, 1200	C-O stretching	Methoxy, Acetate
1155, 1050, 995	C-O-C stretching (ether)	Methoxy

From Raman spectroscopy, alteration to the graphene electronic structure via PICM is discussed in terms of G-band shape. As presented in Figure 2.6a, besides the appearance of D-band, we observed a new peak at lower than 1590 cm^{-1} (denoted as G^-). We found that the newly appeared G^- band downshifts with higher PICM degree (Figure 2.6a). Since the wavenumber of Raman signal of the G-bands is independent of the laser wavelength (Table 2A1), they are likely originated from a first order Raman process. Two peaks in the G-band indicate that two phonon energies are allowed at the point (k = 0). It is known that molecular adsorption could induce phonon symmetry breaking, leading to the degeneracy of the transverse optical (TO) and longitudinal optical (LO) phonon modes.[31] In this study, G-band splitting was observed only in SCFAs with an alkyl chain but neither in pure water nor in formic acid aqueous solution (Figure 2.2). The downshift of the G^- band peak position shows a significant dependence on alkyl chain length, where a larger shift was found on longer alkyl

chains (Figure 2.6b). The fact that longer alkyl chains have higher electron donating nature further supports the above IR analysis, in which we speculate that alkyl chains are covalently attached to the graphene surface. Indeed, a small peak that could be related to the alkyl group was found at ~2943 cm^{-1} (C-H stretching, (CH)[32]) in Raman spectra of highly modified graphene with SCFAs with alkyl chain (see Raman spectra in Figure 2A7 and DFT calculation in Figure 2A8 and Table 2A2).

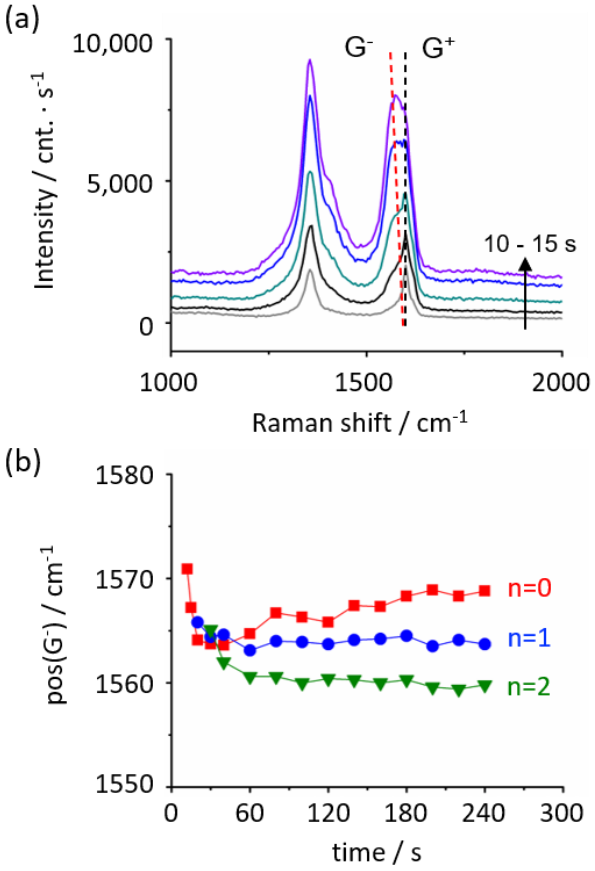

Figure 2.6 G-band splitting and downshifting upon the PICM. (a) Raman spectra from 10 to 15 s during PICM on graphene in an aqueous solution of acetic acid (n = 0). The G-band splits into two peaks and one of them downshifts as a function of time. (b) Position of G^- peak in an aqueous solution of acetic acid (n = 0) (red), propionic acid (n = 1) (green), and butyric acid (n = 2) (purple) as a function of time, respectively.

Given these results, the possible reaction mechanism is illustrated in Scheme 2.1. We consider the PICM reaction in the presence of SCFAs with an alkyl chain proceeds in two reaction stages considering the high oxidation efficiency and species of functional groups on graphene. At the initial stage (stage 1), water plays a critical role and oxidative components, such as hydroxyl or carboxyl groups, are introduced on graphene surfaces. This oxidation is initiated by charge separation (i.e., the generation of excitons/hot electrons in graphene) upon light irradiation to graphene, reacting with surrounding water molecules and radicals are stabilized by water solvation.[14, 22] Once the oxidative groups are introduced on graphene, these polar sites start to 'capture' holes/electrons migrating on graphene and work as an 'active' reaction site, starting the 2nd stage reaction. In stage 2, the presence of SCFAs with an alkyl chain plays a key role. Due to the radical reaction, high density of methyl, methoxy, and acetate groups seem to be finally introduced on the graphene surface. When the SCFAs with an alkyl chain meet the active site, carboxyl radicals ($CH_3(CH_2)_nCOO\cdot$), as well as alkyl radicals ($CH_3(CH_2)_n\cdot$) that are automatically generated via decarboxylation reaction,[33-35] are generated in the solution. These radical species directly attack the pristine graphene surface, functionalizing alkyl and ester groups on the surfaces and/or they attack hydroxyl/carboxyl groups forming ether/ester functionalization. These alkyl groups radicals' reaction is the limiting step in PICM. The two stages properly explain the high PICM efficiency in SCFAs with an alkyl chain. A decrease in reaction rate was indeed observed when increasing the length of the alkyl chains. In stage 2, acetic acid can generate methyl radicals, which are the most reactive because of the primary carbon radical. While propionic and butyric acids can generate ethyl and propyl radicals which are categorized into secondary carbon radicals. Generally, the reaction rate of molecules with smaller molecular weights is faster than those with larger molecular weights.

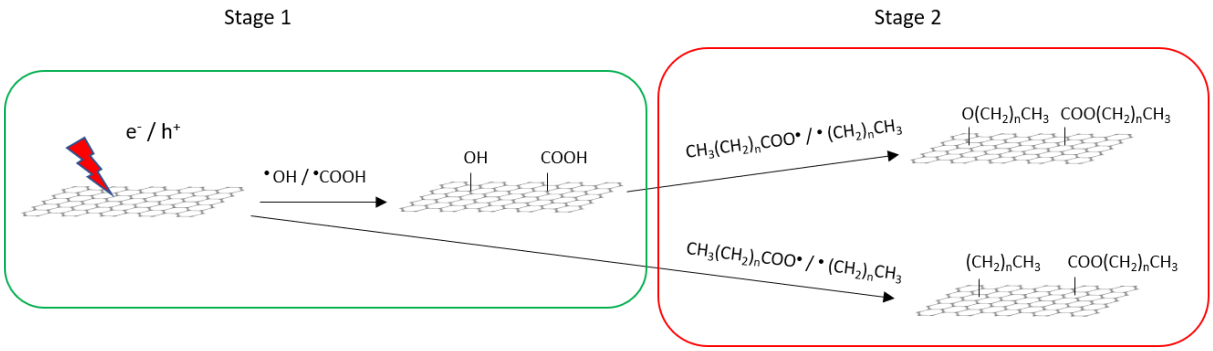

Scheme 2.1 Possible mechanism of the PICM on graphene in an aqueous solution of SCFAs with an alkyl chain.

2.4 Conclusion

We have introduced high functionalization on graphene by SCFAs with an alkyl chain in an aqueous solution using a simple liquid-phase PICM method. By this method, it is easy to wash out the aqueous solution after reaction and can be used to employ modified graphene as a material. We found that, compared to the PICM in water, SCFAs with an alkyl chain drastically enhance the PICM efficiency, most likely due to radical reactions. It takes only several seconds to reach $I_D/I_G \approx 1$. IR and Raman spectroscopy reveal high-density modification of graphene with methyl, methoxy, and acetate groups. A greater downshift of the G-band in Raman spectra was observed upon PICM with longer alkyl chains, suggesting that the charge doping effect can be controlled by the alkyl chain length of the SCFAs. These results suggest that, together with laser-assisted radical reactions, sub-micrometre scaled, site-elective bandgap engineering can be applied to graphene surfaces, opening a venue for micro-scale graphene device applications.

2.5 Experimental method

Sample preparation.

The monolayer graphene on polymer film was purchased from Graphenea. Graphene monolayers were deposited onto a clean coverslip. In short, monolayer graphene sandwiched

between a polymer layer and a sacrificial layer was dipped into deionized water, where the polymer layer was detached and the graphene covered with the sacrificial layer floated on the water surface. A clean coverslip was dipped into the water at a leaned angle to fish out the monolayer graphene / sacrificial layer. The sample was dried in air for 30 min at room temperature and moved to the oven (Standard Electric Furnace, FO201, Yamato) to keep at 150 °C for 1 h and was stored under a vacuum environment for at least 24 h to firmly attach the graphene to the substrate. The sacrificial layer on graphene was removed by hot acetone (50 °C, 1 h) two times and isopropanol (1 h). Then the transferred sample was stored in a vacuum environment for at least 24 h prior to the experiment.

Chemicals

Milli Q water is obtained from a Milli-Q-plus system with a resistivity greater than 18 $M\Omega \cdot cm^{-1}$. Formic acid, acetic acid, propionic acid, and butyric acid were purchased from Tokyo Chemical Industry Co., Ltd. (TCI) and used without further purification.

Raman spectroscopy

Raman spectroscopy was carried out using an inverted optical microscope (Ti-U, Nikon) equipped with a piezoelectric sample stage. A continuous-wave 488 nm laser (Sapphire SF 488-100 CW CDRH) was used for the PICM of graphene. The laser was reflected and guided into an objective (PlanFluor, ×60, N.A. 0.95, Nikon) using a long-pass dichroic mirror (zt488rdcxt, Chroma®) for a 488 nm laser line. The laser power at the sample was ~ 6 MW/cm^2 for photo-covalent functionalization, which was adjusted by attenuators with different optical densities. Raman scattering light from the sample was collected by the same objective and guided to the spectrograph (iHR320, Horiba, cooled to −75 °C) equipped with a 600 lines/mm grating. A long-pass filter (ET500LP for 488 nm line) and a pinhole (diameter 100 μm) are placed before the spectrograph entrance to reject Rayleigh scattering and out-of-focus contribution, respectively. All photo-covalent modification and Raman mapping were conducted by OMEGA software (Combiscope, AIST-NT/ Horiba). Omega software (AIST-

NT/HORIBA), Igor Pro, Origin Lab 9.1, and MATLAB (MathWorks) were used for Raman data analysis. Transmission/wide-field luminescence/wide-field Raman imaging was performed using a charge-coupled device (CCD) camera (ImagEM, Hamamatsu Photonics) operated at −65°C, where a long-pass filter (ET500LP, Chroma) was inserted in front of the camera.

Density functional theory (DFT) calculations

Density functional theory (DFT) calculations were carried out to estimate the Raman peaks related to SCFA. Each structure was fully optimized by the DFT calculations using the B3LYP functional with the 6-31G(d) basis set in *Gaussian 16* software (Gaussian, Inc., Pittsburgh, PA). The theoretical Raman spectrum was calculated for each energy-minimized structures at B3LYP/6-31G(d) level of theory by freezing the coordinate of the graphene moiety.[26]

IR spectroscopy

Graphene was transferred on a $ZnSe_2$ plate prior to the PICM for IR measurement. Monolayer graphene/ $ZnSe_2$ was functionalized in aqueous solution of acetic acid (1 M) by irradiating with visible light from a Xenon lamp. IR spectroscopy was conducted with Nicolet continuμm microscope (Thermo Fisher, Inc.) under transmission mode. The spectral range was set to 4000-650 cm^{-1} with 8 cm^{-1} resolution (Accumulation: 4096 times). The detection area was set to 100 × 100 μm^2. Spectrum processing was carried out with OMNIC and IGOR pro software.

2.6 Appendix

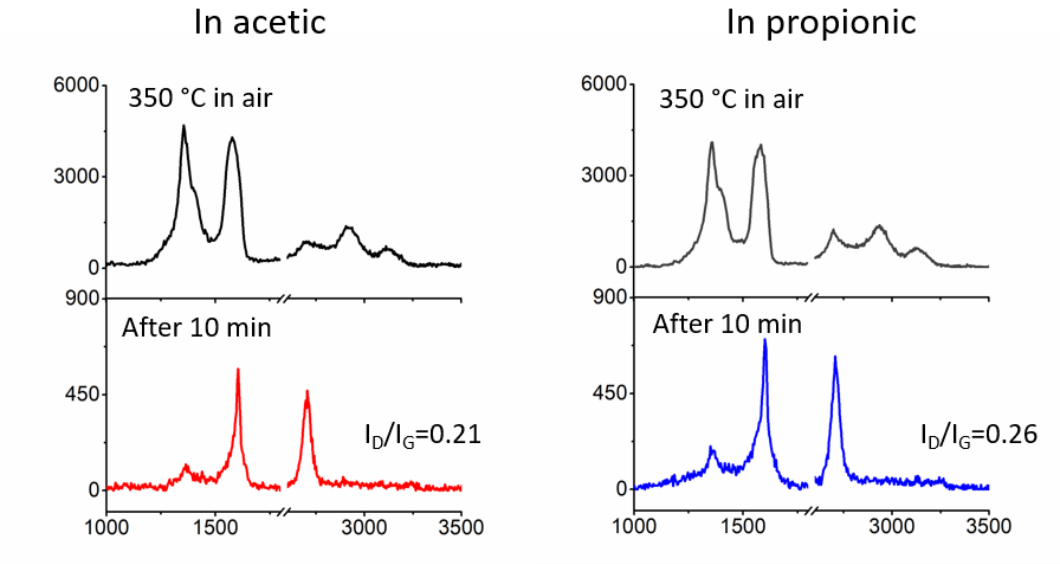

Figure 2A1 Raman spectrum of modified graphene with acetic acid before (top) and after (bottom) heating the graphene at 350 ˚C in air for 10 min.

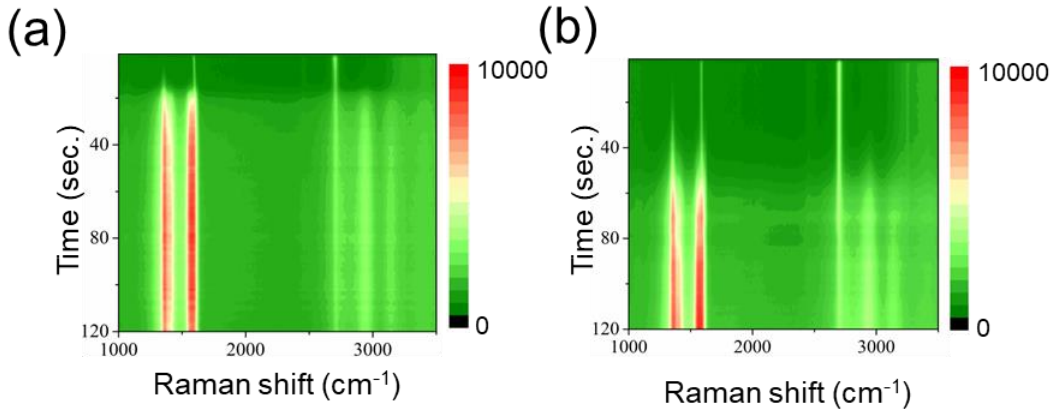

Figure 2A2. A typical in-situ Raman spectroscopy during the PICMs of graphene monolayers in aqueous solution (0.1 M) of propionic acid (a) and butyric acid (b), respectively.

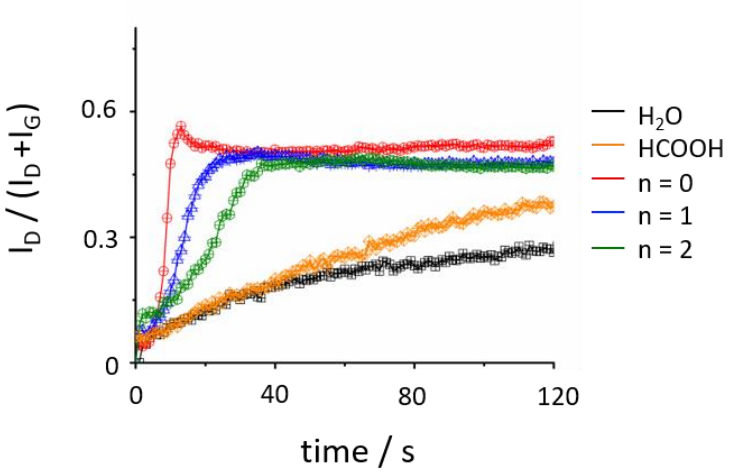

Figure. 2A3 The intensity ratio between D and (D+G) bands ($I_D/(I_D+I_G)$) as a function of time

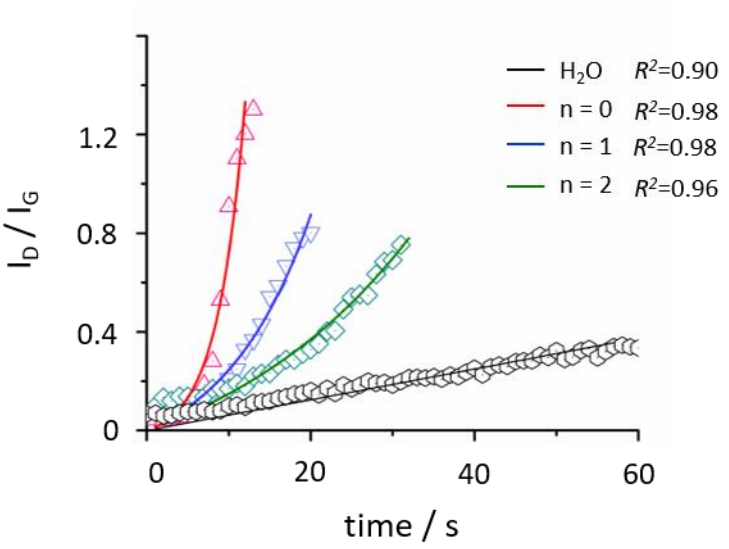

Figure 2A4 Fitting of I_D/I_G at the initial stage with formula 1 (formic is similar with water), R^2: residual square

Modification at wide area

PICM at a wide area was conducted using graphene monolayers supported on SiO_2/Si substrate in 1 M of acetic acid aqueous solution with ~ 6 MW/cm^2 by repeating photolithographic mode at 20×20 μm as shown in Fig. S4. In detail, 20×20 points of 1μm square area of graphene were modified by automatic movements of the sample

stage. Each point of graphene was irradiated with 488 nm laser for 10 s for obtaining over 1 of I_D/I_G value as shown in the I_D/I_G map in Figure 2A5a. Some darker spots in the optical image are visible, which probably correspond to multilayer graphene as reported by the company (marked with yellow circles in Figure 2A5b). Raman information (I_{2D}/I_G=0.6) confirms the black spots are multilayer of graphene. As shown in Figure below, the D/G ratio at the darker spot (spot 2) is slightly lower than that at the bright spot (spot 1), indicating that the PICM efficiently at the multilayer is lower resulting in low covalent modifications. This is one of reason of the weaker luminescence in the missing point. In addition to this, luminescence is expected to be significantly quenched on the multi-layers part of the graphene.

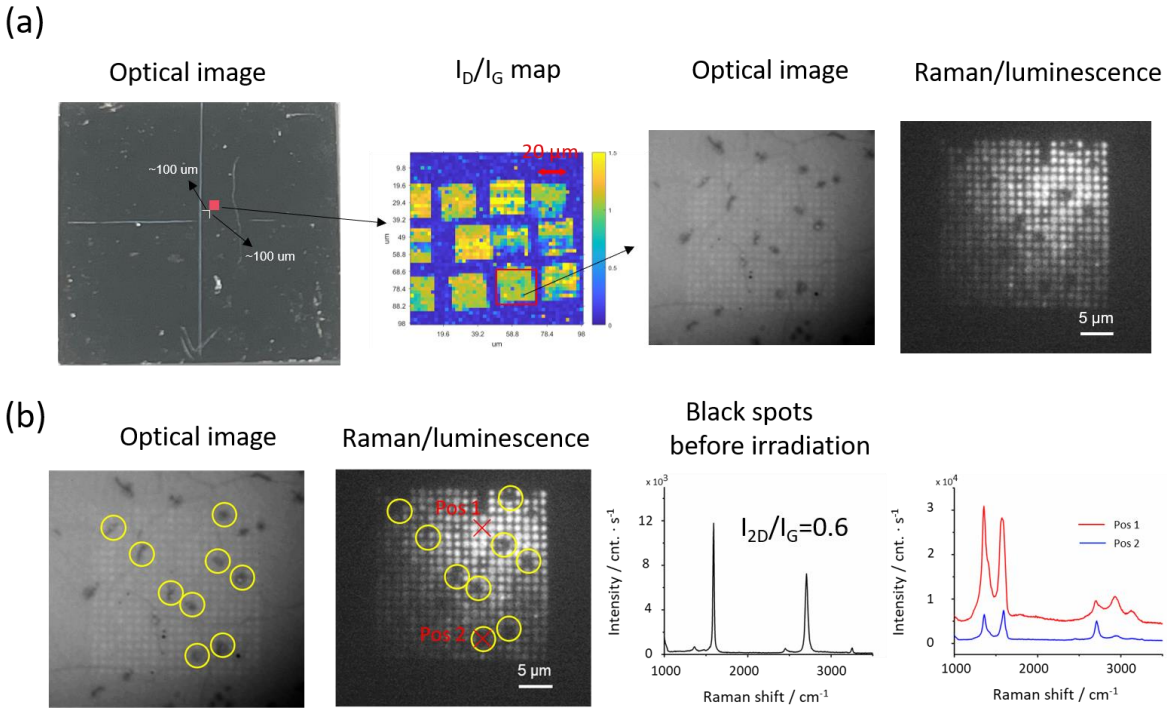

Figure 2A5 Optical and Raman maps of a graphene monolayers modified in an aqueous solution of acetic acid.

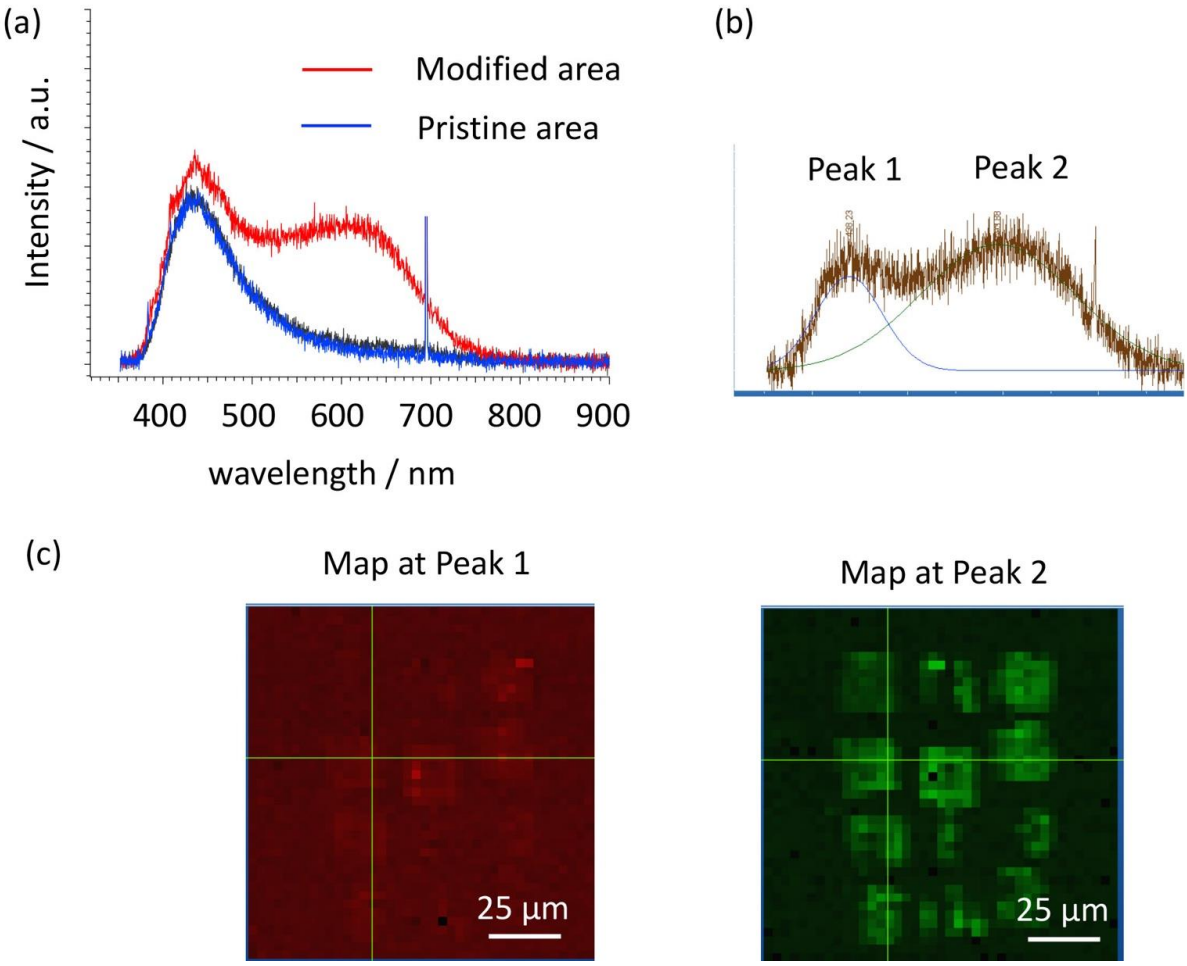

Figure 2A6 Luminescence analysis on the PICM graphene in acetic acid aqueous solution. (a) Averaged luminescence spectra at the modified area (red) and unmodified (pristine) area (blue) of the graphene monolayers. (b) Peak fitting analysis on a luminescence spectrum. The 'peak 1' centered at ~ 435 nm is originated from substrate, while the 'peak 2' at 620 nm is assigned to the luminescence from the functioned graphene. (c) Luminescence intensity map at the 'peak 1' (left) and at the 'peak 2' (right).

Table 2A1 Summary of wavelength dependence at functioned area of graphene

Wavelength (nm)	Energy (eV)	D	G^-	G
488	2.54	1353.9	1564.9	1596.1
532	2.33	1343.9	1566.1	1594.9
633	1.95	1326.5	1566.8	1593.4

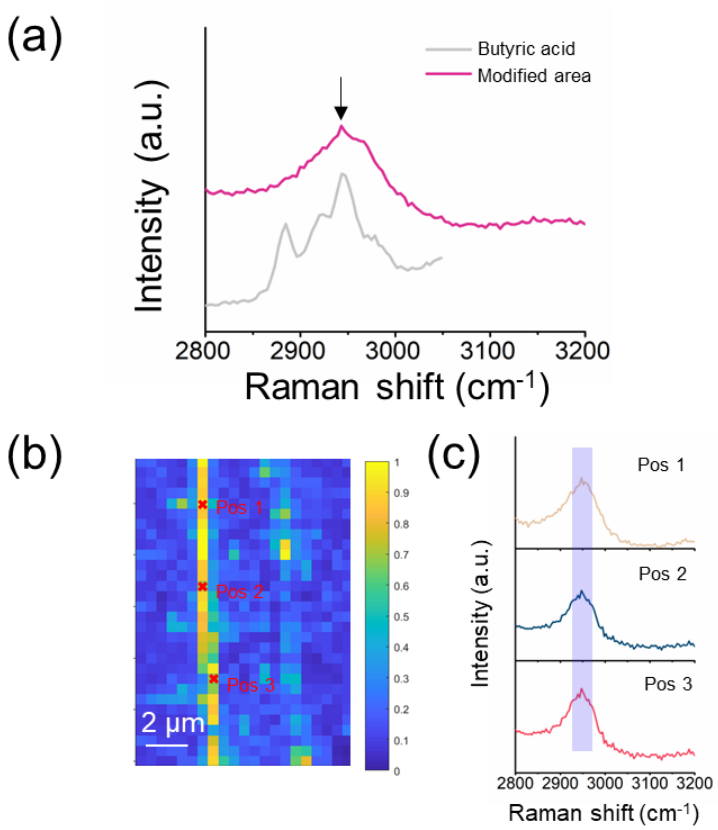

Figure 2A7 (a) Signature of C-H stretching after PICM of graphene in butyric acid; gray line is Raman spectra from the butyric acid solution (highest peak: 2943 cm^{-1}); (b) Photo-pattern two lines in butyric acid; and (c) Corresponded Raman spectra on selected points.

DFT calculations

DFT calculations on alkyl groups covalently attached on graphene were conducted. We assumed that $-CH_3$, $-OCH_3$, $-CH_2COOH$ and $-CH_2COOCH_3$ were covalently attached on graphene along with hydroxy group (-OH) or hydrogen atom (-H), respectively. For this

simulation, the graphene part was frozen and the vibrational modes of -H/-CH_3, -H/-OCH_3, -H/-CH_2COOH, -H/-CH_2COOCH_3, -OH/-CH_3, -OH/-OCH_3, -OH/-CH_2COOH and -OH/-CH_2COOCH_3 were calculated (Figure S6a). The symmetrical CH stretching can be found at around 2950 cm^{-1} (Figure S6b and Table S2). All the vibrational modes are displayed in Figure S6. This simulation further supports the assignment of the observed Raman peak at 2943 cm^{-1} to the alkyl groups from the SCFA.

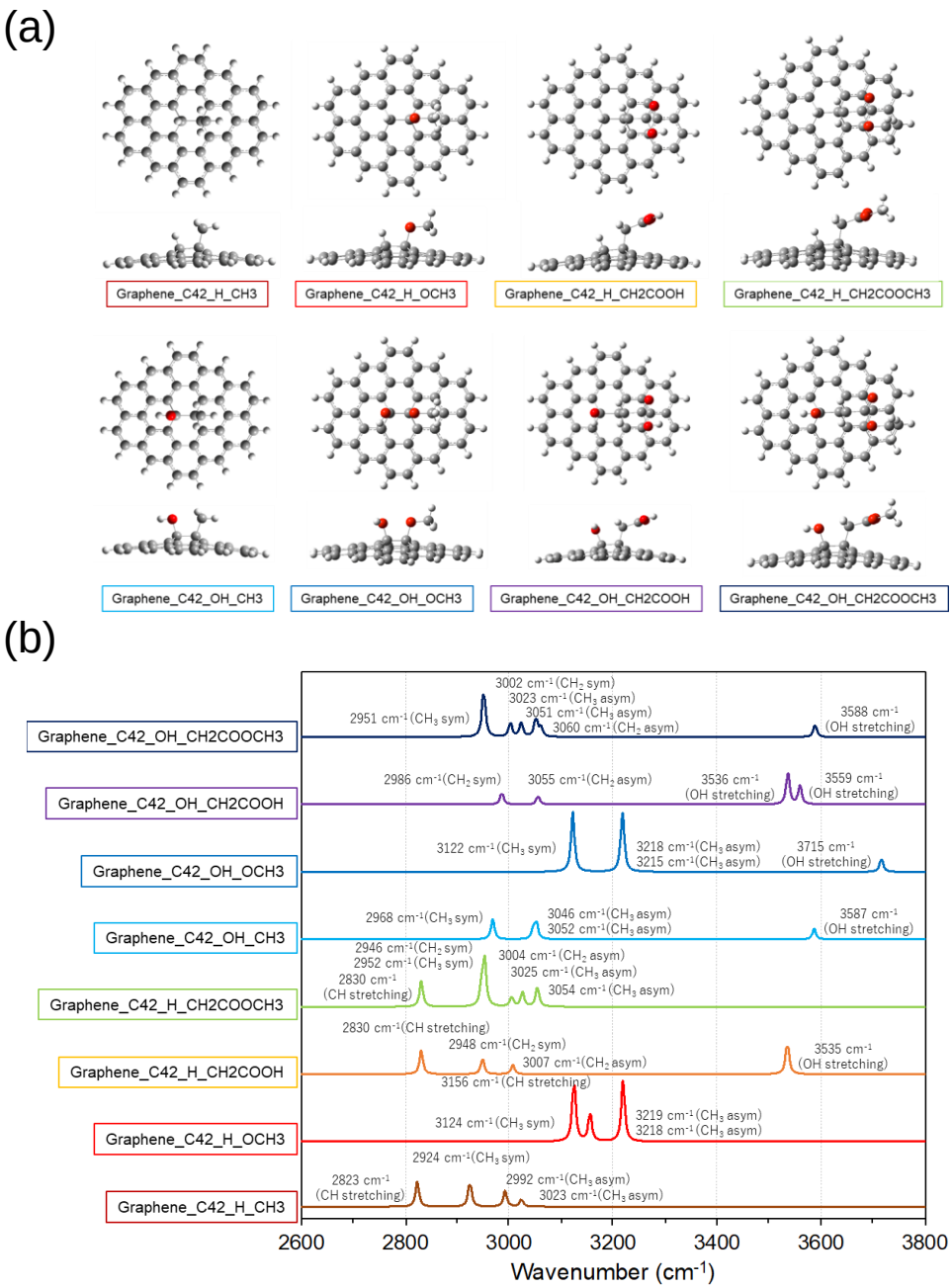

Figure 2A8 DFT calculation in the case of PICM in acetic aqueous solution. (a) Top and side views for the covalent connection of the models; White, gray, and red atoms indicate hydrogen, carbon, and oxygen, respectively. (b) Raman spectra for the eight cases each model (wavenumber scale factor is 0.96).

Table 2A2 Raman peaks related to carboxylic acid estimated with DFT calculation

Possibilities	Peak position (cm^{-1})	Assignment
Graphene / -H /-CH_3	2823	CH stretching
	2924	CH_3 symmetrical stretching
	2992 / 3023	CH_3 asymmetrical stretching
Graphene / -H /-OCH_3	3124	CH_3 symmetrical stretching
	3156	CH stretching
	3219 / 3023	CH_3 asymmetrical stretching
Graphene /-H / -CH_2COOH	2830	CH stretching
	2948	CH_2 symmetrical stretching
	3007	CH_2 asymmetrical stretching
	3535	OH stretching
Graphene /-H / -CH_2COOCH_3	2830	CH stretching
	2946 / 2952	CH_2 / CH_3 symmetrical stretching
	3004 / 3025 / 3054	CH_2 / CH_3 asymmetrical stretching
Graphene / -OH / -CH_3	2968	CH_3 symmetrical stretching
	3046 / 3052	CH_3 asymmetrical stretching
	3587	OH stretching
Graphene / -OH / -OCH_3	3122	CH_3 symmetrical stretching
	3215 / 3218	CH_3 asymmetrical stretching
	3587	OH stretching
Graphene /-OH / -CH_2COOH	2986	CH_2 symmetrical stretching
	3055	CH_2 asymmetrical stretching
	3536 / 3559	OH stretching
Graphene /-OH / -$CH_2COOCH3$	2951 / 3002	CH_3 / CH_2 symmetrical stretching
	3023 / 3051 / 3060	CH_3 / CH_2 asymmetrical stretching
	3588	OH stretching

2.7 References

1. Sun, Z.; Pint, C. L.; Marcano, D. C.; Zhang, C.; Yao, J.; Ruan, G.; Yan, Z.; Zhu, Y.; Hauge, R. H.; Tour, J. M., Towards hybrid superlattices in graphene. *Nat. Commun.* **2011**, *2*, 559.

2. Grigorenko, A. N.; Polini, M.; Novoselov, K. S., Graphene plasmonics. *Nat. Photonics* **2012**, *6*, 749-758.

3. Xiang, Q.; Yu, J.; Jaroniec, M., Graphene-based semiconductor photocatalysts. *Chem. Soc. Rev.* **2012**, *41*, 782-796.

4. Reina, G.; Gonzalez-Dominguez, J. M.; Criado, A.; Vazquez, E.; Bianco, A.; Prato, M., Promises, facts and challenges for graphene in biomedical applications. *Chem. Soc. Rev.* **2017**, *46*, 4400-4416.

5. Ye, R.; Tour, J. M., Graphene at fifteen. *ACS Nano* **2019**, *13*, 10872-10878.

6. Zhao, G.; Li, X.; Huang, M.; Zhen, Z.; Zhong, Y.; Chen, Q.; Zhao, X.; He, Y.; Hu, R.; Yang, T.; Zhang, R.; Li, C.; Kong, J.; Xu, J. B.; Ruoff, R. S.; Zhu, H., The physics and chemistry of graphene-on-surfaces. *Chem. Soc. Rev.* **2017**, *46*, 4417-4449.

7. Lin, L.; Peng, H.; Liu, Z., Synthesis challenges for graphene industry. *Nat. Mater.* **2019**, *18* (6), 520-524.

8. Luo, B.; Zhi, L., Design and construction of three dimensional graphene-based composites for lithium ion battery applications. *Energy Environ. Sci.* **2015**, *8*, 456-477.

9. Sun, Z.; Fang, S.; Hu, Y. H., 3D Graphene Materials: From Understanding to Design and Synthesis Control. *Chem. Rev.* **2020**, *120* (18), 10336-10453.

10. Xu, X.; Liu, C.; Sun, Z.; Cao, T.; Zhang, Z.; Wang, E.; Liu, Z.; Liu, K., Interfacial engineering in graphene bandgap. *Chem. Soc. Rev.* **2018**, *47*, 3059-3099.

11. Chen, Y.; Zhang, B.; Liu, G.; Zhuang, X.; Kang, E. T., Graphene and its derivatives: switching ON and OFF. *Chem. Soc. Rev.* **2012**, *41*, 4688-4707.

12. Xia, Y.; Sun, L.; Eyley, S.; Daelemans, B.; Thielemans, W.; Seibel, J.; De Feyter, S., Grafting Ink for Direct Writing: Solvation Activated Covalent Functionalization of Graphene. *Adv. Sci.* **2022**, *9*, e2105017.

13. Rodriguez Gonzalez, M. C.; Leonhardt, A.; Stadler, H.; Eyley, S.; Thielemans, W.; De Gendt, S.; Mali, K. S.; De Feyter, S., Multicomponent Covalent Chemical Patterning of Graphene. *ACS Nano* **2021**, *15*, 10618-10627.

14. Toyouchi, S.; Wolf, M.; Feng, G.; Fujita, Y.; Fortuni, B.; Inose, T.; Hirai, K.; De Feyter, S.; Uji-i, H., All-Optical and One-Color Rewritable Chemical Patterning on Pristine Graphene under Water. *J. Phys. Chem. Lett.* **2022**, *13*, 3796-3803.

15. Hu, H.; Allan, C. C. K.; Li, J.; Kong, Y.; Wang, X.; Xin, J. H.; Hu, H., Multifunctional organically modified graphene with super-hydrophobicity. *Nano Res.* **2014**, *7* (3), 418-433.

16. Robinson, J. T.; Burgess, J. S.; Junkermeier, C. E.; Badescu, S. C.; Reinecke, T. L.; Perkins, F. K.; Zalalutdniov, M. K.; Baldwin, J. W.; Culbertson, J. C.; Sheehan, P. E.; Snow, E. S., Properties of fluorinated graphene films. *Nano Lett.* **2010**, *10*, 3001-3005.

17. Greenwood, J.; Phan, T. H.; Fujita, Y.; Li, Z.; Ivasenko, O.; Vanderlinden, W.; Van Gorp, H.; Frederickx, W.; Lu, G.; Tahara, K.; Tobe, Y.; Uji-I, H.; Mertens, S. F. L.; De Feyter, S. Covalent Modification of Graphene and Graphite Using Diazonium Chemistry: Tunable Grafting and Nanomanipulation. *ACS Nano* **2015**, *9*, 5520-5535.

18. Bao, L.; Zhao, B.; Yang, B.; Halik, M.; Hauke, F.; Hirsch, A., Hypervalent Iodine Compounds as Versatile Reagents for Extremely Efficient and Reversible Patterning of Graphene with Nanoscale Precision. *Adv. Mater.* **2021**, *33*, 2101653.

19. Zhou, Y.; Loh, K. P., Making patterns on graphene. *Adv. Mater.* **2010**, *22*, 3615-3620.

20. Zhang, W.; Lei, Y.; Ming, F.; Jiang, Q.; Costa, P. M. F. J.; Alshareef, H. N., Lignin Laser Lithography: A Direct-Write Method for Fabricating 3D Graphene Electrodes for Microsupercapacitors. *Adv. Energy Mater.* **2018**, *8*, 1801840.

21. Liu, H.; Ryu, S.; Chen, Z.; Steigerwald, M. L.; Nuckolls, C. and Brus, L. E., Photochemical Reactivity of Graphene, *J. Am. Chem. Soc*. **2009**, *131*, 17099-17101.

22. Mitoma, N.; Nouchi, R.; Tanigaki, K., Photo-oxidation of Graphene in the Presence of Water. *J. Phys. Chem. C* **2013**, *117*, 1453-1456.

23. Xia, K.; Chiang, W. Y.; Lockhart de la Rosa, C. J.; Fujita, Y.; Toyouchi, S.; Yuan, H.; Su, J.; Masuhara, H.; De Gendt, S.; De Feyter, S.; Hofkens, J.; Uji, I. H., Photo-induced electrodeposition of metallic nanostructures on graphene. *Nanoscale* **2020**, *12*, 11063-11069.

24. Edelthalhammer, K. F.; Dasler, D.; Jurkiewicz, L.; Nagel, T.; Al-Fogra, S.; Hauke, F.; Hirsch, A., Covalent 2D-Engineering of Graphene by Spatially Resolved Laser Writing/Reading/Erasing. *Angew. Chem. Int. Ed.* **2020**, *59*, 23329-23334.

25. Venezuela, P.; Lazzeri, M.; Mauri, F., Theory of double-resonant Raman spectra in graphene: Intensity and line shape of defect-induced and two-phonon bands. *Phys. Rev. B* **2011**, *84*, 035433.

26. You, T. T.; Yang, N.; Shu, Y. Q.; Yin, P. G., A DFT study on graphene-based surface-enhanced Raman spectroscopy of Benzenedithiol adsorbed on gold/graphene. *J. Raman Spectrosc.* **2019**, *50* (10), 1510-1518.

27. Eckmann, A.; Felten, A.; Verzhbitskiy, I.; Davey, R.; Casiraghi, C. Raman Study on Defective Graphene: Effect of the Excitation Energy, Type, and Amount of Defects. *Phys. Rev. B* **2013**, *88*, 035426.

28. Chen, C. F.; Park, C. H.; Boudouris, B. W.; Horng, J.; Geng, B.; Girit, C.; Zettl, A.; Crommie, M. F.; Segalman, R. A.; Louie, S. G.; Wang, F., Controlling inelastic light scattering quantum pathways in graphene. *Nature* **2011**, *471* (7340), 617-620.

29. Chien, C. T.; Li, S. S.; Lai, W. J.; Yeh, Y. C.; Chen, H. A.; Chen, I. S.; Chen, L. C.; Chen, K. H.; Nemoto, T.; Isoda, S.; Chen, M.; Fujita, T.; Eda, G.; Yamaguchi, H.; Chhowalla, M.; Chen, C. W., Tunable photoluminescence from graphene oxide. *Angew. Chem. Int. Ed.* **2012,** *51* (27), 6662-6666.

30. Shang, J.; Ma, L.; Li, J.; Ai, W.; Yu, T.; Gurzadyan, G. G., The origin of fluorescence from graphene oxide. *Sci. Rep.* **2012,** *2*, 792

31. Dong, X.; Shi, Y.; Zhao, Y.; Chen, D.; Ye, J.; Yao, Y.; Gao, F.; Ni, Z.; Yu, T.; Shen, Z.; Huang, Y.; Chen, P.; Li, L. J., Symmetry breaking of graphene monolayers by molecular decoration. *Phys. Rev. Lett.* **2009**, *102* (13), 135501.

32. George Socrates. J. Wiley and Sons, Infrared and Raman Characteristic Group Frequencies: Tables and Charts. 3rd edited. Chichester. **2001**. pp.12

33. Lim, Y. B.; Tan, Y.; Turpin, B. J., Chemical insights, explicit chemistry, and yields of secondary organic aerosol from OH radical oxidation of methylglyoxal and glyoxal in the aqueous phase. *Atmos. Chem. Phys.* **2013,** *13*, 8651-8667.

34. Bhattacherjee, A.; Sneha, M.; Lewis-Borrell, L.; Tau, O.; Clark, I. P.; Orr-Ewing, A. J., Picosecond to millisecond tracking of a photocatalytic decarboxylation reaction provides direct mechanistic insights. *Nat. Commun.* **2019,** *10*, 5152.

35. Yoshimi, Y.; Itou, T.; Hatanaka, M., Decarboxylative reduction of free aliphatic carboxylic acids by photogenerated cation radical. *Chem. Commun.* **2007,** 5244-5246.

Chapter 3

A Light-mediated Covalently Patterned Graphene Substrate for Graphene-Enhanced Raman Scattering (GERS)

The results reported in this chapter are based on the following publication:

Feng, G.; Suzuki, N.; Zhang Q.; Li, J.; Inose, T.; Taemaitree, F.; Shameem, K. M. M.; Toyouchi, S.; Fujita, Y.; Hirai, K.; Uji-i, H., A Light-mediated Covalently Patterned Graphene Substrate for Graphene-Enhanced Raman Scattering (GERS). *Chem. Commun.*, 2023, DOI: 10.1039/D3CC03304J.

3.1 Abstract

We report covalently patterned graphene with acetic acid as a new potential candidate for graphene-enhanced Raman scattering (GERS). Rhodamine 6G molecule in direct contact with the covalently modified region shows an enormous enhancement (~25 times) compared to its pristine region at 532 nm excitation. The GERS enhancement with respect to the layer thickness of probed molecule, excitation wavelength, and the covalently attached groups is discussed.

3.2 Introduction

Graphene-enhanced Raman scattering (GERS) is a promising variant of surface-enhanced Raman scattering (SERS), employing two-dimensional graphene as an active substrate to enhance Raman signals from a low quantity of molecular species.[1-5] Unlike the conventional SERS, observed at metal-molecule contact interfaces, GERS demonstrates a clean and robust signal response, characterized by reduced background interferences, enhanced reproducibility, and recyclability.[4] In the GERS system, graphene plays a dual role by effectively quenching autofluorescence and providing a uniform surface for enhanced Raman signals. This unique combination allows for easy analysis of Raman signals from adsorbed molecules exhibiting high photoluminescence (PL). It is postulated that electron transfer and energy transfer between the graphene and the adsorbed molecules are responsible for PL quenching in GERS.[4] The magnitude of the Raman enhancement in GERS likely depends on the highest occupied molecular orbital (HOMO) and lowest unoccupied molecular orbital (LUMO) of adsorbed molecules with respect to the Fermi level of graphene. Moreover, in-depth investigations have revealed that the enhancement factor (EF) in GERS is also influenced by additional factors including the molecular structure, phonon energy associated with the specific vibrational mode, and laser energy employed.[6, 7] The enhancement effect exhibits substantial improvement when the HOMO and LUMO energy levels of the probed molecule fall within the close energy vicinity of graphene's Fermi level (E_F) for a given laser excitation energy.[6-9] Consequently,

there has been a recent surge in research focus on modifying the Fermi energy of the graphene substrate as a means to modulate the EF in GERS. To date, the modulation of graphene's E_F in the context of GERS has primarily been achieved through element doping using chemical vapor deposition[10] and electronic interaction via solution-based molecular deposition[11]. Another approach involves charge doping into graphene utilizing an electrical field device.[7] Nonetheless, these traditional modification routes lack the ability to precisely control the Fermi level of graphene at specific locations or necessitate complex fabrication procedures.

Recently, photo-induced covalent modification (PICM) has been demonstrated as a facile method to tailor the surface properties of graphene in a desired manner.[12-14] PICM enables controlled site-specific chemisorption via photochemical activation with sub-μm precision. The spatially confined light irradiation permits the covalent 2D patterning at user-defined regions on the graphene substrates. Additionally, the grafting density of covalently anchored molecules onto the graphene surface can be controlled by the laser irradiation time, resulting in flexible modulation of the E_F.

Herein, we report that photo-induced covalently modified graphene (PICM-G) substrate exhibits a remarkably high GERS effect on fluorescent organic molecules. PICM in acetic acid aqueous solution presents the highest GERS effect, which could be attributed to the shift of the E_F of graphene due to the covalent functionalization. For the further investigation of GERS effect, Langmuir-Blodgett (LB) technique was employed here to homogenously distribute the dye molecules on the graphene layer.[8,15] 3,3'-Dioctadecyloxacarbocyanine Perchlorate (DiO) and Rhodamine 6G (Rh6G) were selected as probe dye molecules for investigating the GERS effect.

3.3 Results and discussion

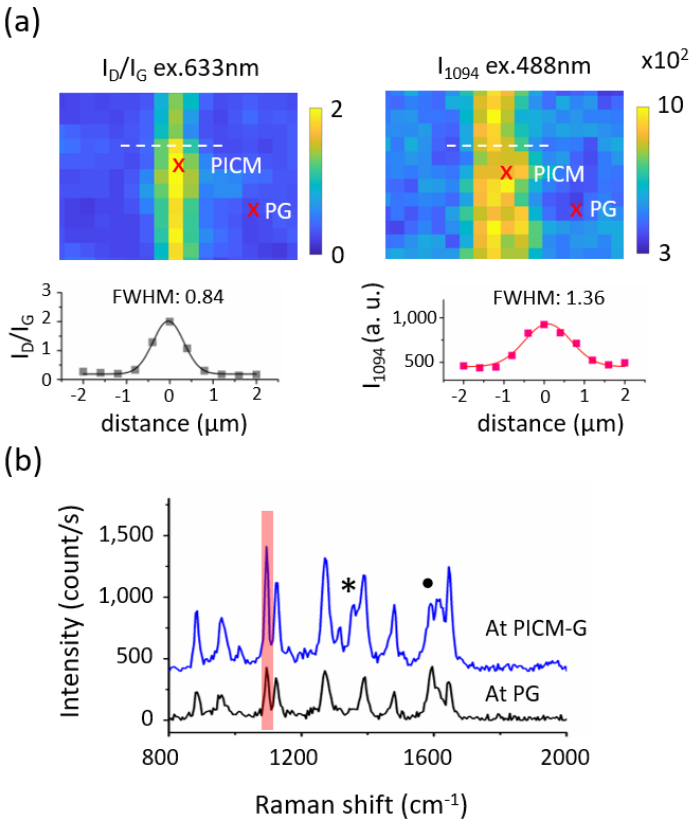

Figure 3.1 GERS of DiO molecules adsorbed on the PICM-G substrate. (a) Raman maps of I_D/I_G excited at 632.8 nm (left top) and I_{1094} excited at 488 nm (right-top), respectively. The bottom plot represents line profile along the white dashed line for each map. The red crosses on the Raman maps represent the regions of PICM and PG, respectively. (b) Raman spectra of DiO molecule at the pristine graphene (PG, black) and covalently patterned (blue) region excited with 488 nm laser. The peaks marked with '*' and '●' correspond to the D and G bands of graphene, respectively. The red highlight represents the peak of DiO at 1094 cm^{-1} used for mapping.

In accordance with our previous work,[14] a 488 nm continuous wave laser was used to covalently pattern the graphene surface with chemical moieties such as -CH_3, -OCH_3, -$COOCH_3$ (for experimental details see supplementary information). A line patterned functionalization as shown in Figure 3.1a was achieved by scanning the tightly focused laser

(488 nm) at the interface between graphene and an aqueous solution of acetic acid (0.1 M). The photogenerated radicals are only formed in those areas where the laser is exposed to the aqueous solution resulting in a spatially controlled grafting of functional groups with the formation of sp^3 carbon defects. The Raman spectra of the PICM region with respect to the pristine graphene (PG) region are presented in Figure 3A1a. Here, a high mean intensity ratio of I_D/I_G (>1.2) along with the presence of the D' peak (1619 cm^{-1}) at the shoulder of the G peak demonstrates the successful covalent modification with a high grafting density at the PICM region.[16] Consistently, the estimated full-width half-maxima (FWHM) of the PICM region (840 nm) was found to be larger than the diffraction limit (300 nm in this study) presumably due to the diffusion of photogenerated radicals over the diffraction spot.

In our initial GERS measurements, DiO molecules (Figure 3A1b) were deposited on the PICM-G by simply immersing it in the DiO solution (1.5 mg/L) and subsequently rinsed with water to remove excess dye molecules. Raman spectra of the adsorbed dye molecules are observed from both PG and PICM-G regions, thanks to the GERS effect (Figure 3.1b). However, a significantly highest signal enhancement has been clearly detected from the PICM-G region than from the PG region (Figure 3.1a right) of 1094 cm^{-1} (I_{1094}), which corresponds to one of the Raman peaks of DiO (Raman spectra of pure DiO see Figure 3A2). The FWHM of the I_{1094} map was estimated to be approximately 1360 nm, which is 1.6 times larger than that of the I_D/I_G map (Figure 3.1a).

The disparity between the FWHM of the I_D/I_G ratio and that of I_{1094} could arise from the heterogeneous density of the adsorbed dye molecule and/or the GERS enhancement. To investigate the GERS effect with respect to the homogeneous distribution and number of layers of the dye molecule, the LB technique was employed. For a good signal-to-noise ratio, three layers of stearic acid labeled with DiO dyes with a molar ratio of [SA] / [DiO] > 10 were used. The details are in Figure 3A3-3A7.

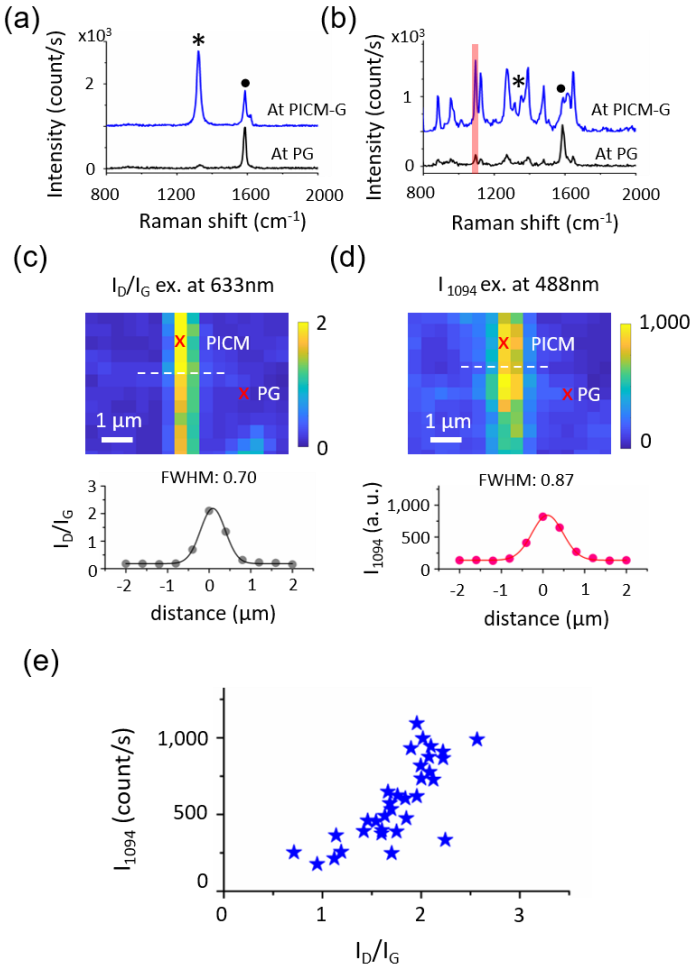

Figure 3.2 Raman maps of LB films labelled with DiO on PICM-G. Raman spectra at the area of PG (black) and PICM-G (blue) excited at 633 nm (a) and 488 nm (b), respectively. The red highlight represents the peak of DiO at 1094 cm^{-1} used for mapping. (c) I_D/I_G ratio map excited at 633 nm (power: 3.08 MW/cm^2). (d) I_{1094} map on the same area as (c) excited at 488 nm (power: 0.78 MW/cm^2). The bottom plot represents the line profile along the white dashed line. (e) Correlation plot between I_D/I_G and I_{1094}. The red highlight on the Raman maps in (c-d) represent the regions of PICM and PG, respectively.

Figure 3.2a and 3.2b display the Raman spectra of a triple LB film of DiO molecules under two different excitation wavelengths of 633 nm and 488 nm, respectively. Interestingly, no distinct Raman signature of the DiO molecule was observed when excited with 633 nm. Instead, both the PG and PICM regions exhibit Raman characteristics associated with graphene. In

contrast, when excited at 488 nm, the spectra exhibit a moderate Raman signal of DiO from the PG region, while enhanced signals are observed from the PICM region. The observed difference in GERS effect with respect to the excitation wavelength can be attributed to the fact that 488 nm is on-resonant to DiO whereas 633 nm is off-resonance (see Figure 3A8). Note that clear Raman peaks of DiO can be identified only in the presence of graphene (Fig. S9). This indicates that the Raman enhancement is attributed to not only the resonance Raman but also to GERS effect. The FWHM of the bright line at the I_{1094} map is estimated to be 870 nm, only 1.24 times wider than that of I_D/I_G (Figure 3.2c-d), which is much narrower than the case of Figure 3.1. This observation suggests that the density of adsorbed dye molecule is relatively homogeneous between the PG and the PICM areas in the LB film compared to the simple deposition of the dye molecules by dipping graphene in the dye solution. Most importantly, the maximum of the I_D/I_G ratio map is located at the maximum of I_{1094} map. Figure 3.2e shows a correlation between I_D/I_G and I_{1094}, where a higher I_D/I_G ratio results in a higher I_{1094}. This suggests that the GERS EF strongly depends on the degree of PICM on graphene.

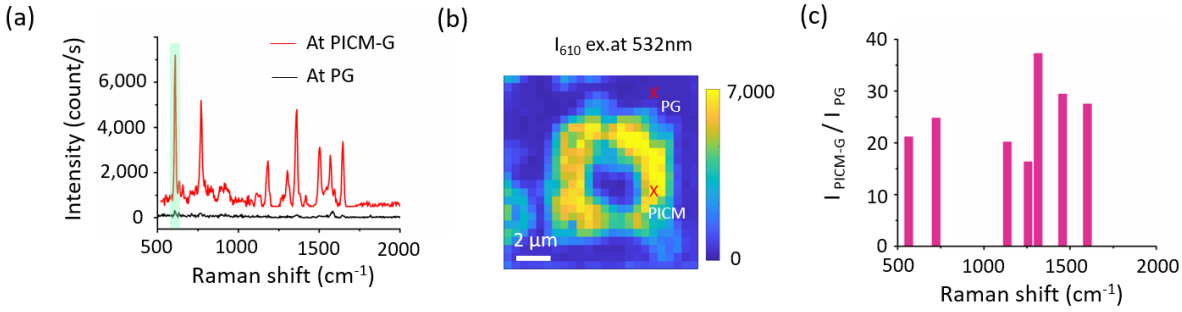

Figure 3.3 (a) GERS of Rh6G on PG and PICM-G excited at 488 nm. The green highlight represents the peak of Rh6G at 610 cm^{-1} used for mapping. (b) GERS mapping of Rh6G (I_{610}, peak intensity at 610 cm^{-1}) from the PG and PICM domain under 532 nm laser excitation (0.98 MW/cm^2). The red crosses on the Raman maps represent the PICM and PG regions, respectively. (c) Peak intensity ratio between the $I_{PICM\text{-}G}/I_{PG}$ across the spectral region.

In order to estimate the GERS effect and versatility of the newly introduced PICM graphene substrate for GERS measurement, we employed the most commonly used Rhodamine 6G (Rh6G) as a probe molecule (adsorbed by immersion) and the results were compared with previously reported works. Figure 3.3a depicts the Raman spectra of Rh6G on the PG and the PICM area under 532 nm laser excitation. Note that the fluorescence background was subtracted from the spectra (see the details in Figure 3A10). The observed Raman bands at 610, 773, 1182, 1312, 1505, and 1647 cm^{-1} are in good agreement with the earlier reports.[17] However, consistent with DiO molecules, the Raman signals are markedly enhanced in the PICM region compared to the PG region. Furthermore, Raman mapping (Figure 3.3b) and the peak ratio ($I_{PICM\text{-}G}/I_{PG}$) analysis (Figure 3.3c) provide additional evidence of signal enhancement in the PICM region. To investigate the enhancement mechanism, we summarized the I_{1647}/I_G as function of excitation energy, where the highest was found around 2.3 eV, indicating resonance Raman scattering effect. Considering no detectable Raman peaks of Rh6G in the absence of graphene (Figure 3A13), GERS effect on Rh6G plays an important role. Note that electromagnetic enhancement is less likely, since surface plasmon lies in the terahertz range rather than in visible to NIR frequency.[6] We further analyzed the Raman shift of both G and 2D peaks at PICM region estimating the shift tendency of graphene's E_F after the covalent modification (Table S1).[18, 19] A downshift of pos (G) indicates electron doping effect, which could be attributed to electron-donating property of methyl, methoxy, functionalized on graphene. As a result, the modified graphene's E_F might shift and comes close to LUMO level of Rh6G (-3.4 eV), promoting the charge transfer between modified graphene and dye molecules. This could lead the Raman enhancement, as suggested in the previous reports.[10, 11]

It has been previously demonstrated that the type of the molecule and its interaction with the graphene substrate significantly influences the GERS effect.[9] To understand the role of the different functional groups on the PICM region in GERS, different chemical groups were covalently anchored to the graphene layer with the aid of a light-triggered radical generation

method. As we reported previously,[13] the PICM under the aqueous solution of acetic acid presumably introduces alkyl, ether, and ester groups on the graphene surface, while water introduces hydroxyls and oxygen species, resulting in the formation of graphene oxide. The Raman spectra of Rh6G show a very distinct enhancement value from these chemical groups as shown in Figure 3A13. The graphene oxide displayed a small enhancement of Rh6G, whereas a significant enhancement was observed from the acetic acid functionalized area. These findings provide evidence that the functional groups within the PICM region play a critical role in determining the EF of GERS.

Table 3.1 Comparison of I_m/I_p on different types of graphene substrates

Medification type	Preparation method	dye	Laser line / nm	Peak/ cm^{-1}	I_m/I_p	Reference
oxide	thermal reaction	Rh6G	532	1647	~1	ref. 20
oxide	PICM in water	Rh6G	532	1647	~1	This work
hydrogenated	thermal reaction	Rh6G	532	1647	~1	ref. 21
covalent with 4-nitrophenyl	diazonium chemistry	Rh6G	532	1647	~2	ref. 11
N-doped	atom substitute	RhB	532	1647	~9	ref. 10
covalent with Acetic acid	PICM	Rh6G	532	1647	~25	This work

In Table 3.1, we provided a comparative summary of the GERS effect for our sample in relation to previous studies. The GERS effect was estimated by calculating the ratio of the peak intensity of the aromatic benzene ring of Rh6G at 1647 cm^{-1} (0.205 eV) from the PICM-G area to that of the PG region (I_m/I_p). Among the previously reported works, N-doped graphene exhibits the highest signal enhancement (I_m/I_p ~9) for the Rh6G molecule, while a moderate enhancement was observed from the functionalized graphene substrate with a 4-nitrophenyl group (I_m/I_p ~2). On the other hand, graphene oxide and hydrogenated graphene did not exhibit a significant enhancement at their defect sites. Remarkably, our PICM-G substrate under the

acetic acid exhibited an enormous signal enhancement of I_m/I_p ~25, which is an order of magnitude higher compared to other reported graphene derivatives. Our findings indicate that PICM graphene has the potential to serve as a promising candidate for future GERS substrates.

3.4 Conclusion

In summary, we have systematically investigated the GERS effect on organic dye molecules from pristine and PICM graphene substrates to address the signal enhancement effect. The covalent patterning is selectively created using a laser writing technique, resulting in a lateral heterojunction comprising both covalent and noncovalent domains. In contrast to the pristine region, the PICM region exhibits a significantly enhanced Raman signal of the dye molecules. The modulation of the electronic structure of graphene can be attributed to the signal enhancement from the PICM region. Likely, the upshift of the EF of graphene can be attributed to the signal enhancement from the PICM region. Our results also demonstrate that the GERS intensity is strongly influenced by the density of the dye molecules and the degree of covalent grafting. In addition, the resonance excitation further enhances the Raman signal of the probed dye molecule on the graphene surface. Finally, the chemical nature of the addends at the PICM region has been investigated to understand the GERS effect. The PICM-G prepared in water exhibits a much lower enhancement than the PICM-G prepared in acetic acid solution, suggesting a strong effect of functional groups for the GERS effect. The results suggest that the PICM-graphene with acetic acid is a promising GERS substrate for (bio-)chemical sensing.

3.5 Experimental method

Sample preparation

The monolayer graphene protected by poly (methyl methacrylate) (PMMA) was purchased from Graphenea and subsequently transferred onto a coverslip. The protective PMMA layer was removed by acetone and 2-propanol. The quality of the single-layer graphene was

monitored after transferring by estimating the I_{2D}/I_G ratio from the Raman spectra (Figure 3A1). Before transferring graphene, the coverslip was ultrasonically washed with acetone, NaOH solution (1 M), and Milli-Q water, respectively. The light-triggered covalent pattering on the graphene layer was selectively achieved by the nanolithography technique. The PCIM was carried out in pure water and acetic acid solution separately in order to attach different functional groups on the graphene surface. A diamond cutter was employed to mark the functionalized region for differentiating the patterned and pristine region.

Chemicals

Milli-Q water obtained from a Milli-Q-plus system with a resistivity greater than 18 MΩ•cm^{-1}. Acetic acid and stearic acid were purchased from Tokyo Chemical Industry Co., Ltd. (TCI). Rhodamine 6G (Rh6G) was purchased from FUJIFILM Wako Pure Chemical Corporation (Japan). DiO dye was purchased from Sigma-Aldrich. All the reagents were used without any further purification.

Langmuir-Blodgett (LB) method

Langmuir-Blodgett (LB) method was carried out to make a homogenous monolayer or multilayer of DiO dye molecules on the graphene substrate. Surface tension was recorded to check the state of the stearic acid and dye molecules on the interface between air and liquid. To systematically investigate the GERS on the modified graphene, we form a combination of stearic acid and DiO dye layers on the graphene surface. DiO dye molecules were dissolved in 0.1 mg/mL (3.51×10^{-4} M) stearic acid (chloroform as solvent). The molar ratio between stearic acid and dye was kept ~10:1. Then, a 100 µl mixture of stearic acid and dye molecules was distributed on the water surface with a micro-syringe. Standing for 30 min to let the dye molecules homogeneously distributed. The target surface tension is set up at 30 mN/mm. The PICM-G was followed to pick up the dye molecules. Since SA layers were carefully picked up at the solid phase, we expect that rearrangement of LB film after deposition was minimized

and thus the dye molecules could be homogeneously distributed both on the PG and the PICM-G region.

Raman spectroscopy

Raman spectroscopic measurements were carried out using an inverted optical microscope (Ti-U, Nikon) equipped with a piezoelectric sample stage. A continuous-wave 488 nm (Sapphire SF 488-100 CW CDRH) laser was used for the photoinduced covalent functionalization (PICM) on the graphene layer. The PICM was achieved with an input power of ~6 MW/cm^2, while the Raman measurements were carried out by reducing the power to ~0.78 MW/cm^2 with the same laser. Alongside two other lasers (532, and 633 nm) were also employed for the Raman measurements. The input power density during the Raman measurements was controlled by the combination of neutral density filters. The laser beam was focused using a 60 X objective lens (Nikon), and the Raman scattering signals was collected using the same objectives in a backscattering geometry. The collected Raman signals were guided to a liquid nitrogen-cooled CCD spectrograph (iHR320, Horiba) having a grating of 600 grooves/mm. A corresponding long-pass filter (Chroma) was placed just before the spectrograph for blocking the Rayleigh scattering during the Raman measurements. The PICM and Raman mapping were conducted by OMEGA software (Combiscope, AIST-NT/ Horiba). Origin Lab 9.1 and MATLAB (MathWorks) were used for the Raman data analysis.

Atomic force microscopy (AFM) measurement

AFM was carried out with an OmegaScope™ (AIST-NT, HORIBA) system in tapping mode at ambient conditions. Al reflecting coating (160 AC-NA) AFM cantilever was used to obtain images resolved by 512×512 or 1024×1024 pixels. Omega software (AIST-NT/HORIBA) and Gwyddion software were utilized for AFM data analysis.

3.6 Appendix

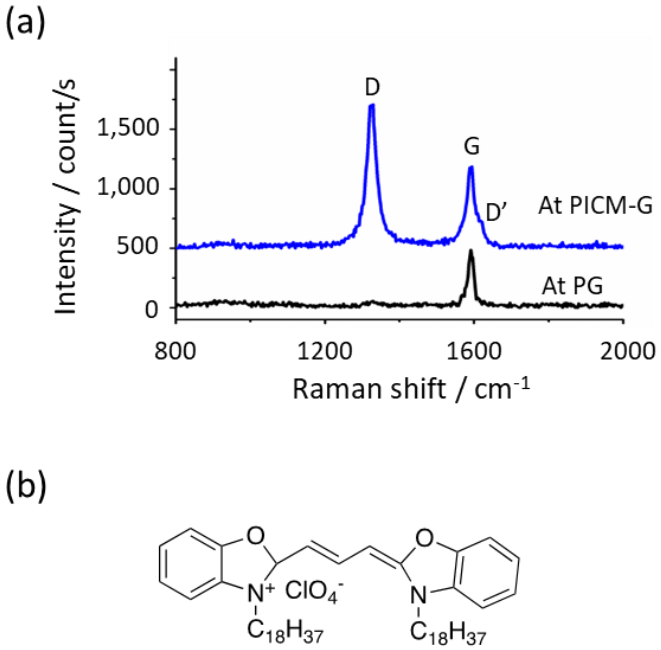

Figure 3A1 (a) Raman spectra of graphene heterojunction consisting of pristine (black) and chemically patterned region (blue), measured by 633 nm (to reduce the effect of laser on patterned functionalization, low excitation energy (633nm) was used for Raman scattering). The patterned region manifests a pronounced defect-induced D band at 1326 cm^{-1} together with the characteristic G band of graphene at 1594 cm^{-1}, while the areas with no laser exposure resemble the pristine features, exhibiting an I_D/I_G ratio of <0.2; (b) Chemical structure of DiO molecule.

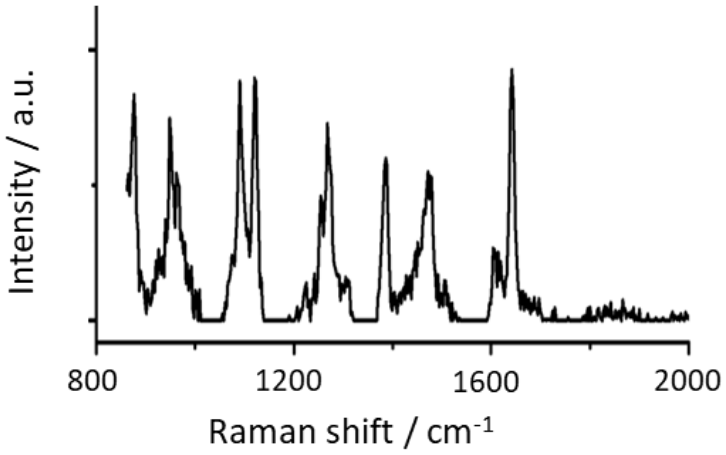

Figure 3A2. Raman spectra of pure DiO dye excited by 633 nm.

Langmuir-Blodget film for GERS measurements

As depicted in Figure 3A4, a mixture of stearic acid (SA) and DiO was distributed on the water surface. SA, an amphoteric molecule, was used to trap and distribute the dye molecules. After compressing the layer to the saturated pressure, the layers were picked up on a graphene surface. Figure 3A5 shows the Raman spectra of one to three LB layers on the PICM-G. While no obvious Raman signal of DiO was detected from a single LB layer, clear peaks of DiO have been observed from double and triple layers of LB films. It is worth mentioning here that only D and G bands of graphene were detected (see Figure 3A7) in the case of LB layers composed of pure SA without any dyes. The lack of Raman signals from the first layer is presumably due to the ultralow concentration of the adsorbed DiO molecule. To confirm our prediction, we further prepared a single LB layer on the PICM-G region with a high concentration of DiO ([DiO] / [SA] > 0.1). In this case, Raman signals were observed from the single layer (Figure 3A8), indicating that the GERS intensity is influenced by the density of dye molecules present on surface. However, a high concentration of DiO in the LB layers causes spatial heterogeneity of GERS intensity. This heterogeneity is most likely due to the rearrangement of LB layers after the deposition according to our AFM study (Figure 3A6). Thus, in the following

experiments, triple LB layers with the molar ratio of [SA] / [DiO] > 10 were used to obtain homogeneously distributed DiO molecules on surface.

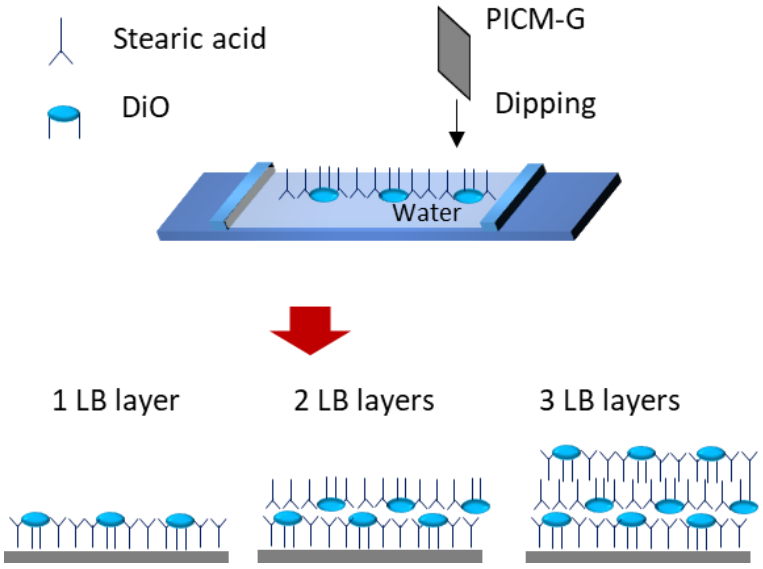

Figure 3A3. Schematic drawing of LB of DiO dye molecules on the PICM-G substrate.

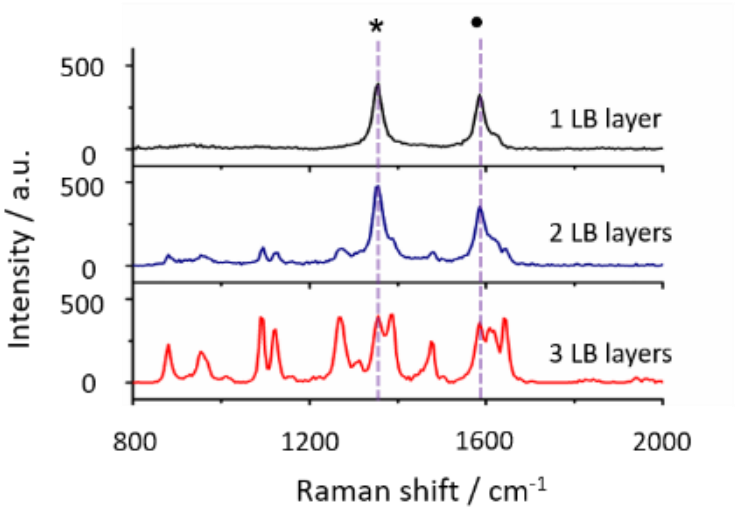

Figure 3A4 Raman spectra of DiO molecule with different layer numbers of the LB film on the PICM graphene substrate. Raman signals of DiO molecules are detected over double LB layers. The peaks marked with '*' and '●' correspond to the D and G bands of the graphene, respectively.

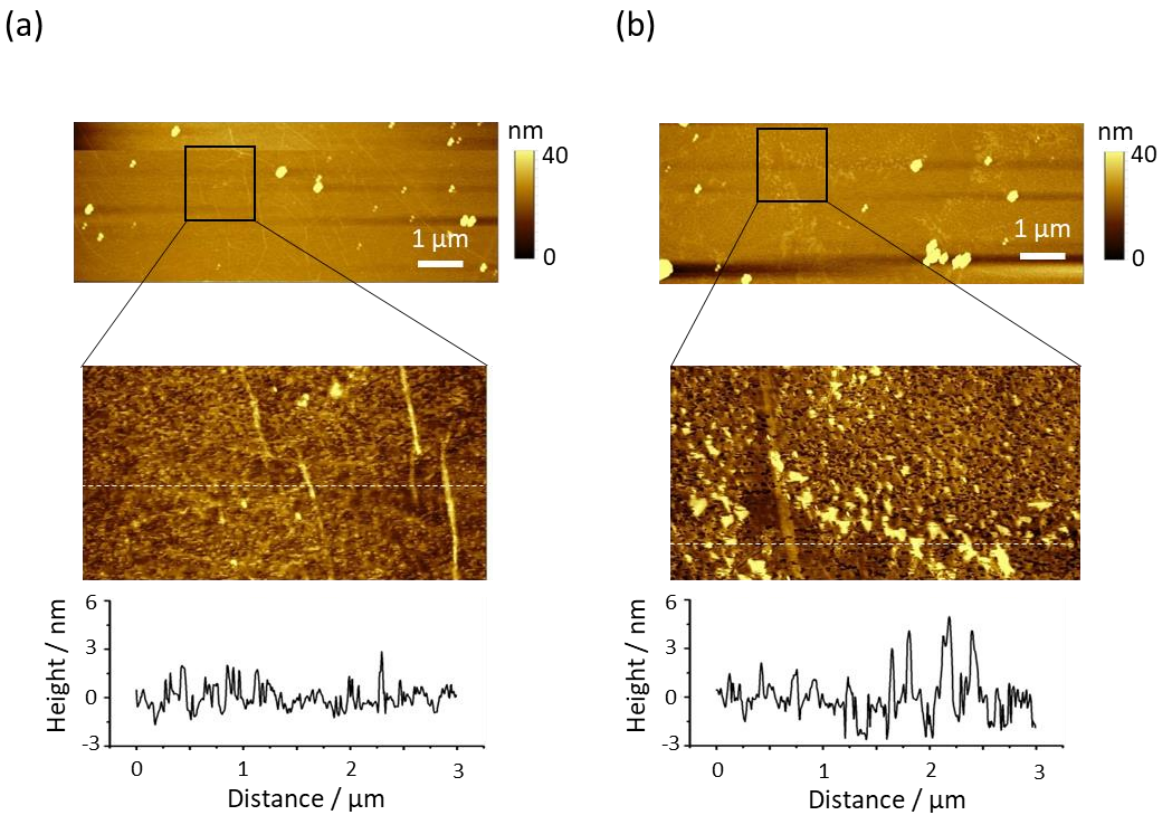

Figure 3A5 AFM measurement on single LB layer at the molar ratio of [SA] / [DiO] ~10: 1 (a) and ~10: 3 (b), respectively. The corresponding height profiles are presented at the bottom.

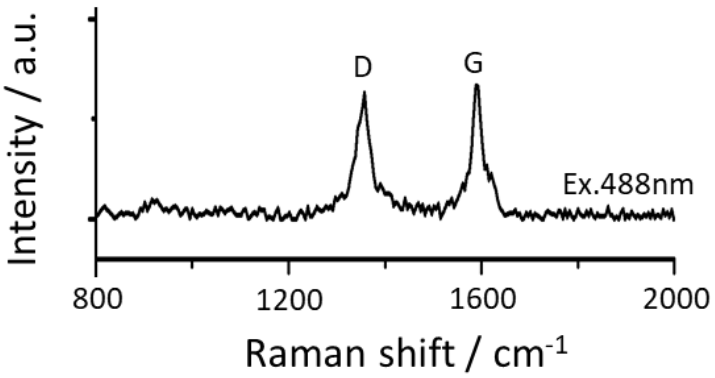

Figure 3A6. Raman response of pure SA on the PICM region.

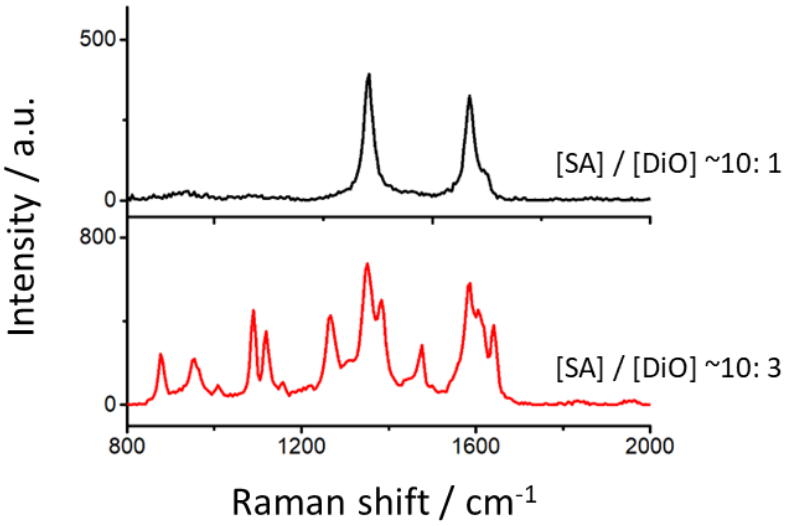

Figure 3A7. Raman spectra of monolayer LB layer of DiO with low (black, [SA] / [dye]~10: 1) and high concentration (red, [SA] / [dye]~10: 3).

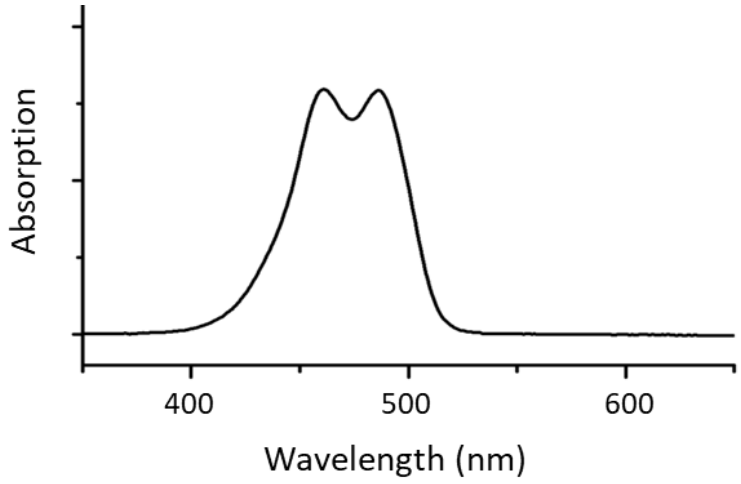

Figure 3A8. UV-visible absorption of DiO dye.

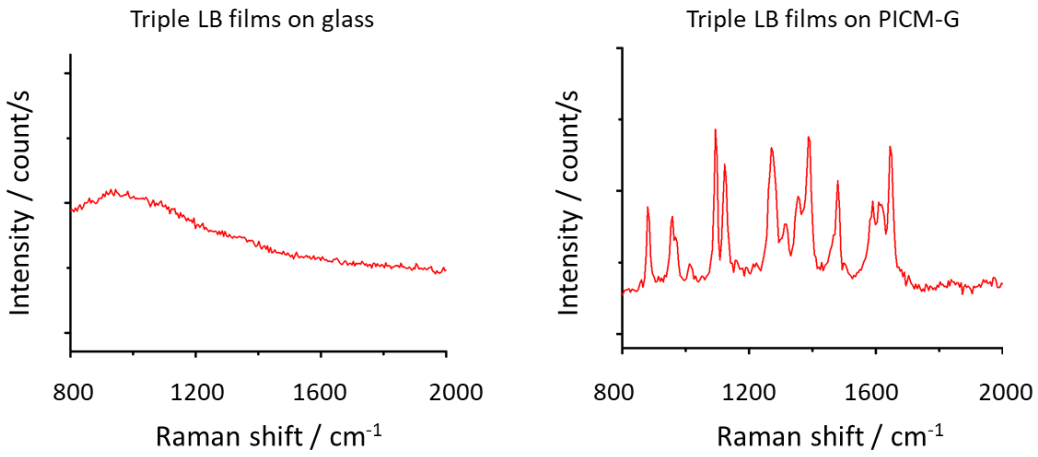

Fig. S9. Raman spectra of triple LB films of DiO on glass substrate and PICM-G substrate, respectively. Measured by 488 nm.

The background correction of Raman spectra

Top panel in Figure 3A10 displays raw Raman spectra of Rhodamine 6G on the PG and the PICM-G area, respectively. Although the fluorescence was suppressed by graphene, the emission appears in the Raman spectra as a background. To identify Raman peaks better, the fluorescence background was subtracted from the spectra by a simple polynomial fitting (the bottom panel in Figure 3A10).

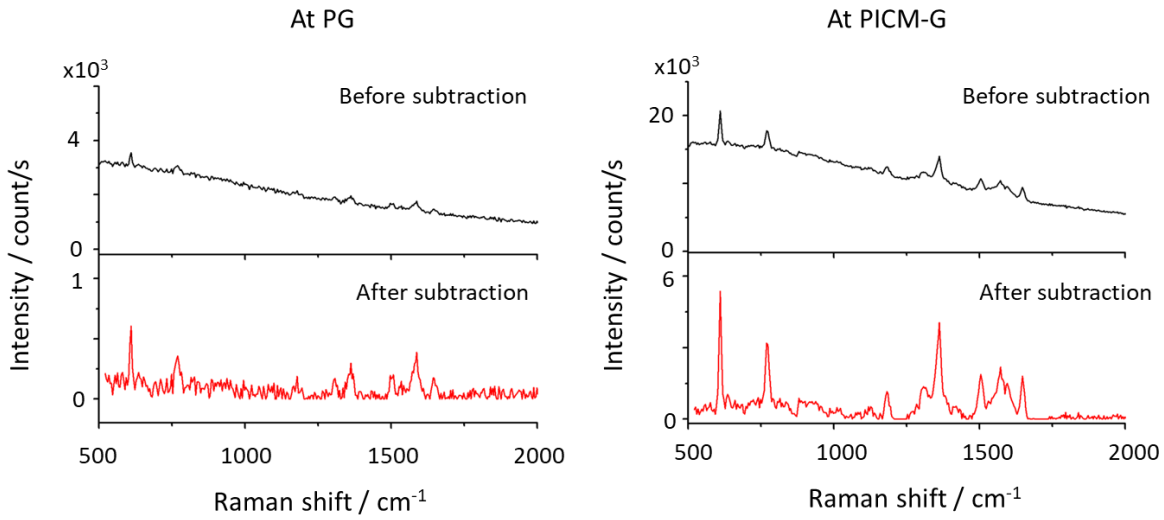

Figure 3A10. GERS performance for Rh6G adsorbed on the PG and PICM-G region before (black) and after subtraction (red), respectively.

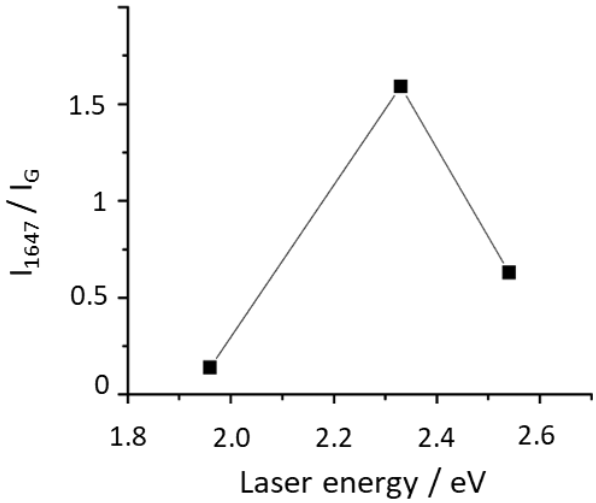

Figure 3A11. The enhancement factor (normalized by G band) as function of laser excitation energy: 488 nm (2.54 eV), 532 nm (2.33 eV), 633 nm (1.96 eV).

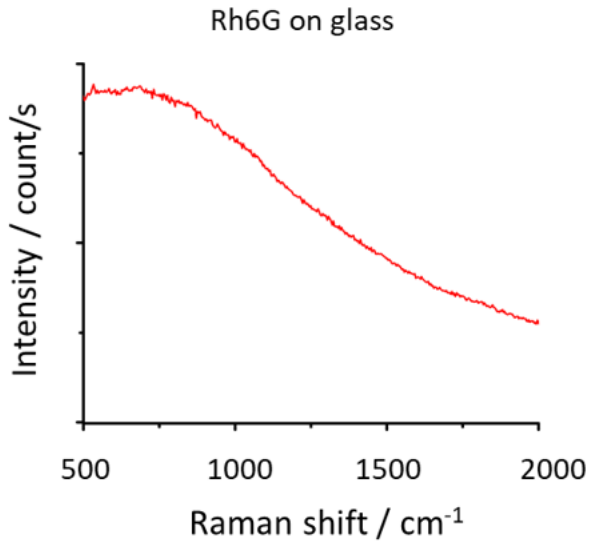

Figure 3A12. Raman spectra of Rh6G distributed on glass substrate, measured by 532 nm.

Table 3A1. Average values of Pos(G), Pos(2D) and the corresponding shifts

Type of graphene	Pos (G) /cm^{-1}	Shift of pos (G) /cm^{-1}	Pos (2D)	Shift of pos (2D) /cm^{-1}
Pristine	1588.0±2.3	-3.8	2639.6±3.53	0.3
PICM in acetic acid	1584.2±2.2		2639.9±3.18	

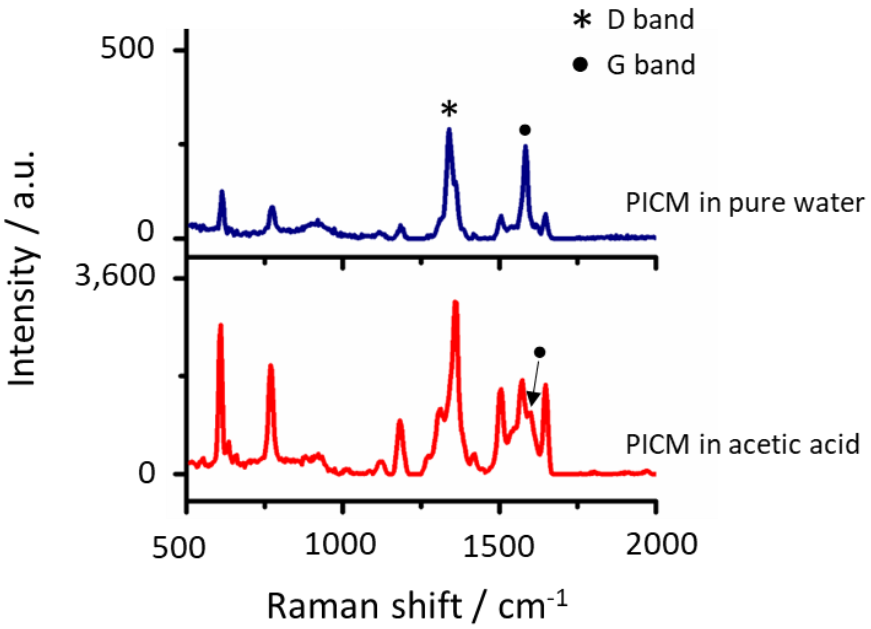

Figure 3A13. Comparison of GERS performance of R6G on graphene layers modified with PICM in pure water (top) and acetic acid (bottom), respectively. (Excitation at 532 nm with 0.98 MW/cm^2).

3.7 References

1. Xu, W.; Mao, N.; Zhang, J., Graphene: a platform for surface-enhanced Raman spectroscopy. *Small* **2013**, 9 (8), 1206-1224.

2. Qiu, C.; Zhou, H.; Yang, H.; Chen, M.; Guo, Y.; Sun, L., Investigation of n-Layer Graphenes as Substrates for Raman Enhancement of Crystal Violet. *J. Phys. Chem. C* **2011**, 115 (20), 10019-10025.

3. Ling, X.; Wu, J.; Xu, W.; Zhang, J., Probing the effect of molecular orientation on the intensity of chemical enhancement using graphene-enhanced Raman spectroscopy. *Small* **2012**, 8 (9), 1365-1372.

4. Zhang, N.; Tong, L.; Zhang, J., Graphene-Based Enhanced Raman Scattering toward Analytical Applications. *Chem. Mater.* **2016**, 28 (18), 6426-6435.

5. Xie, L.; Ling, X.; Fang, Y.; Zhang, J.; Liu, Z. Graphene as a Substrate to Suppress Fluorescence in Resonance Raman Spectroscopy. *J. Am. Chem. Soc.* **2009**, 131, 9890– 9891.

6. Ling, X.; Xie, L.; Fang, Y.; Xu, H.; Zhang, H.; Kong, J.; Dresselhaus, M. S.; Zhang, J.; Liu, Z., Can graphene be used as a substrate for Raman enhancement? *Nano Lett.* **2010**, 10 (2), 553-61.

7. Huang, S.; Ling, X.; Liang, L.; Song, Y.; Fang, W.; Zhang, J.; Kong, J.; Meunier, V.; Dresselhaus, M. S., Molecular selectivity of graphene-enhanced Raman scattering. *Nano Lett.* **2015**, 15 (5), 2892-2901.

8. Ling, X.; Zhang, J., First-layer effect in graphene-enhanced Raman scattering. *Small* **2010**, 6 (18), 2020-2025.

9. Xu, H.; Chen, Y.; Xu, W.; Zhang, H.; Kong, J.; Dresselhaus, M. S.; Zhang, J., Modulating the charge-transfer enhancement in GERS using an electrical field under vacuum and an n/p-doping atmosphere. *Small* **2011**, 7 (20), 2945-2952.

10. Feng, S.; Dos Santos, M. C.; Carvalho, B. R.; Lv, R.; Li, Q.; Fujisawa, K.; Elias, A. L.; Lei, Y.; Perea-Lopez, N.; Endo, M.; Pan, M.; Pimenta, M. A.; Terrones, M. Ultrasensitive Molecular Sensor Using N-doped Graphene through Enhanced Raman Scattering. *Sci. Adv.* **2016**, 2, e1600322.

11. Valeš V.; Kovaříček, P., Fridrichová, M.; Ji, X.; Ling, X.; Kong, J.; Dresselhaus, M.S.; Kalbáč, M., Enhanced Raman scattering on functionalized graphene substrates. *2D Mater.* **2017**, 4, 025087.

12. Toyouchi, S.; Wolf, M.; Feng, G.; Fujita, Y.; Fortuni, B.; Inose, T.; Hirai, K.; De Feyter, S.; Uji-i, H., All-Optical and One-Color Rewritable Chemical Patterning on Pristine Graphene under Water. *J. Phys. Chem. Lett.* **2022**, 13, 3796-3803.

13. Edelthalhammer, K. F.; Dasler, D.; Jurkiewicz, L.; Nagel, T.; Al-Fogra, S.; Hauke, F.; Hirsch, A., Covalent 2D-Engineering of Graphene by Spatially Resolved Laser Writing/Reading/Erasing. *Angew. Chem. Int. Ed.* **2020**, *59*, 23329-23334.

14. Feng, G.; Inose, T.; Suzuki, N.; Wen, H.; Taemaitree, F.; Wolf, M.; Toyouchi, S.; Fujita, Y.; Hirai, K.; Uji, I. H., Liquid-phase photo-induced covalent modification (PICM) of single-layer graphene by short-chain fatty acids. *Nanoscale* **2023**, 15, 4932–4939.

15. Oliveira, O. N., Jr.; Caseli, L.; Ariga, K., The Past and the Future of Langmuir and Langmuir-Blodgett Films. *Chem. Rev.* **2022**, 122 (6), 6459-6513.

16. Rodríguez González, M. C.; Leonhardt, A.; Stadler, H.; Eyley, S.; Thielemans, W.; De Gendt, S.; Mali, K. S.; De Feyter, S. Multicomponent Covalent Chemical Patterning of Graphene. *ACS Nano* **2021**, 15, 10618−10627.

17. Guthmuller, J.; Champagne, B. Resonance Raman Scattering of Rhodamine 6G as Calculated by Time-Dependent Density Functional Theory: Vibronic and Solvent Effects. *J. Phys. Chem. A* **2008**, 112, 3215– 3223.

18. J. E. Lee, G. Ahn, J. Shim, Y. S. Lee and S. Ryu, *Nat. Commun.*, **2012**, 3, 1024.

19. G. Velpula, R. Phillipson, J. X. Lian, D. Cornil, P. Walke, K. Verguts, S. Brems, I. H. Uji, S. De Gendt, D. Beljonne, R. Lazzaroni, K. S. Mali and S. De Feyter, *ACS Nano*, **2019**, 13, 3512-3521.

20. Sil, S.; Kuhar, N.; Acharya, S.; Umapathy, S. Is Chemically Synthesized Graphene 'Really' a Unique Substrate for SERS and Fluorescence Quenching? *Sci. Rep.* **2013**, 3, 3336.

21. Vales, V.; Drogowska-Horna, K.; Guerra, V. L. P.; Kalbac, M., Graphene-enhanced Raman scattering on single layer and bilayers of pristine and hydrogenated graphene. *Sci. Rep.* **2020**, 10 (1), 4516.

Summary and perspective

In summary, firstly, we investigated the PICM of graphene in short-chain fatty acids (SCFAs) at the liquid-phase. By using this method, chemically covalent graphene can be easily achieved with high efficiency. The site-specific point in D band Raman mapping presents that modification of graphene only happens at the laser focused area, demonstrating the reaction is generated by the irradiated laser. The PICM efficiency estimated by the *in-situ* Raman by monitoring the intensity of D band show that SCFAs with an alkyl chain (acetic acid, propionic acid, and butyric acid) drastically enhance the PICM efficiency, compared to the PICM in water and formic acid. It takes only several seconds to reach $I_D/I_G \approx 1$ in the case of acetic acid. These results indicate that alkyl chains play a vital role in chemically covalent modification of graphene. Furthermore, we found that the covalent area of graphene can emit the luminescence, which could be attributed to the modulated electronic structure generating the semiconductor property of graphene. IR and Raman spectroscopy reveal that functional groups on graphene are most likely methyl, methoxy, and acetate groups for PICM in acetic acid solution. A greater downshift of the G-band was observed in Raman spectra upon PICM with longer alkyl chains, suggesting that the charge doping effect can be controlled by the alkyl chain length of the SCFAs. In the end, two stages of radicals' reaction were proposed considering the high oxidation efficiency and species of functional groups on graphene. These results suggest that sub-micrometre scaled and site-elective bandgap engineering can be applied to graphene surfaces using laser-assisted radical reactions.

Secondly, applying the photo-induced covalent modification of graphene (PICM-G), the graphene-enhanced Raman scattering (GERS) is studied for detecting a low quantity of molecular species, further investigating the electronic property of the chemically modified graphene. As a result, we found that the GERS effect at the covalent area is higher than the

pristine area, which could be attributed to the upshifted Fermi level of graphene after covalent modification. By the help of Langmuir-Blodgett (LB) method, the dye molecules on PICM-G can be homogeneously distributed and the heterogeneity between pristine and covalent region is minimized. We found that the maximum of the I_D/I_G at the PICM-G area is located at the maximum of I_{1094} (the peak intensity at 1094 cm^{-1} of DiO). The correlation between I_D/I_G and I_{1094} shows that a higher I_D/I_G ratio results in a higher I_{1094}. These results suggest that the GERS effect strongly depends on the degree of covalent modification. In addition, PICM-G substrate presents the highest GERS effect on Rh6G compared to the previous works. The GERS effects of PICM-G prepared in pure water was much weaker than PICM-G prepared in acetic acid aqueous solution, suggesting the key role of functional groups on graphene in determining the GERS enhancement. These findings seriously investigate the GERS effect of PICM-G and indicate that the PICM graphene has the potential to serve as a promising candidate for future GERS substrates.

Our results reported in this thesis provide a high-efficiency method to generate liquid-phase PICM of graphene, which can tailor the chemical nature and electronic structure of graphene. The reliable strategy using SCFAs with an alkyl chain for covalent modification of graphene would boost the study of sub-micrometer scaled and site-controllable bandgap engineering of graphene and related applications. The reconstruction of sp^2 hybridized carbon of PICM graphene at high temperature (reversibly remove chemical defects of PICM graphene) would boost the study on cross utilization of semiconducting and conducting property of graphene. Furthermore, applying this liquid-phase PICM method would boost the study of GERS substrate, such as improving the enhancement factor of GERS, investigating the chemical mechanism. All in all, these findings would boost the study of graphene on nanodevice, catalysis, biological detecting, and tracing, extending the potential applications of graphene.

List of publications

1. **Feng, G.**; Inose, T.; Suzuki, N.; Wen, H.; Taemaitree, F.; Wolf, M.; Toyouchi, S.; Fujita, Y.; Hirai, K.; Uji-i, H., Liquid-phase photo-induced covalent modification (PICM) of single-layer graphene by short-chain fatty acids. *Nanoscale*, **2023**, 15, 4932–4939.

2. **Feng, G.**; Suzuki, N.; Zhang Q.; Li, J.; Inose, T.; Taemaitree, F.; Shameem, K. M. M.; Toyouchi, S.; Fujita, Y.; Hirai, K.; Uji-i, H., A Light-mediated Covalently Patterned Graphene Substrate for Graphene-Enhanced Raman Scattering (GERS). *Chem. Commun.*, 2023, DOI: 10.1039/D3CC03304J.

3. Toyouchi, S.; Wolf, M.; **Feng, G.**; Fujita, Y.; Fortuni, B.; Inose, T.; Hirai, K.; De Feyter, S.; Uji-i, H., All-optical and one-color rewritable chemical patterning on pristine graphene under water. *J. Phys. Chem. Lett.* **2022**, 13, 17, 3796-3803.

Conferences

1. 2021.10.01 The 7th Hokkaido University Cross-Departmental Symposium. (Poster presentation, online)

2. 2021.11.04-11.05 The fourth International Workshop on Symbiosis of Biology and Nanodevices. (Poster presentation, online)